



22nd European Molecular Beam Epitaxy Workshop



March 9-13, Auron, France, 2025

<https://eurombe2025.sciencesconf.org>



Invited talk : 23min + 7min questions
Oral : 15min + 5min questions

22nd EuromBE, March 9-13, 2025

	Sunday, 09.03	Monday, 10.03	Tuesday, 11.03	Wednesday, 12.03	Thursday, 13.03
8:00	Salle Roversy	Salle Roversy registration	Salle Roversy registration	Salle Roversy registration	Movie Theater Le Riounet registration
8:30	opening	11: L. Ceruffi	14: M. Brehm	17: W. Wegscheider	110: T. Hakkarainen
9:00	S1: Antimonides	12: D.V. Dinh	S4: Ultra-low temperature, Photonics	S7: Quantum	S10: Quantum dots
9:30	break	S2: Nitrides	break	break	break
10:00	break	Lunch Boxes	break	break	break
10:30	break	Lunch Boxes	15: A. Patanè	18: G. Krizman	111: E. Luna
11:00	break	Lunch Boxes	11:00	11:00	11:00
11:30	break	Lunch Boxes	S5: 2D Materials	S8: Novel materials - topological	S11: Novel materials - Photovoltaic
12:00	break	Lunch Boxes	11:30	11:30	11:30
12:30	break	Lunch Boxes	12:00	12:00	12:00
13:00	break	Lunch Boxes	12:30	12:30	12:30
13:30	break	Lunch Boxes	13:00	13:00	13:00
14:00	break	Lunch Boxes	13:30	13:30	13:30
14:30	break	Lunch Boxes	14:00	14:00	14:00
15:00	break	Lunch Boxes	14:30	14:30	14:30
15:30	break	Lunch Boxes	15:00	15:00	15:00
16:00	break	Lunch Boxes	15:30	15:30	15:30
16:30	break	Lunch Boxes	16:00	16:00	16:00
17:00	break	Lunch Boxes	16:30	16:30	16:30
17:30	break	Lunch Boxes	17:00	17:00	17:00
18:00	break	Lunch Boxes	Poster session 1 - drinks	Poster session - drinks	19: D. Lanzoni
18:30	break	Lunch Boxes	16: B. Amstutz	S9: New concepts	18:00
19:00	break	Lunch Boxes	S6: Production	18:30	18:30
19:30	break	Lunch Boxes	18:00	18:00	19:00
20:00	break	Lunch Boxes	18:30	18:30	19:30
20:30	break	Lunch Boxes	Debate & Cocktail-buffet. Why and how could be achieved MBE at lower economic and ecological costs?	Riber User Meeting - Banquet	20:00
21:00	break	Lunch Boxes	Movie Theater Le Riounet	Hotel Restaurant Bataclan	20:30
21:30	break	Lunch Boxes	Veeco User Meeting, Le Dandy Club	21:00	21:00
22:00	break	Lunch Boxes	21:30	21:30	21:30
			22:00	22:00	22:00

Specific information for events:

- **Monday evening: Veeco User Meeting**

At the “Dandy” club.

- **Tuesday evening: Debate & Cocktail-buffet.**

“Why and how could be achieved MBE at lower economic and ecological costs?”

At Movie Theater Le Riounet

We are pleased to welcome you to the cinema hall from 19:30 (with drinks and snacks) before we start the debate.

The debate is expected to last for about one hour.

- **Wednesday evening: Riber User Meeting - Banquet**

At Hotel Restaurant Bataclan

There will be a shuttle that brings you from Salle « Roverly » to the restaurant.

Pick-up point: Salle « Roverly »

- 1st departure: 19h20

- 2nd departure: 19h45



It is recommended to take multi-purpose shoes with you.

There is a few hundred meters of walking on the snow from the shuttle drop-off to the restaurant.

- **Shuttle departure to Nice Airport** (pick-up point at movie theater “Le Riounet”):

- 1st departure: 12h30

- 2nd departure: 14h

For any question or specific information
please join our WhatsApp community:





Steering Committee

Régis André	<i>Institut Néel, Grenoble, France</i>
Gavin Bell	<i>University of Warwick, United Kingdom</i>
Vladimir Dubrovskii	<i>Academic University, St. Petersburg, Russia</i>
Martin Eickhoff	<i>University of Bremen, Germany</i>
Lutz Geelhaar	<i>Paul-Drude-Institut, Berlin, Germany</i>
Nicolas Grandjean	<i>EPFL, Lausanne, Switzerland</i>
Mircea Guina	<i>Tampere University of Technology, Finland</i>
Alvaro de Guzman Fernandez	<i>Universidad Politecnica de Madrid, Spain</i>
Mark Hopkinson	<i>University of Sheffield, United Kingdom</i>
Sergey Ivanov	<i>Ioffe Institute, St. Petersburg, Russia</i>
Stefano Sanguinetti	<i>Università degli Studi di Milano-Bicocca, Italy</i>
Fabrice Semond	<i>Université Côte d'Azur, CRHEA, CNRS, Valbonne, France</i>
Czeslaw Skierbiszewski	<i>UNIPRESS, Warsaw, Poland</i>
Lucia Sorba	<i>Istituto Nanoscienze-CNR, Pisa, Italy</i>
Gunther Springholz	<i>Johannes Kepler University, Linz, Austria</i>
Eric Tournié	<i>Université Montpellier 2, France</i>
Shu Min Wang	<i>Chalmers University of Technology, Sweden</i>
Werner Wegscheider	<i>ETH Zurich, Switzerland</i>



Local Organization Committee:

Mohamed Al Khalfioui

Julien Brault

Yvon Cordier

Anne-Marie Cornuet

Minh-Tuan Dau

Christiane Deparis

Jean-Yves Duboz

Maxime Hugues

Hélène Rotella

Fabrice Semond

Stéphane Vézian



Sponsored by:



Invited talk : 23min + 7min questions
 Oral : 15min + 5min questions



Monday, 10.03	
08:00	Registration
08:30	Opening
Session 1 : Antimonides : chairman Eric Tournié	
09:00	Invited talk I1 : MBE growth of mid-IR interband cascade lasers , <u>Laurent Cerutti</u> , IES, University of Montpellier, CNRS, F-34000 Montpellier, France
09:30	S1.1 : Antimonide based heterostructures: MBE growth strategies for infrared applications , <u>Volker Daumer</u> , Fraunhofer Institute for Applied Solid State Physics IAF, Tullastraße 72, 79108 Freiburg, Germany
09:50	S1.2 : InAs/GaInSb W-Quantum Well based Interband Cascade Lasers for Mid Infrared Emission , <u>Matthew Bentley</u> , Department of Physics, Lancaster University, LA1 4YB, UK
10:10	S1.3: Formation of one dimensional nanostructures in the molecular beam epitaxy of antimony triselenide , <u>Piotr Wojnar</u> , Institute of Physics, Polish Academy of Sciences, Warsaw, Poland
10:30	S1.4: Interband cascade lasers emitting below 3 μm grown on GaAs substrate , <u>Maeva Fagot</u> , IES, University of Montpellier, CNRS, F-34000 Montpellier, France
10:50	break
Session 2: Nitrides : Chairman Maxime Hugues	
11:10	Invited talk I2: Properties of ScN and (Sc,Al)N alloys grown by plasma-assisted molecular beam epitaxy , <u>Van Duc Dinh</u> , Paul-Drude-Institut für Festkörperelektronik, 10117 Berlin, Germany
11:40	S2.1: Ammonia-source molecular beam epitaxy of ScAlN/GaN heterostructures for high-power high-frequency applications , <u>Yvon Cordier</u> , Université Côte d'Azur, CNRS, CRHEA, Valbonne, FRANCE
12:00	S2.2: Fabrication of a-plane AlN pseudosubstrates grown by Molecular Beam Epitaxy , <u>Amalia Fernando Saavedra</u> , ISOM and Dept. Ingeniería Electrónica, ETSI Telecomunicación, 28040 Madrid, Spain
12:20	S2.3: Growth of Fully Relaxed (In,Ga)N Pseudo-Substrates by a Two-Step Protocol Without Ex-situ Patterning , <u>Huaide Zhang</u> , Paul-Drude-Institut für Festkörperelektronik, 10117 Berlin, Germany
12:40	S2.4: Epitaxy of self-assembled Al_{1-x}Sc_xN nanowires on metallic TiN: Towards vertical and flexible piezoelectric nanogenerators , <u>Philipp John</u> , Paul-Drude-Institut für Festkörperelektronik, 10117 Berlin, Germany
13:00	Lunch Boxes
16:30	S2.5: Tuning the morphology and structure of In-rich InGaN nanocolumns suitable for biomedical application , <u>Matteo Canciani</u> , University of Milano-Bicocca, Via R. Cozzi, 55, Milano, 20126
16:50	S2.6: New generation of near-UV Laser Diodes by Plasma Assisted MBE , <u>Marcin Siekacz</u> , Institute of High Pressure Physics PAS, ul. Sokolowska 29/37, Warsaw, Poland
17:10	S2.7: AlGaN based Heterostructures grown on h-BN by quasi van der Waals Molecular Beam Epitaxy for Ultra-Violet Light Emitting Diodes , <u>Julien Brault</u> , Université Côte d'Azur, CNRS, CRHEA, Valbonne, 06560, France
Session 3: Oxides : Chairwoman Amalia Patané	
17:30	Invited talk I3: Harnessing Redox Epitaxy for Tailored Functionalities at Oxide Heterointerfaces , <u>Martina Müller</u> , Universität Konstanz, Fachbereich Physik, Germany
18:00	S3.1: κ-Ga₂O₃ thin films and related heterostructures grown by Suboxide-MBE and conventional MBE <u>Alexander Karg</u> , Universität Bremen, Institute of Solid State Physics, Bremen, Germany
18:20	S3.2: Elevated cryogenic permittivity of epitaxial SrTiO₃ films on silicon by stoichiometry and thickness control , <u>Andries Boelen</u> , Imec, B-3001 Leuven, Belgium
18:40	S3.3: Strong optical anisotropy in epitaxial SrO(SrTiO₃)_n Ruddlesden–Popper thin layers <u>Mohamed Bounab</u> , INL-UMR5270/CNRS, Ecole Centrale de Lyon, Ecully (France)
19:00	
20:00	Veeco user meeting



I1: MBE growth of mid-IR interband cascade lasers

M. Fagot,¹ D. A. Diaz-Thomas,¹ A. Gilbert,¹ Y. Rouillard,¹ J.-B. Rodriguez,¹ E. Tournié^{1,2} and
L. Cerutti^{1,*}

¹IES, University of Montpellier, CNRS, F-34000 Montpellier, France ²Institut
Universitaire de France (IUF), F-75005 Paris, France

*E-mail: laurent.cerutti@umontpellier.fr

Interband cascade lasers (ICLs) were first proposed 30 years ago [1] and have since become essential for a wide range of applications within the 3–6 μm wavelength range [2,3] thanks to their operation in continuous wave above room temperature and a power consumption below 0.5 W. However, the active region of ICLs is particularly complex and relies on the alternance of few-monolayers thin layers of binary antimonides and alloys with non-common atoms. Therefore, the molecular beam epitaxy (MBE) growth of ICLs remains challenging. In fact, the extensive group-V intermixing at the interfaces, the different optimal growth temperatures required for the various layers, and the sensitivity to thermal annealing can affect the properties such as threshold current and emission wavelength [4, 5].

However, despite the high sensitivity of ICL to their growth conditions, these structures are surprisingly very tolerant to high crystalline defect densities such as dislocations. In contrast to interband diode lasers, which are very sensitive to dislocations with a rapid degradation of their performance [6], ICL grown on highly mismatched substrates such as GaAs and Si exhibit very similar performances without degradation during ageing [7]. These properties open the way for the direct integration of mid-infrared lasers on GaAs or Si photonic integrated circuits for the development of compact and low-power consumption optical sensors.

In this talk, we will first detail the influence of the growth conditions on the properties of the QWs constituting the ICL active region and then review the growth and performance of ICLs on different substrates emitting between 3.3 and 4.7 μm .

- [1] R.Q. Yang *et al*, Superlattices and Microstructures, **17**, 77 (1995)
- [2] H. Wu *et al*, Sensors and Actuators B: Chemical, **297**, 126753 (2019)
- [3] P. Didier *et al*, Photonics Research, **11**, 582 (2023)
- [4] C. Canedy *et al*, Journal of Vacuum Science and Technology B, **28**, C3G8 (2010)
- [5] D.A. Díaz-Thomas *et al*, Optics Express, **27**, 31425 (2019)
- [6] J. li *et al*, Advanced Photonics Research, **5**, 2300348 (2024)
- [7] M. Fagot *et al*, Optics Express, **32**, 11057 (2024)

This work was partially funded by France 2030 program (EquipEx EXTRA and HYBAT, ANR-11-EQPX-0016, ANR-21-ESRE-0026), the French Occitanie Region (LASIDO project), the French Agency for Defense and Innovation (AID-DGA) and the Banque Publique d'Investissement (Hyquality Project DOS0188007/00).





S1.1 : Antimonide based heterostructures: MBE growth strategies for infrared applications

V. Daumer*, L. Kirste, R. Müller, R. Rehm, A. Vogt, M. Wagstaffe

Fraunhofer Institute for Applied Solid State Physics IAF, Tullastraße 72, 79108

Freiburg, Germany

*volker.daumer@iaf.fraunhofer.de

The 6.1 Å materials family, which includes InAs, GaSb, and AlSb, along with their ternary and quaternary alloys and corresponding type-II superlattices (T2SLs), allows for extensive wavelength tuning across the infrared (IR) spectrum. This versatility in detector design enables the creation of advanced device concepts and high-performance, bandgap-engineered IR technologies suitable for a range of applications. By growing these materials lattice-matched on GaSb substrates through molecular beam epitaxy (MBE), we can effectively combine them to fulfill specific requirements. At Fraunhofer IAF, we harness these materials to design and develop IR detectors and arrays for the extended shortwave infrared (eSWIR), mid-wavelength infrared (MWIR), long-wavelength infrared (LWIR), and various combinations thereof.

Alternatively to extended InGaAs on InP substrate, which suffers from a high dislocation density resulting in limited performance, we have recently developed lattice matched InGaAsSb heterojunction photodiodes on GaSb substrate for the extended short-wavelength infrared (eSWIR) spectral range from 1.7 up to 3.0 μm . Initial results demonstrate first-rate performance with low dark current and high detectivity, which will be presented.

For the thermal infrared in the range from 3 up to 12 μm covering MWIR to LWIR, T2SLs based on InAs/InAsSb and InAs/GaSb are developed. The activities range from basic studies up to pilot line production with detectors at TRL 8. In the latter case reproducibility and process-accompanying quality control are of great importance and will be addressed in this talk.

Recent developments on large-format, Ga-free type-II superlattice (T2SL) detectors are focused on achieving high operating temperatures (HOT) in the mid-wavelength infrared (MWIR) range. Epitaxial growth studies have been conducted to enhance material quality, supported by extensive structural and electro-optical characterization. We are currently involved in several collaborative European projects to demonstrate a non-dependent supply chain for antimony based high quality infrared detectors. With its material expertise, Fraunhofer IAF is a reliable partner for industrial customers without a suitable MBE facility of their own.





S1.2 : InAs/GaInSb W-Quantum Well based Interband Cascade Lasers for Mid Infrared Emission

M. Bentley*¹, P. J. Carrington², Q. Zhuang¹

¹Department of Physics, Lancaster University, LA1 4YB, UK

²School of Engineering, Lancaster University, LA1 4YW, UK

*m.bentley1@lancaster.ac.uk

Mid-infrared emitters, emitting in the 2-5 μm wavelength range, offer a wide range of applications, including; atmospheric pollution monitoring, chemical process control, thermal imaging, and noninvasive medical diagnosis. To fully realise the potential of mid-infrared emitters in these applications a high-performance room temperature tuneable laser diode with low power consumption is required. Interband Cascade Lasers (ICLs) offer the potential for low threshold current densities and as such lowpower while being able to generate continuous wave (CW) high optical power emission at room temperature [1]. W-Quantum Well (WQW) active regions offer great flexibility in band-structure engineering through modifying each QW individually. This provides a two-dimensional density of states for both electrons and holes (high differential gain), high wavefunction overlap despite their type-II band alignment (high gain) and a reduction in Auger recombination. Through combining an ICL with a WQW active region to produce an Interband-Cascade W-Quantum Well Laser (ICWQWL) highperformance room temperature laser diode has been achieved [2].

This work will present details on the growth and characterisation of ICWQWLs grown via molecular beam epitaxy (MBE) at Lancaster University. The WQW consists of InAs electron confinement wells and GaInSb hole confinement wells in a InAs/GaInSb/InAs configuration, which can achieve tuneable emission in the 3.6 μm range close to room temperature [3]. To achieve electron injection and collection InAs/AlSb and AlSb/GaSb superlattices were used respectively. A series of samples were first produced utilizing these WQW, injection, and collection layers, to assess material quality via X-ray diffraction (XRD) measurements and lower temperature photoluminescence (PL). Device fabrication was then performed in Lancaster University's Quantum Technology Centre (QTC) using standard cleanroom processing techniques yielding Fabry-Perot ridge contact laser devices with cavity lengths of 1mm ridge widths of 10, 20, and 50 μm . Initial 1mm cavity length 10 & 20 μm ridge width laser devices yielded threshold currents of 576 & 580mA and peak emission wavelengths of 3.56 & 3.60 μm respectively at room temperature.

- [1] C. S. Kim, M. Kim, J. Abell, W. W. Bewley, C. D. Merritt, C. L. Canedy, I. Vurgasftman and J. R. Meyer, "Mid-infrared distributed-feedback interband cascade lasers with continuous-wave single-mode emission to 80 °C," *Applied Physics Letters*, no. 061104, p. 101, 2012.
- [2] C. L. Canedy, W. W. Bewley, J. R. Lindle, I. Vurgaftman, C. S. Kim, M. Kim and J. R. Meyer, "High-power continuous-wave midinfrared type-II "W" diode lasers," *Applied Physics Letters*, no. 211105, p. 86, 2005.
- [3] G. K. Veerabathran, S. Sprengel, A. Andrejew and M. -C. Amann, "Room-temperature certical-cavity surface-emitting lasers at 4 μm with GaSb-based type-II quantum wells," *Applied Physics Letters*, no. 071104, p. 110, 2017.

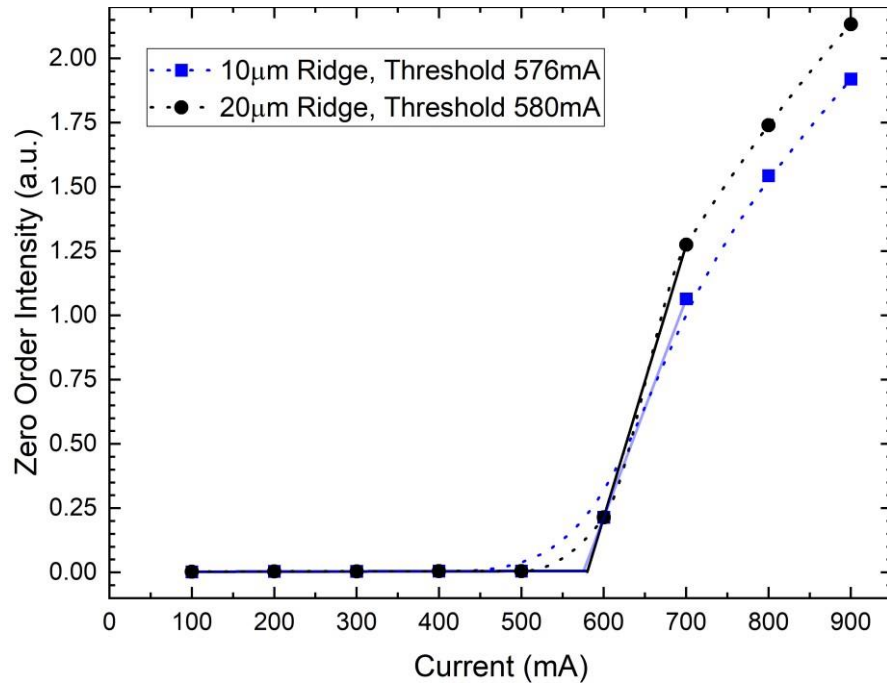


Figure 1: Room temperature current-Intensity characteristics of 1mm cavity length FabryPerot laser with 10 & 20µm ridge contact.

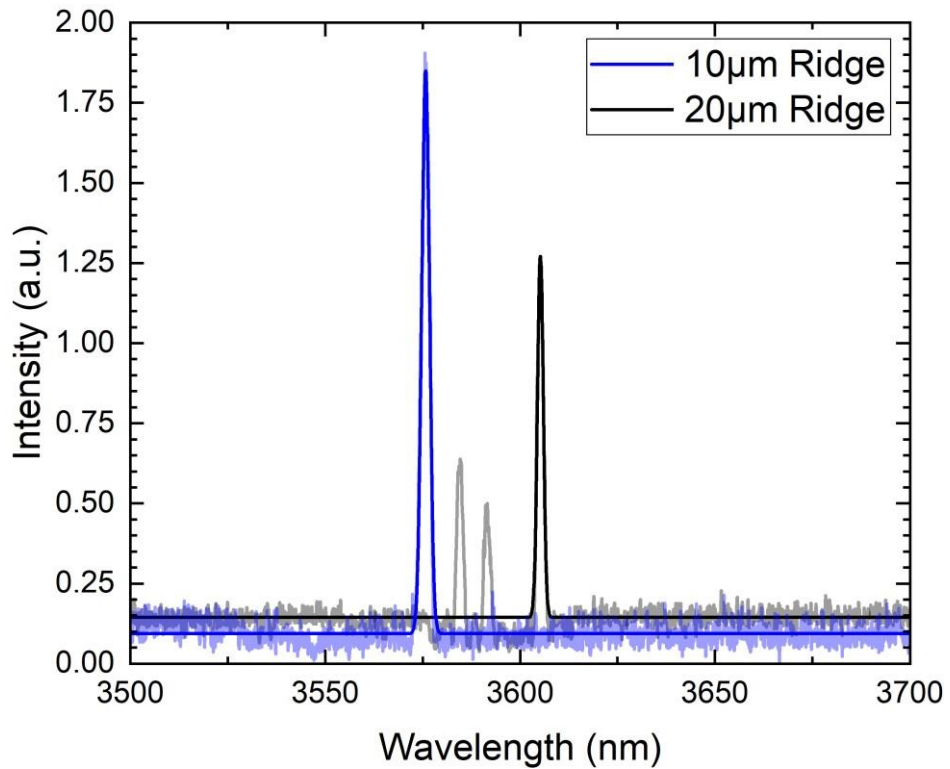


Figure 2: Room temperature electroluminescence (EL) spectra of 1mm cavity length FabryPerot laser with 10 & 20µm ridge contact under 600mA drive current 1% duty cycle.



S1.3: Formation of one dimensional nanostructures in the molecular beam epitaxy of antimony triselenide

P. Wojnar^{1,2*}, S. Chusnutdinow^{1,2}, A. Kaleta¹, M. Aleszkiewicz¹, S. Kret¹, J.Z. Domagala¹, P. Ciepielewski^{1,3}, T. Wojtowicz²

¹ Institute of Physics, Polish Academy of Sciences, Warsaw, Poland

² International Research Centre MagTop, Institute of Physics, Polish Academy of Sciences, Warsaw, Poland

³ Lukaszewicz Res Network, Institute of Microelectronics & Photonics, Warsaw, Poland

*E-mail : wojnar@ifpan.edu.pl

Antimony triselenide belongs to the family of one-dimensional semiconductors, which could be used for downscaling semiconductor channels in transistors even to the limit of a single atomic chain [1]. Its crystal structure consists of one dimensional ribbons held together by weak Se-Se van der Waals interactions. The interest in bulk antimony triselenide has been boosted mainly by its applications in photovoltaic devices leading to the development of Sb₂Se₃-based solar cells with the efficiency exceeding 10% [2]. The advantages of using antimony triselenide for these purposes are the high absorption coefficient, the appropriate value of the band gap that allows the absorption of the solar spectrum, single-phase structure and low toxicity.

In this work, the growth of antimony triselenide by molecular beam epitaxy on GaAs substrates with various crystalline orientations is reported [3]. It is demonstrated that this semiconductor spontaneously forms tiny, monocrystalline, highly anisotropic Sb₂Se₃ nanostripes with the areal density of the order of 10⁹ cm⁻² and the cross-section dimensions of the order of a few nanometers implying a significant contribution of the quantum confinement to their electronic landscape. They lie always in the surface plane and their orientation corresponds to one of <1-10> azimuths of the substrate, Figure 1. With increasing deposition time all three dimensions: the length, the width and the height of these nanostructures increase simultaneously, with the length usually one order of magnitude larger than the two other parameters. The monocrystalline nature of Sb₂Se₃ lattice within a single nanostructure is demonstrated by transmission electron microscopy. Raman scattering and X-ray diffraction confirm its high crystalline quality.

To confirm that there is an epitaxial relationship between the substrate and the nanostripes, and thus the crystalline orientation of the substrate is an important parameter that directly affects the orientation of the nanostripes' growth direction, antimony triselenide is grown on three differently oriented GaAs substrates. It is found that in the case of (111)B oriented GaAs substrate three equivalent growth directions of the nanostripes are preferred corresponding to [1-10], [10-1] and [01-1] crystallographic directions of the substrate. In the case of (100) oriented GaAs substrate, there are only two equivalent growth directions: the [011] and [01-1] directions, while in the case of (110) oriented GaAs substrate, there is only one preferred orientation of the nanostripes: the [1-10] direction.

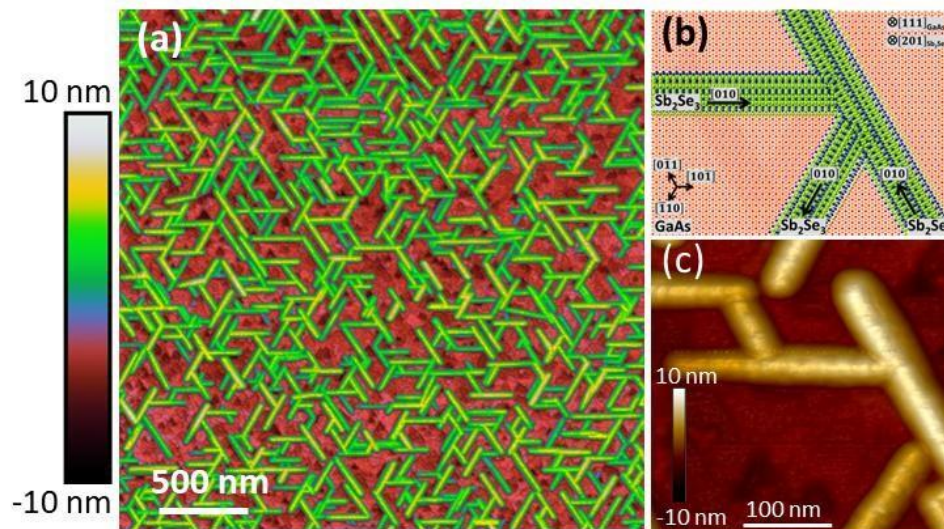


Figure 1 (a) Antimony triselenide nanostructures on (111)B GaAs substrate measured by atomic force microscope (AFM). (b) Crystallographic model illustrating three possible Sb_2Se_3 orientations on (111)B GaAs substrate. One dimensional nano-stripes grow always along $\langle 0\bar{1}1 \rangle$ directions of GaAs substrate (c) Close-up of a AFM image showing the orientation of the nanostructures.

References

- [1] Meng Y, Wang W, Ho JC *One dimensional atomic chains for ultimate scaled electronics ACS Nano* 2022; 16, 13314
- [2] Duan, Z. *et al. Sb₂Se₃ Thin-Film Solar Cells Exceeding 10% Power Conversion Efficiency Enabled by Injection Vapor Deposition Technology Adv. Mater.* 2022, **34**, 2202969
- [3] P. Wojnar *et al. Spontaneous formation of monocrystalline nanostructures in the molecular beam epitaxy of antimony triselenide, Nanoscale* 2024 **16**, 19477-19484

This research was partially supported by the Foundation for Polish Science through the IRA Programme “MagTop” no. FENG.02.01-IP.05-0028/23 co-financed by EU from the funds of Priority 2 of the European Funds for a Smart Economy Program 2021–2027 (FENG)



S1.4: Interband cascade lasers emitting below 3 μm grown on GaAs substrate

M. Fagot,^{1,*} D. A. Diaz-Thomas,¹ Y. Rouillard,¹ J.-B. Rodriguez,¹ E. Tournié^{1,2} and
L. Cerutti¹

¹IES, University of Montpellier, CNRS, F-34000 Montpellier, France ²Institut
Universitaire de France (IUF), F-75005 Paris, France

*E-mail: maeva.fagot@umontpellier.fr

Interband cascade lasers (ICLs) are mainly used in the 3 – 5 μm range, as diode lasers dominate below 3 μm due to their high efficiency and low threshold current. However, beyond 2.5 μm , diode laser performance begins to degrade, due to increased internal losses and non-radiative Auger recombination, causing an exponential increase in threshold current density [1]. GaSb-based laser diodes grown on Si have recently shown promising threshold currents, only three times higher than on native substrates [2], but suffer from rapid degradation, limiting their reliability. ICLs, on the other hand, are highly tolerant to dislocations within their operating window [3,4] and have demonstrated an extrapolated mean time of failure exceeding 35 years. While much efforts have been focused on extending ICL performance at longer wavelengths [5], little has been done to explore their potential at shorter wavelengths. Extending the operating range of ICLs below 3 μm could bridge the performance gap between 2.5 and 3 μm , leveraging the unique advantages of their design to improve laser technology in this spectral range.

This work presents our latest results on type-II ICLs designed to emit at 2.7 μm , grown on both GaSb and GaAs substrates. The laser structure includes a five-stage active region, situated between two 350 nm separate confinement heterostructures and two AlSb/InAs superlattice claddings. The ICL structure was first grown on GaSb to assess performance, then on GaAs substrate for comparison. Laser ridges are fabricated using standard photolithography process, creating 8 μm -wide and 2 mm-long cavities with uncoated facets. The light-current-voltage (L-I-V) characteristics of the lasers, taken under pulsed operation (DC 1%, 10 kHz) at 20°C and presented Figure 1, show a slightly higher threshold current for GaAs (100 mA vs 80 mA for GaSb) while maintaining a similar slope efficiency ($\sim 130 \text{ mW/A}$ for both GaSb and GaAs). The ICL on GaAs, however, has a higher series resistance (5.9 Ω vs 2.7 Ω for GaSb). Spectra (shown in insert) reveal emission between 2.8 and 2.9 μm for both structures, with a slight shift in the GaAs device likely caused by the higher As content in its active region. Aging tests will be conducted to evaluate the laser durability at this wavelength. These findings open the way for efficient devices on Si below 3 μm .

[1] K. S. Gadedjisso-Tossou *et al*, *Semicond. Sci. Technol.* **28**, 015015 (2012).

[2] A. Remis *et al*, *J. Appl. Phys.* **133**, 093103 (2023).

[3] L. Cerutti *et al*, *Optica* **8**, 1397 (2021).

[4] M. Fagot *et al*, in *The 23rd International Conference on Molecular Beam Epitaxy*, Matsue, Japan (2024).

[5] J. A. Massengale *et al*, *Semicond. Sci. Technol.* **38**, 025009 (2022).

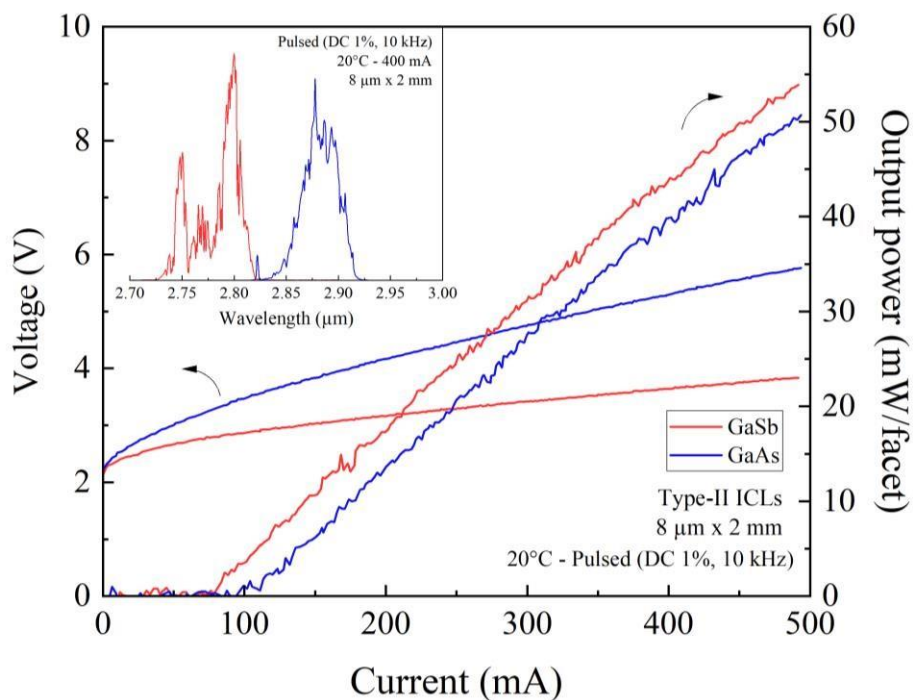


Figure 1: Pulsed L-I-V curves for 8 μm x 2 mm type-II ICLs grown on GaSb (red) and GaAs (blue) substrates.

Insert: Emission spectra of ICLs measured under pulsed operation at 20°C with an injection current of 400 mA.

This work was partially funded by France 2030 program (EquipEx EXTRA and HYBAT, ANR-11-EQPX-0016, ANR-21-ESRE-0026), the French Occitanie Region (LASIDO project), the French Agency for Defense and Innovation (AID-DGA) and the Banque Publique d'Investissement (Hyquality Project DOS0188007/00).



I2: Properties of ScN and (Sc,Al)N alloys grown by plasma-assisted molecular beam epitaxy

**D. V. Dinh^{1,*}, M. Yuan¹, J. Lähnemann¹, F. Peiris², S. Mandal³, O. A. Williams³, Z. Chen⁴,
P. V. Santos¹, L. Geelhaar¹, O. Brandt¹**

⁽¹⁾ Paul-Drude-Institut für Festkörperelektronik, 10117 Berlin, Germany.

⁽²⁾ Department of Physics, Kenyon College, Gambier, 43022 Ohio, United States.

⁽³⁾ School of Physics and Astronomy, Cardiff University, Cardiff CF24 3AA, United Kingdom

⁽⁴⁾ Huawei Technologies Co Ltd, Ottawa, Ontario, Canada

*Corresponding author email: dinh@pdi-berlin.de

In this work, we review our recent studies on the plasma-assisted molecular beam epitaxy of ScN, a group-IIIb transition-metal nitride, as well as its alloys with conventional group-IIIa wurtzite nitrides, focusing on the formation of wurtzite (Sc,Al)N.

Although ScN was first synthesized over five decades ago, its electrical and optical properties remain not fully understood. Regardless the growth method, ScN has usually been found to be heavily doped, making it a highly degenerate semiconductor. The uncontrolled doping and its consequences hinder the understanding of the intrinsic electrical and optical properties of ScN, and also impede many of its potential applications. We have recently shown that lattice-matched ScN layers on wurtzite GaN can be nondegenerate with comparatively low electron densities and high electron mobilities. Temperature-dependent Hall-effect measurements provide insights into the dominant scattering mechanisms [1].

Wurtzite (Sc,Al)N alloys are of great interest due to their strong piezoelectric response. Despite numerous studies, their lattice constants remain controversial. By optimizing the growth conditions of (Sc,Al)N on GaN, we were able to produce thick layers that allowed us to accurately measure their lattice constants. We found that Sc_{0.1}Al_{0.9}N layers are lattice-matched to GaN. This knowledge has supported the development of (Sc,Al)N on polycrystalline diamond substrates for surface-acoustic-wave devices [2].

[1] D. V. Dinh, O. Brandt, Phys. Rev. Appl. 22, 014067 (2024).

[2] M. Yuan, D. V. Dinh, S. Mandal, O. A. Williams, Z. Chen, O. Brandt, P. V. Santos, J. Phys. D: Appl. Phys. 57, 495103 (2024).





S2.1: Ammonia-source molecular beam epitaxy of ScAlN/GaN heterostructures for high-power high-frequency applications

C. Elias, S. Chenot, M. Nemoz, F. Bartoli, A. Courville,

V. Gallardo Mödinger, P. Vennéguès, M. Hugues, Y. Cordier*

¹Université Côte d'Azur, CNRS, CRHEA, Valbonne, FRANCE

*yvon.cordier@crhea.cnrs.fr

ScAlN is a wide bandgap semiconductor with large piezoelectric and spontaneous polarization coefficients ensuring a very high charge density at the interface with GaN, which makes it a promising barrier layer for HEMTs in view of power switching and RF/mm-wave power amplifier applications. Furthermore, it can benefit ferroelectric properties opening the way for new applications. The development of the epitaxy of this alloy has started with plasma-assisted MBE, followed by MOVPE. More recently, we have demonstrated the feasibility of the growth with ammonia source MBE under nitrogen-rich regime and an optimum temperature was identified for the growth of $\text{Sc}_x\text{Al}_{1-x}\text{N}$ barriers quasi-lattice matched on GaN ($x \sim 14\%$) [1]. The advantages of this growth regime in terms of growth rate, alloy composition and homogeneity [2] have been demonstrated. HEMT heterostructures have been grown on GaN-on-Si and GaN-on-Sapphire templates, demonstrating two-dimensional electron gases (2DEGs) with charge densities N_s -cv ranging from 2×10^{13} to $4 \times 10^{13}/\text{cm}^2$ depending on the nominal thickness of the ScAlN barrier which was varied from 5 nm to 25 nm. Functional transistors with 9 μm source-drain spacing have been fabricated on these heterostructures. Drain current density exceeds 700 mA/mm on 10 nm barrier and 1 A/mm on 25 nm barrier (twice the one obtained on our standard AlGaIn/GaN devices) while a limited gate leakage current could be observed up to a drain voltage of 100 V. This result is of primary importance as the gate leakage through the ScAlN barrier has been reported as a major concern [3]. However, the surface of ScAlN rapidly oxidizes and suffers a lack of stability during the device process. For this reason, in-situ grown cap layers such as GaN and AlN have been studied. According to Hall effect measurements, the room-temperature electron mobility in the 2DEG of most of the samples ranges from 500 to about 1000 $\text{cm}^2/\text{V}\cdot\text{s}$ depending on the quality of the interface between ScAlN and GaN which features a 1-2 nm AlN exclusion layer. The typical 2DEG sheet resistances range between 240 and 300 Ω/sq . In absence of the AlN exclusion layer, the resistance rises to 785 Ω/sq . Furthermore, optimizations of the growth of a 10 nm barrier HEMT lead to a sheet resistance of 210 Ω/sq , a promising result for the fabrication of high-performance transistors. This work is partly supported by the French technology facility network RENATECH, the French National Research Agency (ANR) through the 'Investissements d'Avenir' program GaNeX (ANR-11LABX-0014 and the project TWINS (ANR-23-CE51-0011) as well as ECSEL JU project GaN4AP under Grant Agreement No. 101007310.

[1] C. Elias et al, Appl. Phys. Lett. Materials 11, 031105 (2023).

[2] S. Ndiaye et al, Appl. Phys. Lett. 123, 162102 (2023). [3] P. Döring et al, Appl. Phys. Lett. 123, 032101 (2023).

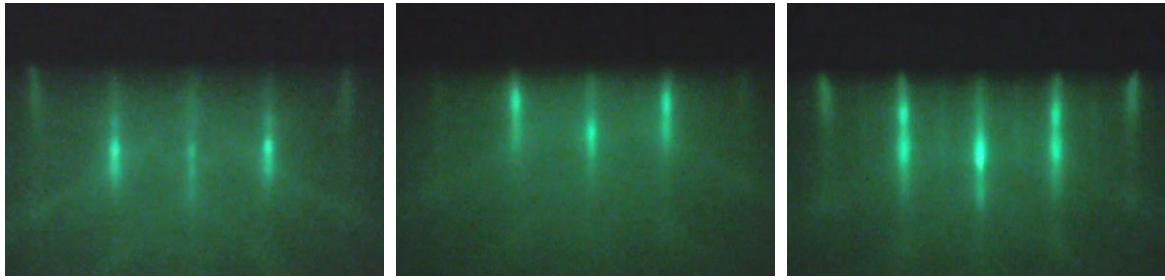


Fig. 1: RHEED patterns of the surface of ScAlN (left) capped with AlN (centre) or GaN (right).

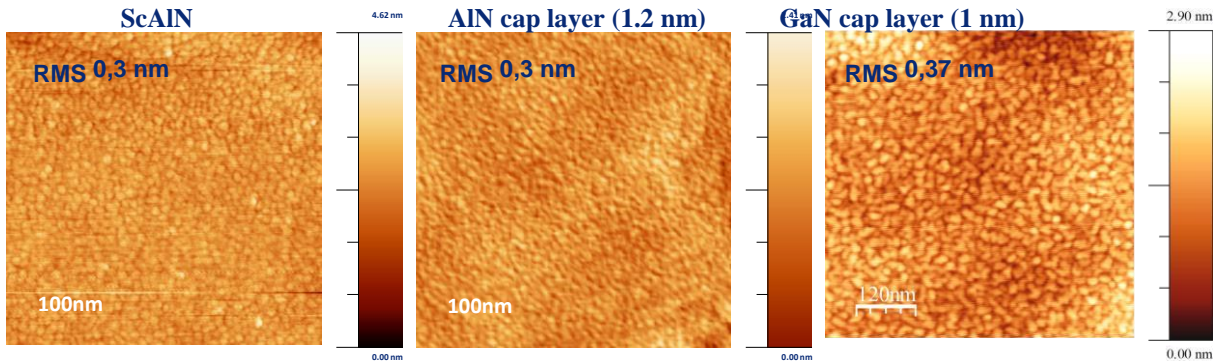


Fig. 2: Tapping mode atomic force microscopy images showing the morphology of ScAlN (left) capped with AlN (centre) or GaN (right).

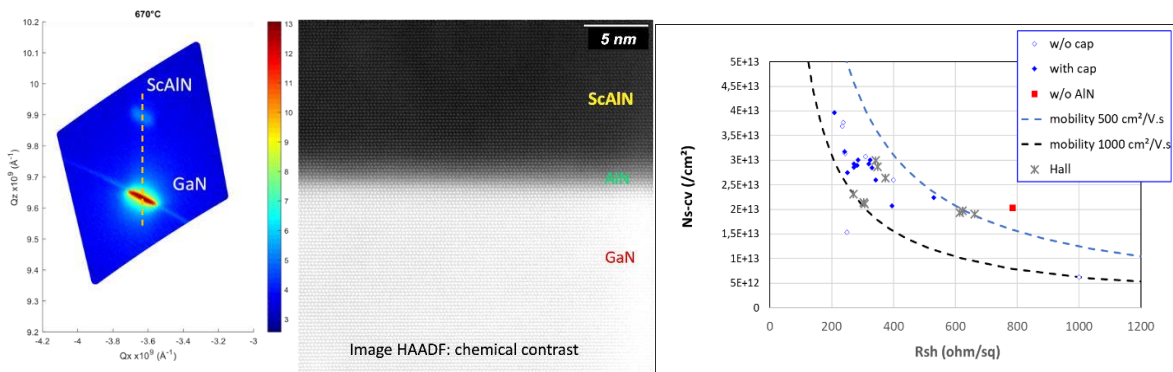


Fig. 3: Left: X-ray diffraction reciprocal space map around the (10 $\bar{1}$ 5) node showing the in-plane lattice matching of ScAlN with GaN. Centre: high-resolution cross-section transmission electron microscopy view of the HEMT interface. Right: transport properties of the ScAlN/GaN HEMTs.

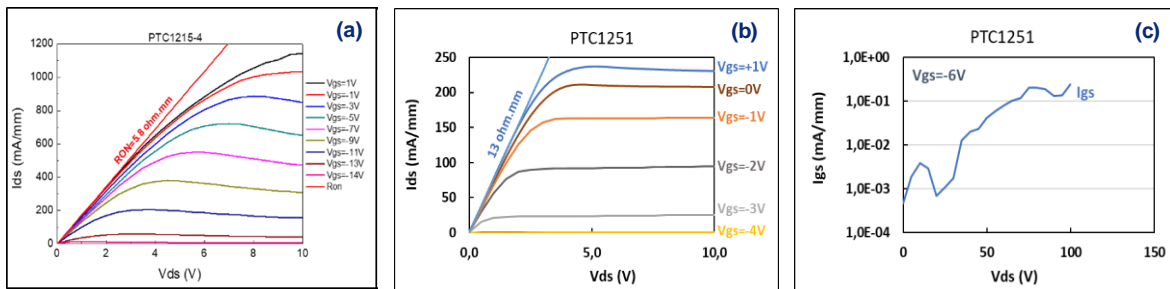


Fig. 4: DC output characteristics $I_{ds}(V_{ds}, V_{gs})$ of 2 μ m gate transistors with 9 μ m source-drain spacing fabricated on the ScAlN/GaN HEMT grown on Silicon with (a) a 25 nm barrier and (b) a 10 nm barrier. (c) Gate leakage of the 10 nm barrier HEMT in 3-terminal off-state configuration.



S2.2: Fabrication of a-plane AlN pseudosubstrates grown by Molecular Beam Epitaxy

A. Fernando Saavedra,¹ A. Bengoechea-Encabo,² M. Xie,² M. A. Sánchez-García,¹ and E. Calleja¹

¹ISOM and Dept. Ingeniería Electrónica, ETSI Telecomunicación, Universidad Politécnica de Madrid, Av. Complutense 30, Ciudad Universitaria, 28040 Madrid, Spain, ²Tianrui Semiconductor Materials (Suzhou) Ltd.co., the Third Zone of Datong rd. 20, Suzhou New District, 215151 Suzhou, P.R. China.

e-mail: amalia.fsaavedra@fundetel.upm.es

High quality native AlN substrates used to develop ultraviolet (UV) and deep UV (DUV) emitters, such as light emitting diodes (LEDs) and laser diodes (LDs)^{1,2} are an extremely successful choice. Unfortunately, suitable low-cost, large-area AlN native substrates are not available, and AlN is typically grown hetero-epitaxially on substrates like silicon, sapphire or SiC. These approaches generate a high density of threading dislocation (TDs)^{3,4} which is detrimental to electron mobility and reduces the quantum efficiency of UV emitters⁵. In addition, the strong internal electric field, present along the polar direction, may be detrimental to device performance because it modifies the carrier distribution and potential profile in Quantum Wells (QWs) and favors the emission energy shift by screening effects. These negative effects can be avoided by growing devices on non-polar AlN buffers.

This work reports on the growth by Plasma Assisted Molecular Beam Epitaxy (PAMBE) of a-plane AlN pseudo-substrates on r-sapphire by controlled coalescence of ordered AlN nanocrystals (etched nanopillars, NPs) following three steps: i) growth of a-plane AlN buffer on r-sapphire, ii) etching down of the AlN buffer to obtain an array of ordered AlN NPs, and iii) AlN overgrowth until full coalescence.

Prior the growth of the a-plane AlN buffer, the r-sapphire substrate was nitridated for 30 min with a N flux of 7.5 nm/min at 860 °C. AlN growth was then performed at 860 °C under nominal fluxes of 7.9 nm/min and 8.3 nm/min for Al and N respectively. After that, a square pattern of ordered Ni dots was defined by e-beam lithography on the AlN buffer. Etching by inductively coupled plasma with a Cl/Ar mixture resulted in an ordered array of AlN NPs. Finally, PAMBE overgrowth on the AlN NPs arrays was performed with the same nominal fluxes for Al and N (i.e. 3 nm/min).

Two samples were prepared with areas having NPs with different pitch (350, 450 nm) and diameters (110 nm – 200 nm). The samples were analyzed by Scanning Electron Microscopy, Atomic Force Microscopy and Transmission Electron Microscopy to study the AlN coalescence into a continuous film and how the different geometries and sizes of the NPs affect the quality of the final AlN layer. Previous work on *m*-plane GaN⁶ using similar approach shows a preferential growth rate on the NPs along the *c*-direction and a significant reduction of extended defect density in the coalesced film compared to the initial GaN buffer.

[1] Y. Taniyasu, M. Kasu, T. Makimoto, *Nature*, **2006**, 441, 325-328.

[2] A. Khan, K. Balakrishnan, T. Katona, *Nature Photonics*, **2008**, 2, 77-84.

[3] N. Teraguchi, A. Suzuki, Y. Saito, T. Yamaguchi, T. Araki, Y. Nanishi, *J. Cryst. Growth*, **2001**, 230, 392397.

[4] N. Onojima, J. Suda, H. Matsunami, *Appl. Phys. Lett.*, **2002**, 80, 76-78.

[5] M. Kneissl, T. Kolbe, C. Chua, V. Kueller, N. Lobo, J. Stellmach, A. Knauer, H. Rodriguez, S. Einfeldt, Z. Yang, N.M. Johnson, M. Weyers, *Semicond. Sci. & Technol.*, **2011**, 26, 014036.

[6] A. Fernando-Saavedra, S. Albert, A. Bengoechea-Encabo, A. Trampert, M. Xie, M.A. Sánchez-García, E. Calleja, *J. Cryst. Growth*, **2023**, 617, 127272.





S2.3: Growth of Fully Relaxed (In,Ga)N Pseudo-Substrates by a Two-Step Protocol Without Ex-situ Patterning

Huaide Zhang*, Jingxuan Kang, Oliver Brandt, Lutz Geelhaar

Paul-Drude-Institut für Festkörperelektronik, Leibniz-Institut im Forschungsverbund Berlin e.V.,
Hausvogteiplatz 5-7, 10117, Berlin, Germany

*zhang@pdi-berlin.de

The band gap of (In,Ga)N spans the entire visible spectrum. This semiconductor is thus a promising candidate for the fabrication of red-green-blue light emitting diodes (LEDs) from one and the same material class. Blue and green (In,Ga)N LEDs have been commercialized, but the quantum efficiency of red (In,Ga)N LEDs is insufficient for practical purposes. This limitation arises from the large lattice mismatch between the active region with increased In content of around 40% and GaN. The large strain in the QW results in large internal fields, reducing the recombination rate. Also, certain point defects (such as Ca) become increasingly active in nonradiative recombination. We note that in general bulk group-III nitride substrates are expensive, and the long-standing success of blue (In,Ga)N LEDs is a result of mature procedures for the growth of GaN template layers on sapphire and SiC substrates.

In this study, we present a simple yet effective two-step growth protocol without patterning that results in essentially fully relaxed (In,Ga)N pseudo-substrates on GaN templates. The key concept is to grow by plasma-assisted molecular beam epitaxy first a rough (In,Ga)N layer under N-rich conditions and second proceed with overgrowth under metal-rich conditions that leads to a smooth surface.

In detail, the first (In,Ga)N layer is grown at 500 °C under N-rich conditions for 30 min. These growth conditions lead to a spotty reflection high energy electron diffraction (RHEED) pattern typical for a rough surface. The In content and degree of strain relaxation are determined from x-ray diffraction reciprocal space maps (RSM). The In content varies between samples in the range 25 to 42%, and the relaxation degree reaches up to 95%. The thickness of the layer with In content 42% and relaxation degree 95% as measured by scanning electron microscopy is about 200 nm. Characterization by atomic force microscopy (AFM) reveals a surface with a root mean square (RMS) roughness of 4.4 nm in an area of $2 \times 2 \mu\text{m}^2$.

That N-rich growth leads to a rough surface for group-III nitrides is well known. The main innovation of this study is the demonstration that the surface can be smoothed again in the case of (In,Ga)N. To this end, (In,Ga)N overgrowth is carried out at 550 °C under metal-rich conditions for 60 min. The RHEED pattern exhibits streaks with undulations in intensity, and AFM analysis shows a surface morphology with a clearly reduced RMS roughness of 1.8 nm. These properties are achieved for an In content of $\approx 30\%$ and a strain relaxation degree of $\approx 80\%$. A layer with a lower In content of 24% and similar relaxation degree and surface roughness is obtained by reducing the In flux during growth and increasing the substrate temperature. The photoluminescence spectra acquired at room temperature exhibit a single emission band centered at 574 nm and 543 nm, respectively. The full widths at half maximum (FWHM) are 53 nm (225 meV) and 28 nm (118 meV), respectively. The latter value indicates excellent homogeneity, and the increase compared to a reference (In,Ga)N sample emitting in the blue spectral range and grown directly on a GaN template is related to more pronounced alloy disorder for higher In content.

In conclusion, we have demonstrated the growth of (In,Ga)N layers with high In content up to 42%, smooth surface, and essentially full strain relaxation. These properties stand out in comparison to other approaches for the fabrication of pseudo-substrates, and the facile two-step growth protocol can easily be scaled up. Therefore, this

advancement represents a critical step toward the realization of high-performance red (In,Ga)N LEDs for next-generation micro-LED applications.

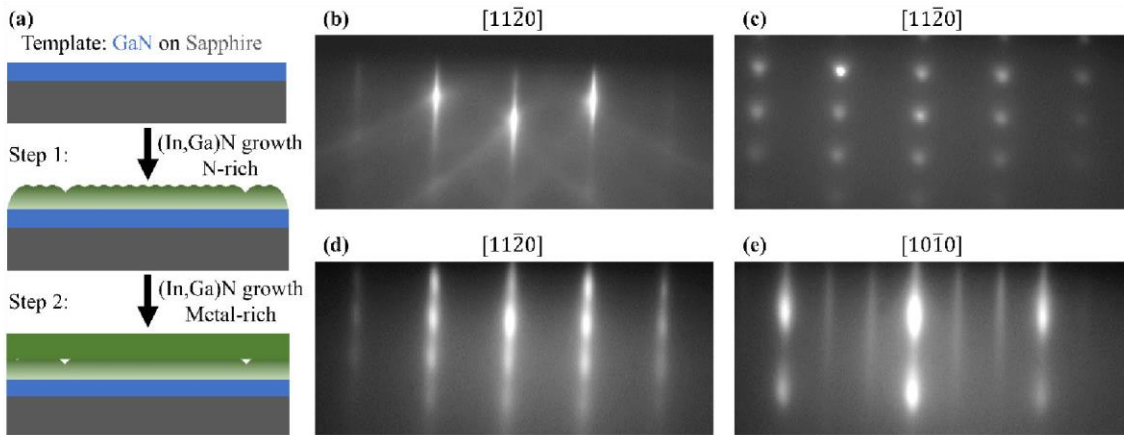


Figure 1: (a) Schematic of the two-step growth protocol for the fabrication of relaxed (In,Ga)N pseudo-substrates. RHEED patterns of (b) the GaN(0001) template along the $[11\bar{2}0]$ direction, (c) the first (In,Ga)N layer along the $[11\bar{2}0]$ direction, and the second (In,Ga)N layer along the (d) $[11\bar{2}0]$ and (e) $[10\bar{1}0]$ directions. The spotty and streaky patterns show the surface smoothing during overgrowth. The $(\sqrt{3} \times \sqrt{3})R30^\circ$ surface reconstruction seen in (e) reflects that growth was carried out with an In adlayer at the growth front.

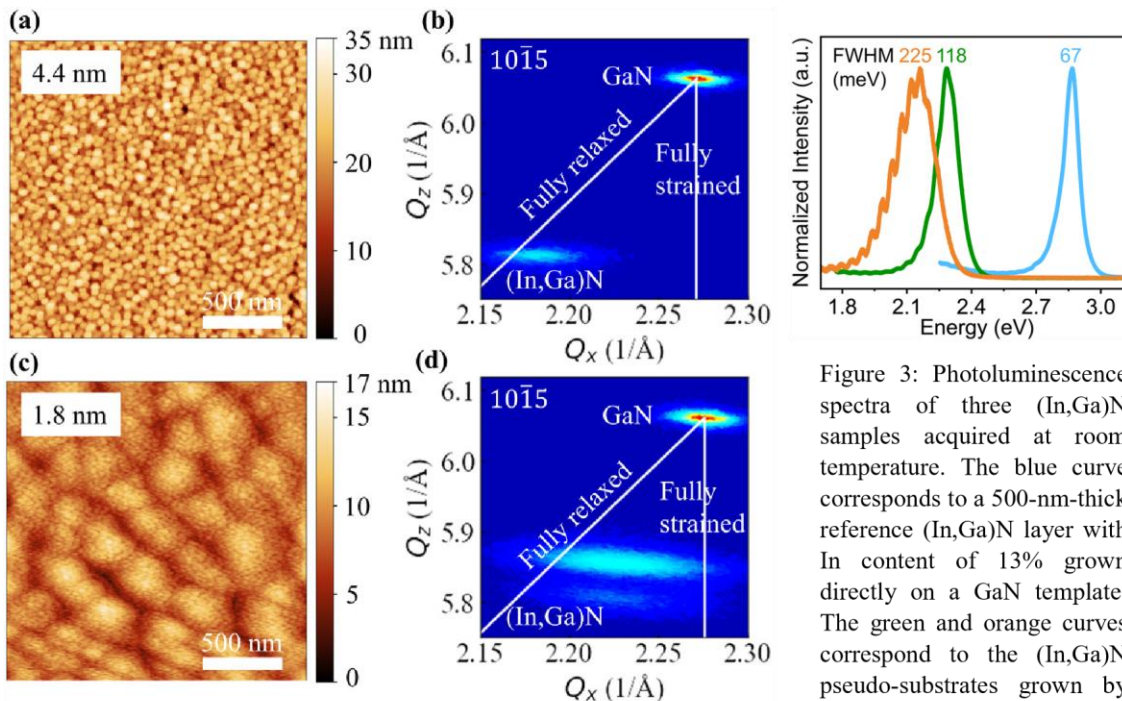


Figure 2: (a) AFM topograph of the first (In,Ga)N layer with a RMS roughness of 4.4 nm. (b) RSM of the first (In,Ga)N layer around the $10\bar{1}5$ reflection revealing a strain relaxation degree of 95% and In content of 42%. (c) AFM topograph of the second (In,Ga)N layer with a RMS roughness of 1.8 nm. (d) RSM of both the first and second (In,Ga)N layer around the $10\bar{1}5$ reflection indicating a strain relaxation degree of 80% and In content of 30%.

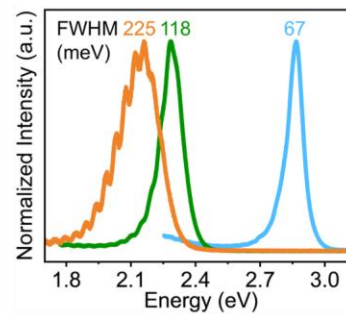


Figure 3: Photoluminescence spectra of three (In,Ga)N samples acquired at room temperature. The blue curve corresponds to a 500-nm-thick reference (In,Ga)N layer with In content of 13% grown directly on a GaN template. The green and orange curves correspond to the (In,Ga)N pseudo-substrates grown by the two-step protocol with In contents of 24 and 30% in the second layer, respectively. The text labels indicate the FWHMs of the spectra.



S2.4: Epitaxy of self-assembled $\text{Al}_{1-x}\text{Sc}_x\text{N}$ nanowires on metallic TiN: Towards vertical and flexible piezoelectric nanogenerators

P. John,^{1*} A. Notarangelo,¹ H. Tornatzky,¹ A. F. Campbell,¹ R. Songmuang,² N. Buatip,²
I. Florea,³ P. Vennéguès,³ J. Lähnemann,¹ A. Trampert,¹ T. Auzelle,¹ O.
Brandt,¹ and L. Geelhaar¹

¹Paul-Drude-Institut für Festkörperelektronik,

Leibniz-Institut im Forschungsverbund Berlin e.V., 10117 Berlin, Germany

²Université Grenoble Alpes, CNRS, Grenoble INP, Institut Néel, 38000 Grenoble, France ³Université
Côte d'Azur, CRHEA, CNRS, 06905 Sophia-Antipolis Cedex, France

*john@pdi-berlin.de

The incorporation of Sc into the hexagonal wurtzite lattice of AlN is an effective way to extend the functionalities of the group III-nitride semiconductor family. Ternary $\text{Al}_{1-x}\text{Sc}_x\text{N}$ exhibits giant piezoelectricity, ferroelectricity and exciting non-linear optical properties, which are already utilized in novel devices. New functionalities, such as flexibility and enhanced piezoelectric response may arise from the growth in the form of nanostructures.

In this work, we demonstrate the molecular beam epitaxy of ternary $\text{Al}_{1-x}\text{Sc}_x\text{N}$ nanowires. We start with the previously established, self-assembled growth of AlN nanowire stems on metallic TiN thin films [1], which are subsequently overgrown with ternary $\text{Al}_{1-x}\text{Sc}_x\text{N}$ varying both substrate temperature and metal flux ratio. At high substrate temperatures (> 800 °C), a phase separation of the ternary $\text{Al}_{1-x}\text{Sc}_x\text{N}$ is observed, accompanied by nanowire branching and Raman signals characteristic for cubic rock-salt ScN. In contrast, moderate substrate temperatures below 800 °C favor the formation of wurtzite $\text{Al}_{1-x}\text{Sc}_x\text{N}$ nanowires, with a morphology characterized by inverse nanowire tapering. Still, Sc is homogeneously incorporated with concentrations of $0 \leq x \leq 0.35$, as investigated by energy-dispersive x-ray spectroscopy (EDX) and scanning transmission electron microscopy (STEM). The E_2^{high} and $A_1(\text{TO})$ Raman modes of AlN are broadened upon Sc-incorporation, suggesting wire-to-wire inhomogeneities and/or disorder in the $\text{Al}_{1-x}\text{Sc}_x\text{N}$ alloy. Their consistent red-shift observed as a function of Sc concentration confirms its enhanced incorporation into the wurtzite lattice.

Pure wurtzite $\text{Al}_{1-x}\text{Sc}_x\text{N}$ nanowires are processed into vertical piezoelectric nanogenerators, for which the metallic TiN substrate serves as bottom electrode. The output response resulting from a sinusoidal force excitation indicates metal-polarity and is compared to that of AlN and GaN nanowirebased reference samples [2].

The growth of wurtzite $\text{Al}_{1-x}\text{Sc}_x\text{N}$ nanowires on conductive substrates and the demonstration of first nanogenerators paves the way towards the development of flexible piezoelectric energy harvesters with improved device performance.

[1] P. John *et al.*, *Nanotechnology* **34**, 465605 (2023).

[2] N. Buatip *et al.*, *ACS Appl. Nano Mater.* **7**, 15798 (2024).

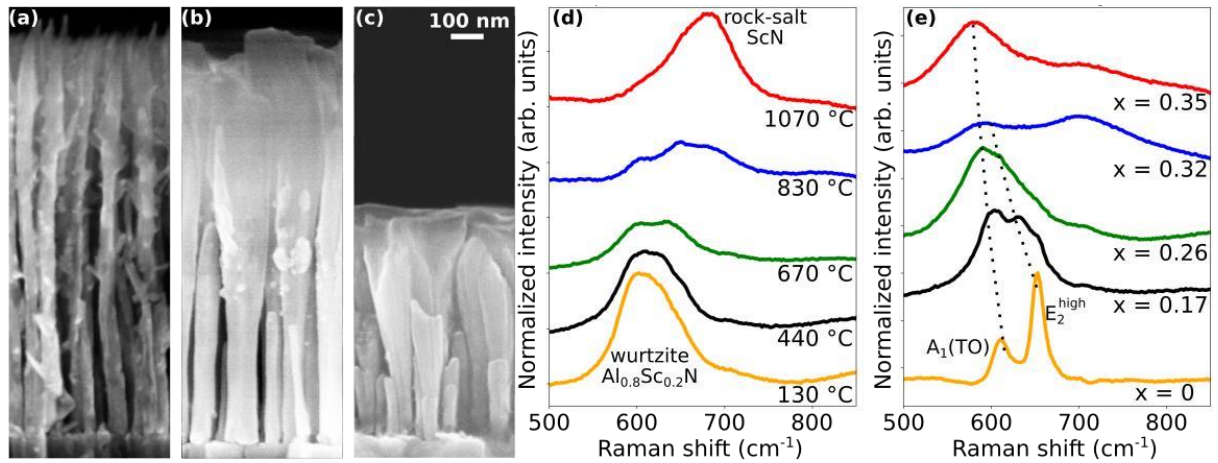


Fig. 1: Cross-section secondary electron micrographs of $\text{Al}_{0.8}\text{Sc}_{0.2}\text{N}/\text{AlN}$ nanowires grown at (a) 1150 °C, (b) 830 °C and (c) 440 °C. The scale bar is identical for all micrographs. Raman spectra of (d) $\text{Al}_{0.8}\text{Sc}_{0.2}\text{N}/\text{AlN}$ nanowires grown at different temperatures and (e) $\text{Al}_{1-x}\text{Sc}_x\text{N}/\text{AlN}$ nanowires with different Sc concentrations grown at 440 °C. The spectra are taken at room temperature with a 473 nm excitation laser.

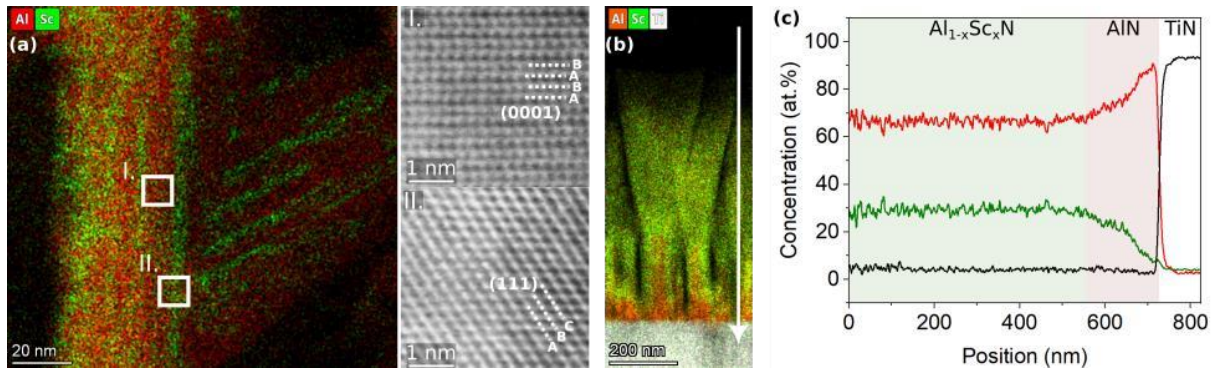


Fig. 2: (a) STEM-EDX map of a branched $\text{Al}_{0.8}\text{Sc}_{0.2}\text{N}/\text{AlN}$ nanowire grown at 1150 °C, indicating regions of Al-rich wurtzite (inset I) and Sc-rich rock-salt phases (inset II). (b) STEM-EDX map of an inversely tapered $\text{Al}_{0.74}\text{Sc}_{0.26}\text{N}/\text{AlN}$ nanowires, indicating homogeneous Sc incorporation. (c) STEM-EDX profile along the direction indicated by the white arrow in (b) and confirming the nominal Sc concentration.

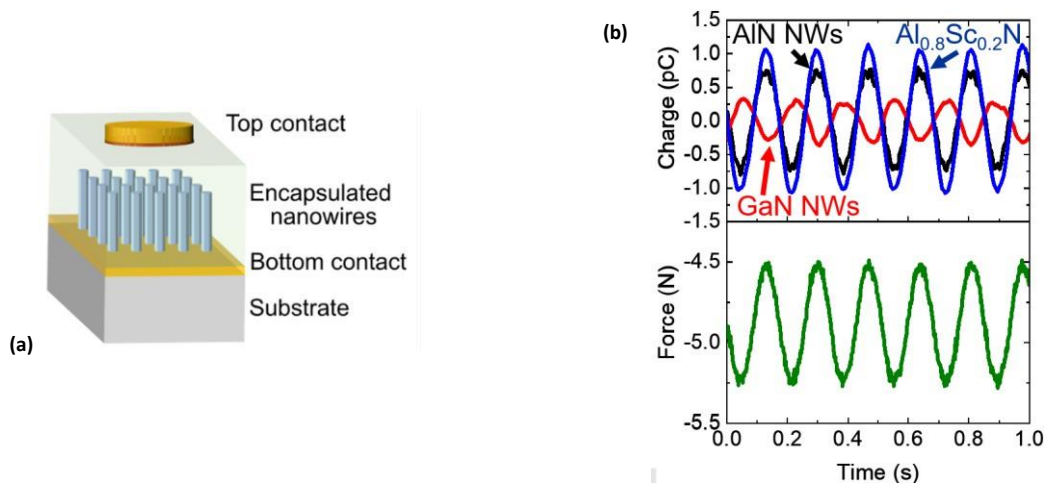


Fig. 3: (a) Schematic of a vertical nanowire-based piezoelectric generator. (b) Charge output of an $\text{Al}_{0.8}\text{Sc}_{0.2}\text{N}/\text{AlN}$ nanowire generator in response to a sinusoidal force excitation, compared to GaN and AlN reference devices.



S2.5: Tuning the morphology and structure of In-rich InGaN nanocolumns suitable for biomedical application

Matteo Canciani*, Oksana Koplak, Stefano Vichi, Sergio Bietti and Stefano Sanguinetti

University of Milano-Bicocca, Via R. Cozzi, 55, Milano, 20126, e-mail:

**m.canciani2@campus.unimib.it*

Developing wearable transdermal biosensors for real-time health monitoring is a very attractive and promising field of research and medical application. Among the materials studied, InGaN heterostructures stand out for their chemical stability, biocompatibility, low cytotoxicity, and high carrier mobility. Biosensors based on InN/InGaN quantum dots (QDs) exhibit twice the sensitivity and five times faster response compared to InN thin films, surpassing the classical Nernstian limit by leveraging the super-Nernstian behavior enabled by InN QD surface nanostructuring¹. The study presented analyzes the nanostructured InGaN growth made using Plasma-Assisted Molecular Beam Epitaxy (PA-MBE) on Si (111) substrates. The significant lattice mismatch is used to promote a nanocolumnar morphology, while achieving high indium content, critical for optimizing surface energy states and enabling ohmic contact, requires low substrate temperatures to prevent indium desorption and InN decomposition².

Accurate structural analysis, detailed surface morphology, and key growth parameters as In/Ga ratio, substrate temperature, and III/V flux ratio, were carried out using X-Ray Diffraction (XRD) and Atomic Force Microscopy (AFM). To monitor the individual nanocolumns' chemical composition and local structure, Energy Dispersive X-ray Spectroscopy (EDX), Electron backscatter diffraction (EBSD), and Transmission Electron Microscopy (TEM) measurements were performed, confirming the high indium content (60%) with nanocolumns exhibiting excellent epitaxial alignment along the (001) plane with a negligible misorientation of only 1° (Figure 1b). Samples with elevated indium levels displayed larger column diameters, correlating with indium higher thermal diffusion coefficient (Figure 1c). The mechanisms governing the growth and geometry of InGaN nanocolumns were investigated through scanning electron microscopy (SEM), examining both top and side views (Figure 1). SEM observations also uncovered fascinating phenomena during nanocolumn vertical growth, contributing to the optimized design and enhanced performance of biosensor materials.

This study is fundamental for enabling a comprehensive understanding of the growth mechanisms of InGaN nanocrystals (NCs) on silicon (Si) substrates. It establishes a foundation for optimizing the crystal quality, dealing with the formation of different crystal structures (i.e. wurtzite and zinc-blende) and the size of the nanocrystals, which is crucial for future QDs depositions. Moreover, it represents a significant step in the optics of assembly of the biosensor and in testing its overall performance.

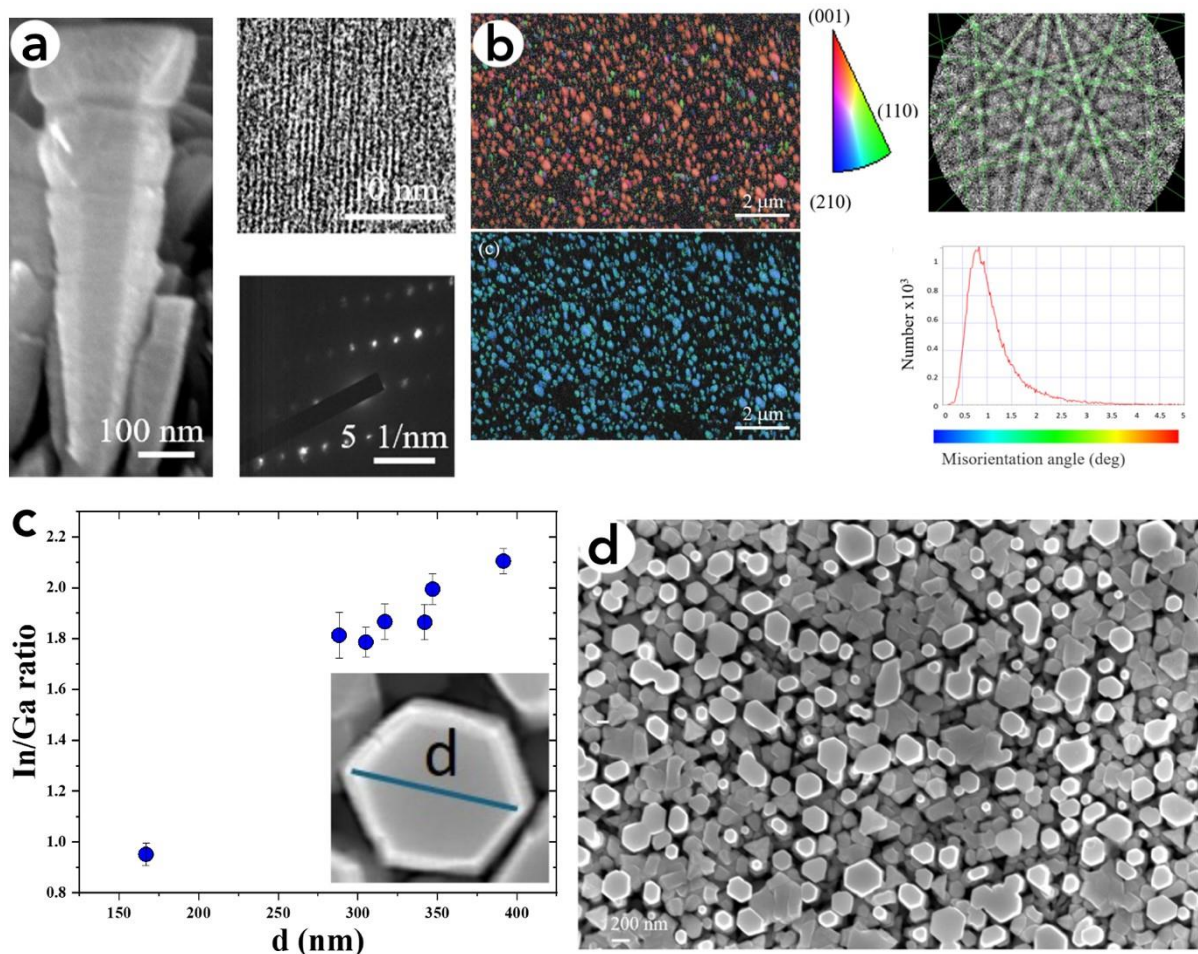


Figure 1. a) SEM side view and TEM images of a nano-column (NC). b) EBSD analysis of the sample and corresponding Kikuchi pattern. The Kernel Average Misorientation map shows a negligible misorientation of 1° . Data acquired using a FE-SEM JEOL IT710HR microscope with QUANTAX EBSD & EDS Bruker detectors. c) Relation between the NCs basis radii with the In/Ga ratio made via EDX analysis. D) SEM top view of a sample with nanocolumns.

References:

- [1] Richard Nötzel, National Science Review, **2017**, 4, 184-195.
- [2] Azadmand, Vichi, Cesura, Bietti, Chrastina, Bonera, Vanacore, Tsukamoto, Sanguinetti, *Nanomaterials*, **2022**, 12, 3887.

Acknowledgments: The authors thank project n. PNC0000003 - AdvaNced Technologies for HumancentrEd Medicine - ANTHEM.



S2.6: New generation of near-UV Laser Diodes by Plasma Assisted MBE

M. Siekacz,^{1,*} G. Muziol,¹ M. Sawicka,¹ M. Żak,¹ M. Hajdel,¹ O. Gołyga,¹ and C. Skierbiszewski,¹

¹ Institute of High Pressure Physics PAS, ul. Sokołowska 29/37, Warsaw, Poland

*msiekacz@unipress.waw.pl

The ultraviolet (UV) laser diodes (LDs) attract attention due to their wide range of applications, e.g. in the field of gas detection, lithography, biomedical, 3D printing, purification, sterilization etc. In this paper we will focus on group-III nitride-based LDs operating in the near ultraviolet range. Interestingly, despite the abundance of potential applications and significant resources devoted to development of UV LDs, their commercial success is yet to come. There are a number of issues which hinder their implementation in many potential applications. Some of those are: i) lack of proper substrates – devices grown on standard GaN substrates suffer from large band-to-band light absorption, ii) lattice mismatch between AlGaIn claddings and GaN substrates – significant strain leads to relaxation through generation of extended defects, and iii) increased degradation rate for short-wavelength LDs.

In this work we focus on novel architecture of UV LDs with GaN quantum well (operating at $\lambda=360$ nm). Instead of classical LD structure with GaN waveguides and AlGaIn claddings (Fig.1a) we used an AlGaIn waveguide and air claddings (Fig. 1b). The structure of LDs is grown by plasma assisted molecular beam epitaxy (PAMBE). The upper air cladding is created by implementation of the tunnel junction (TJ), which allow for side contact deposition (outside of laser ridge). The air above mesa acts as upper cladding. The bottom cladding is made from low Al content porous AlGaIn. The proof of concept of LDs with TJ and bottom porous GaN claddings was already demonstrated for true-blue LDs grown by PAMBE [1-2]. We will discuss the development of low resistance AlGaIn/AlGaIn TJ which do not absorb 360 nm UV light as well as electrochemical etching of nanoporous AlGaIn cladding. The simulation of laser diode optical mode confinement, absorption losses for different parameters of TJ and AlGaIn cladding porosification will be shown.

Acknowledgements:

This work was supported by the National Centre for Research and Development grant INNOGLOBO/II/62/DUVLas/2023

[1] M. Sawicka et. al., Optics Express 30, 10709 (2022)

[2] G. Muziol et.al., Optics Express 28, 35321 (2020).

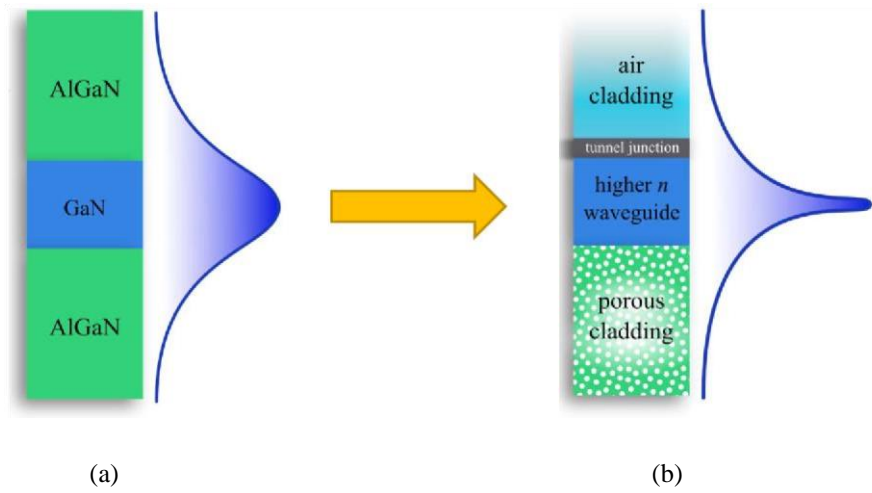


Fig. 1: Comparison of standard LD with AlGaN claddings (a) and LD with air claddings (b)



S2.7: AlGa_xN based Heterostructures grown on h-BN by quasi van der Waals Molecular Beam Epitaxy for Ultra-Violet Light Emitting Diodes

J. Brault^{1,*}, S. Mitra¹, S. Chenot¹, S. Shetty¹, M. Nemoz¹, M. Al Khalifioui¹, P. Vuong², V. Ottapilakkal², S. Sundaram², A. Ibanez³, P. Valvin³, G. Cassabois³, B. Gil³, A. Ougazzaden^{2,4}

¹ Université Côte d'Azur, CNRS, CRHEA, Valbonne, 06560, France

² IRL 2958 Georgia Tech – CNRS, Georgia Tech Europe, Metz, 57070, France

³ UMR 5221, L2C and Université Montpellier 2, Montpellier, 34095, France

⁴ School of Electrical & Computer Engineering, Georgia Tech, Atlanta, GA 30332, USA

*E-mail: julien.brault@crhea.cnrs.fr

Ultra-wide bandgap aluminum gallium nitride (Al_xGa_{1-x}N) materials are widely investigated for numerous applications taking advantage of their direct bandgap going from 3.4 to 6 eV. Despite the lack of bulk substrates, which remain difficult to find and very expensive, Al_xGa_{1-x}N heterostructures have led to the development of a broad range of optical and electronic devices [1], in particular regarding ultra-violet (UV) light emitting diodes (LEDs) grown on sapphire substrates [2]. Indeed, UV LEDs focus a lot of attention due to strategic applications (e.g. in environment, medical fields). Quasi van der Waals (VDW) epitaxy is attractive due to its potential to minimize the impact of the lattice-mismatch between the substrate and the heterostructure, as well as the ability to transfer the structure onto a designated substrate, enabling the creation of devices with innovative functionalities. Along this view, hexagonal boron nitride (h-BN) has demonstrated effectiveness in the growth of nitride-based LEDs [3,4].

By using molecular beam epitaxy (MBE), we have first shown the growth of AlN on h-BN [5], AlN being used as a template for the fabrication of Al_xGa_{1-x}N heterostructures. Next, we obtained an emission in the deep UV with the fabrication of strain-induced Al_yGa_{1-y}N quantum dots [6].

Here, we have studied the growth conditions and characterization of Al_xGa_{1-x}N heterostructures on h-BN templates. The templates were deposited on sapphire via metal organic vapor phase epitaxy, followed by MBE grown Al_{0.7}Ga_{0.3}N / AlN heterostructures. The structural properties of the layers were investigated by atomic force microscopy, scanning electron microscopy and X-Ray diffraction measurements. An improvement of the structural quality was observed as the AlN and Al_{0.7}Ga_{0.3}N thicknesses were increased, as well as a significant influence of the h-BN template thickness. As a next step, Si-doped n-type Al_{0.7}Ga_{0.3}N layers were used as templates for the fabrication of Al_{0.3}Ga_{0.7}N (nominal composition) QDs based UV LEDs. Surfaces exhibiting RMS roughnesses around 2-3 nm at the micro-scale were obtained and electroluminescence in the UVC, down to 270 nm, was obtained at room temperature. The electric characteristics were investigated through current-voltage and transmission line method measurements, while EL and optical power were also examined, showing different operation modes as a function of the injected current. This work was supported by ANR funding DOPALGAN <ANR-22-CE51-0035> and GANEX (ANR-11-LABX-0014).

[1] B. Gil, Physics of Wurtzite Nitrides & Oxides, Springer Series (2014); [2] M. Kneissl et al., Nat. Photonics 13, 233 (2019); [3] Shin, J., et al., Nature 614, 81–87 (2023); [4] S. Sundaram et al., Journal of Crystal Growth 507, 352, (2019); [5] A. Zaiter, et al., Materials 15, 8602 (2022); [6] A. Zaiter, et al., Nanomaterials 13, 2404 (2023).

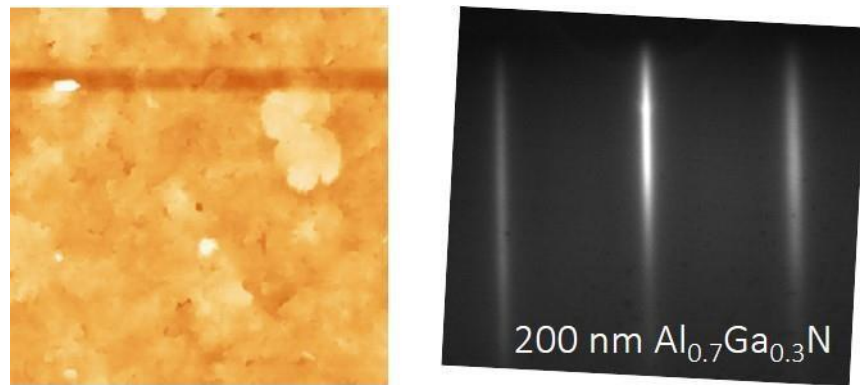


Fig. 1: (left) Atomic force microscopy image ($2 \times 2 \mu\text{m}^2$) of an MBE $\text{Al}_{0.7}\text{Ga}_{0.3}\text{N}$ layer grown on h-BN and (right) a reflection high energy electron diffraction photograph of the same layer at the end of the growth showing a streaky pattern.

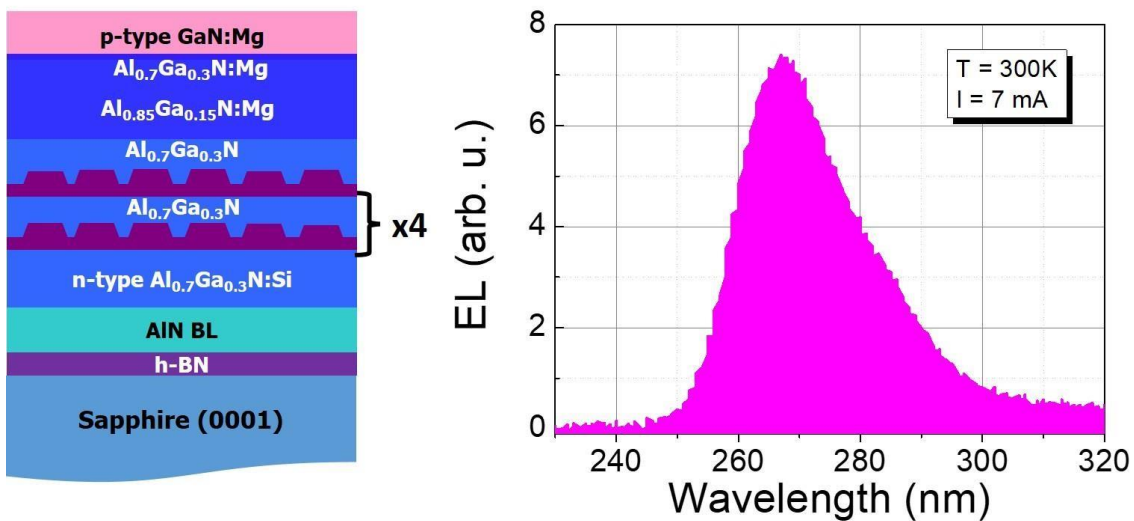


Fig. 2: (left) Schematic of the ultra-violet (UV) LED structure with five planes of $\text{Al}_{0.3}\text{Ga}_{0.7}\text{N}$ (nominal composition) quantum dots and (right) electroluminescence (EL) spectrum of an LED device ($310 \times 310 \mu\text{m}^2$) showing an emission in the deep UV, centered at 267 nm.



I3: Harnessing Redox Epitaxy for Tailored Functionalities at Oxide Heterointerfaces

Martina Müller

Universität Konstanz, Fachbereich Physik, Germany martina.mueller@uni-konstanz.de

The tunability of the oxygen content in complex oxides and heterostructures has emerged as a key to designing their physical functionalities. Controlling the interface reactivity by redox reactions provides a powerful means to deliberately set distinct oxide phases and emerging properties – down to the monolayer limit. With regard to metal-oxide growth, the importance of the choice of oxide substrate materials has typically been downplayed with regard to reduction-oxidation reactions. Only lately, the huge potential of this determining factor was received for the design of oxide functionalities via interfacial oxide exchange, such as magnetic oxides. This way, we have accomplished to i) realize the growth metastable oxide phases [1,2], to ii) control reversibly phase transitions of multivalent Fe oxides [3] and iii) tailor 2D electronic and hole states at oxide heterointerfaces [4]. The emerging properties are uncovered by the unique capabilities of photoelectron spectroscopy using hard X-rays to access bulk and interface properties in an element selective way.

Here we will consider two examples. First, by exploiting the active oxygen supply of the substrate material without the need for external oxygen dosing, high-quality, crystalline ultrathin films of the Heisenberg ferromagnet europium monoxide (EuO) can be stabilized on YSZ (001). This so-called redox-assisted growth mode (or, vice versa, the extreme case of a distillation growth) was monitored from end to end by in situ X-ray photoelectron emission spectroscopy and electron diffraction techniques. The evolution of Eu 3d core levels allows us to disentangle the processes of interfacial oxygen diffusion and vacancy formation in stabilizing the very first monolayers of EuO on YSZ (001). A convenient background correction analysis is presented, which allows us to quantify the critical $\text{Eu}^{3+}/\text{Eu}^{2+}$ ratio in the ultrathin film regime. We concluded on the key mechanisms of redox-assisted EuO/YSZ (001) thin film synthesis, which merge in a universal three-process growth model (see Fig. 1) that may serve as guideline for redox-assisted synthesis of metastable lowdimensional oxides.

Second, we provide evidence for individually emerging hole- and electron-type 2D band dispersions at Fe-SrTiO₃ heterostructures [4]. The emergence of p- or n-type bands is closely linked to the Fe oxidation state which enables the possibility to tune the interface properties to set or even switch between negatively (n) charged electrons or positively (p) charged holes. One of the main processes that controls the interface properties is the oxygen exchange between the film and the substrate.

Using an UHV-MBE system, we grow high-quality ultrathin TM (e.g. Fe, Co) oxide films on SrTiO₃ substrates by systematically varying the growth parameters, e.g. (i) growth temperature, (ii) substrate annealing, and (iii) metal film thickness. The present work discusses the effect of different growth parameters on the interfacial properties like oxygen vacancies, the oxidation state of the redox-formed TM oxide as well as the concentration of defects in SrTiO₃, which strongly influences the valence band alignment between electron and hole band bending. In this way, we can effectively control the properties of the 2D interface to ultimately add ferroic functionalities to these confined electronic states. In summary, exploiting the tunability of the oxygen content in the materials and

understanding interface formation are versatile strategies in designing new functional properties through controlled interfacial oxygen exchange.

References

- [1] Patrick Lömker and Martina Müller, *Redox-controlled epitaxy and magnetism of oxide interfaces*, Physical Review Materials 3, 061401(R) (2019)
- [2] Paul Rosenberger and Martina Müller, *Europium Oxide: Growth guide for the first monolayers on oxidic substrates*, Physical Review Materials 6, 044404 (2022)
- [3] Martina Müller, Patrick Lömker, Paul Rosenberger, Mai Hussein Hamed, David N. Mueller, Ronja A. Heinen, T. Szyjka and Lutz Baumgarten, *Hard X-ray photoelectron spectroscopy of tunable oxide interfaces*, Journal of Vacuum Science and Technology A, 40, 013215 (2022)
- [4] Pia Maria Düring, Paul Rosenberger, Lutz Baumgarten, Fatima Alarab, Frank Lechermann, Vladimir N. Strocov, and Martina Müller, *Tunable 2D Electron- and 2D Hole States Observed at Fe/SrTiO₃ Interfaces*, Advanced Materials 230917 (2024)

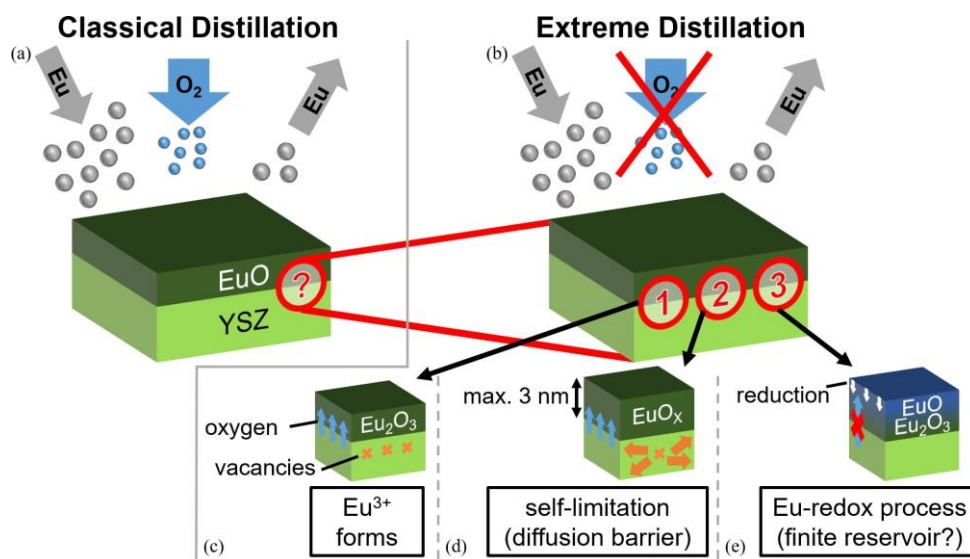


Fig. 1: Sketch of the three-process growth model for EuO/YSZ (001). While mainly hidden under (a) classical distillation conditions the individual processes are best observable under (b) extreme distillation conditions, i.e., the absence of externally supplied oxygen gas. (c) In process 1, a first oxygen-rich layer forms, which (d) acts as diffusion barrier and reduces the oxygen flux from the substrate towards the film surface, resulting in a self-limitation of the growth to a maximum EuO film thickness of about $d_{\text{max}} \approx 3 \text{ nm}$. (e) Finally, an Eu-redox process is part of the growth process whenever the supply of Eu metal is larger than the oxygen supply at the surface (either as O₂ gas or by diffusion). Taken from Ref [1].



S3.1: κ -Ga₂O₃ thin films and related heterostructures grown by Suboxide-MBE and conventional MBE

A. Karg,^{1,*} M. Schowalter,^{1,2} A. Hinz,¹ M. Alonso-Orts,^{1,2} S. Figge,¹ P. Vogt,^{1,3}

A. Rosenauer,^{1,2} and M. Eickhoff,^{1,2}

¹Universität Bremen, Institute of Solid State Physics, Bremen, Germany ²Universität Bremen, MAPEX Center for Materials and Processes, Bremen, Germany ³Max Planck Institute for solid state research, Stuttgart, Germany

*karg@uni-bremen.de

The wide-bandgap semiconductor Ga₂O₃ is considered a promising material for high-power electronic devices, benefiting essentially from its large bandgap and the associated high breakdown field strength. The five polymorphs of Ga₂O₃ also exhibit unique material properties^[1]. Widely investigated is the thermodynamically stable monoclinic β -Ga₂O₃, from which bulk substrates are commercially available^[2], and precise n-type doping that enables high carrier mobilities has been established^[3]. However, the primary focus of this contribution is on the metastable orthorhombic κ -Ga₂O₃. Due to its crystal structure, it is assumed to possess a spontaneous polarization along the c-axis, which makes the realization of high sheet carrier densities at heterointerfaces feasible^[4].

In this study we focus on two key aspects of κ -Ga₂O₃ growth, the stabilization of the metastable polymorph and the realization of heterostructures. Here, we initially demonstrate the growth of the κ phase and discuss the phase stabilization and the growth process using suboxide-MBE (S-MBE) as a novel MBE technique and conventional MBE (C-MBE), both combined with the use of the known additive tin^[5,6]. The growth regimes in which a phase transformation from β -Ga₂O₃ to κ -Ga₂O₃ occurs are identified and characteristics of the obtained layers are compared.

Additionally, we focus on the growth of Ga₂O₃-based heterostructures using both growth techniques (S-MBE and C-MBE). The study examines the combination of different polymorphs in superlattice heterostructures, specifically β -Ga₂O₃/ κ -Ga₂O₃. This provides through scanning transmission electron microscopy insights into the atomic arrangement of both polymorphs at the interfaces. Furthermore, κ -Ga₂O₃/ κ -(Al,In,Ga)₂O₃ heterostructures are studied and the strain state in κ -Ga₂O₃/ κ -InGaO/ κ -AlGaO heterostructures is investigated^[7], since fully strained structures are promising candidates for the realization of carrier accumulation at heterointerfaces.

[1] Roy et al., J. Am. Chem. Soc. **74**, 719-722 (1952)

[2] Galazka et al., Cryst. Res. Technol. **45**, 1229-1236 (2010)

[3] Maccioni et al., Appl. Phys. Express **9**, 041102 (2016)

[4] Kang et al., J. Phys. Condens. Matter **29**, 234001 (2017)

[5] Vogt et al., U.S. Patent No. 11,462,402 (2022)

[6] Karg et al., J. Appl. Phys. **132**, 195304 (2022)

[7] Karg et al., APL Mater. **11**, 091114 (2023)

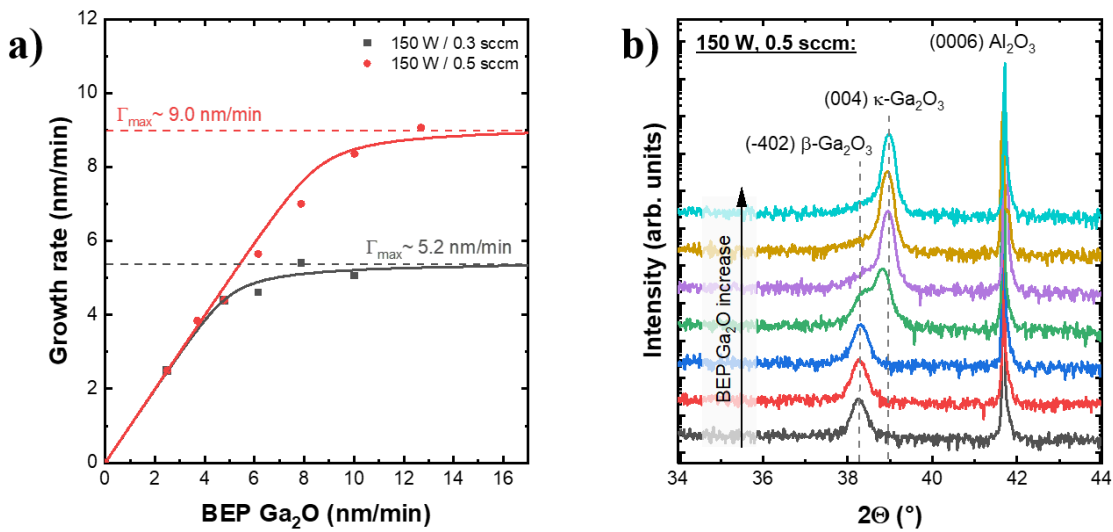


Fig. 1: a) Ga₂O₃ growth rate as a function of gallium suboxide (Ga₂O) flux. For both series grown at different plasma settings, the adsorption-controlled regime with a constant growth rate is reached, indicating the single-step growth mechanism of κ -Ga₂O₃ when using S-MBE. b) XRD spectra of the series grown at 150 W and 0.5 sccm revealing the phase transition from β - to κ -Ga₂O₃ when increasing the Ga₂O flux.

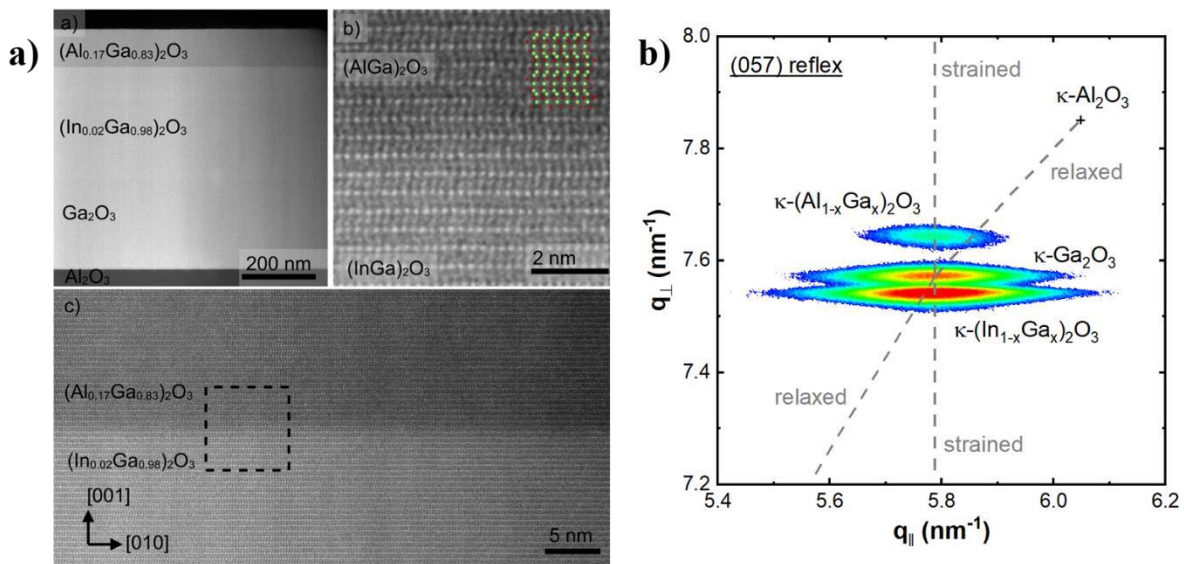


Fig. 1: a) STEM images of a κ -Ga₂O₃/ κ -(In,Ga)₂O₃/ κ -(Al,Ga)₂O₃ heterostructure, showing a sharp distinct transition between the κ -(In,Ga)₂O₃ and κ -(Al,Ga)₂O₃ layer. b) The corresponding reciprocal space map of the heterostructure displayed in a) indicates the pseudomorphic growth throughout the layer sequence [7].



S3.2: Elevated cryogenic permittivity of epitaxial SrTiO₃ films on silicon by stoichiometry and thickness control

Andries Boelen^{1,2}, Marina Baryshnikova¹, Anja Ulrich^{1,3}, Kamal Brahim^{1,4}, Christian Haffner¹ and Clement Merckling^{1,2}

1. *Imec, B-3001 Leuven, Belgium*

2. *Department of Materials Engineering (MTM), KU Leuven, B-3001 Leuven, Belgium*

3. *Department of Information Technology (INTEC), Photonics Research Group, Ghent University, B-9052 Ghent, Belgium* 4. *Department of Electrical Engineering (ESAT), KU Leuven, B-3001 Leuven, Belgium*

Strontium titanate (SrTiO₃, STO) stands out as a promising material for various electronic applications thanks to its exceptional dielectric properties. Its intrinsic parameters allow a direct growth on silicon, it shows nonlinear optical behaviour and importantly, its bulk dielectric permittivity of several hundred at room temperature is very high and increases further to $\sim 10^4$ at cryogenic temperatures thanks to its quantum paraelectric behaviour [1].

Molecular beam epitaxy (MBE) is one of the few techniques which allows epitaxial growth of STO directly on industry-relevant Si substrates. The large lattice mismatch between STO and Si (-39.1%) can be reduced tremendously to only few percents when the STO lattice rotates 45° with respect to Si, i.e., (001) [100]_{STO}// (001) [110]_{Si}, allowing direct heteroepitaxy [2]. However, maintaining precise stoichiometry and high crystalline quality in this process remains a significant challenge. Establishing this is essential to obtain STO with bulk-like dielectric properties and to minimize leakage current and optical absorbance. In this study, the importance of cationic stoichiometry and the effect of thickness are investigated for STO thin films epitaxially grown on (001)-oriented silicon substrates.

During epitaxy, the Sr molecular beam is gradually disturbed by the high oxygen environment generally conduct to a Ti-rich STO layer. We employed real-time reflection high-energy electron diffraction (RHEED) as a feedback loop mechanism to counteract Sr source oxidation and maintain a constant flux. Additionally, high-temperature post-growth annealing treatments in O₂ were investigated to promote layer relaxation and reduce oxygen vacancy concentration, thereby improving the physical, electrical, and optical properties of stoichiometric STO. As a result, high-quality STO thin films exceeding 100 nm were successfully fabricated featuring a bulk-like out-of-plane lattice parameter and refractive index, as well as rocking curve full width at half maximum (FWHM) below 0.2°, smooth surface ($R_q < 0.2$ nm) and a leakage current density below 1E-7 A/cm² [3].

This epitaxy process for MBE growth of high-quality thick STO layers on silicon (001)-oriented substrates is essential for optimizing dielectric properties, such as the dielectric permittivity. By establishing a correlation between cationic stoichiometry, crystallinity, and STO thickness, we achieve significant enhancement of the effective permittivity at cryogenic temperatures, reaching value of over 2,500 for our stoichiometric 105 nm STO film. To our knowledge, this is the highest reported permittivity for STO thin films on silicon. This study paves the way for using STO thin films as active materials in advanced devices for various applications, including energy storage and quantum information technology.

References:

[1] Müller, K., Burkard, H., “SrTiO₃: An intrinsic quantum paraelectric below 4K,” *Phys. Rev. B*, (1979), 19, 3593–3602.

[2] R. A. McKee, F. J. Walker, and M. F. Chisholm, “Crystalline Oxides on Silicon: The First Five Monolayers,” *Phys. Rev. Lett.*, vol. 81, no. 14, pp. 3014–3017, Oct. 1998, doi: 10.1103/PhysRevLett.81.3014.

[3] A. Boelen, M. Baryshnikova, A. Ulrich, K. Brahim, J. Van de Vondel, C. Haffner, and C. Merckling, "Stoichiometry and Thickness of Epitaxial SrTiO₃ on Silicon (001): An Investigation of Physical, Optical, and Electrical Properties," *APL Materials*, manuscript submitted for publication, 2025.

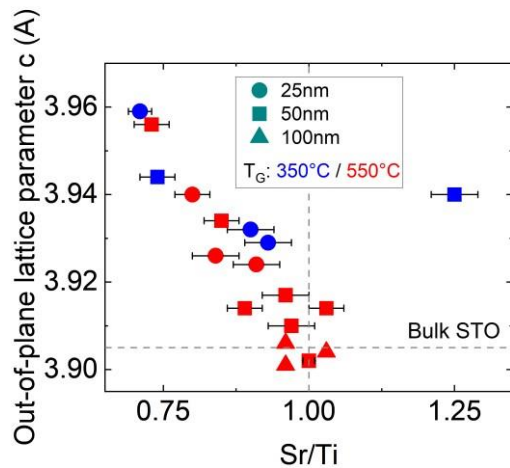


Figure 1: Out-of-plane lattice parameter (c) as a function of Sr/Ti ratio for STO films with varying thickness and growth temperature T_G . For obtaining a bulk-like lattice parameter, perfect cationic stoichiometry, high growth temperatures and layers > 50 nm need to be fulfilled.

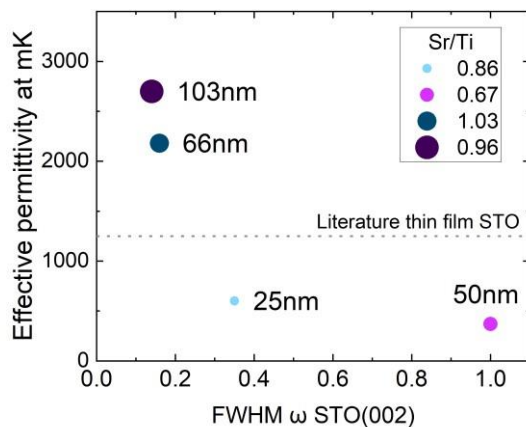


Figure 2: Effective permittivity ϵ_{eff} near 0 K as a function of the STO (002) rocking curve FWHM. Cationic stoichiometry ($Sr/Ti = 1$) and increasing STO thickness result in lower FWHM and higher effective permittivity.



S3.3: Strong optical anisotropy in epitaxial SrO(SrTiO₃)_n Ruddlesden–Popper thin layers

M. Bounab¹, C. Furgeaud¹, S. Cueff¹, L. Berguiga¹, R. Bachelet¹, M. Bouras¹, L. Largeau², G. Saint-Girons^{1*}

¹ INL-UMR5270/CNRS, Ecole Centrale de Lyon, Ecully (France)

² C2N-UMR9001/CNRS Université Paris-Saclay, Palaiseau (France)

*guillaume.saint-girons@ec-lyon.fr

Optical anisotropy is at the hearth of many essential optical devices ranging from phase-matching elements or modulators¹ to more exotic devices exploiting unconventional optical modes,² with potential applications ranging from sensors, displays and medicine to non-linear and quantum optics.³ Device fabrication requires anisotropic materials to be integrated compactly, in the form of thin films, with silicon based photonic circuits. Flexibility in controlling anisotropy is also required for device design. So-called optical metamaterials based on planar/multilayer nanostructuring enable strong birefringence and significant flexibility for permittivity engineering, but generally their morphology complicates their integration into devices.⁴ Intrinsically anisotropic homogeneous materials are quite few in number, present a fixed anisotropy that cannot be engineered, are barely available in the form of thin films, and their elaboration processes are not compatible with the constraints of the photonics industry.⁵ A homogeneous material exhibiting strong and controllable optical anisotropy, compactly integrable as thin-film in silicon photonic platforms, is therefore still lacking.

In this contribution we will show that SrTiO₃ (STO) based Ruddlesden-Popper thin layers (noted STORP_N, general formula Sr_{N+1}Ti_NO_{3N+1}), grown by molecular beam epitaxy by inserting an extra SrO plane every N STO unit cells in the STO lattice, present a strong optical anisotropy, higher than the highest values reported in the literature in the UV and visible ranges. In contrast to known highly anisotropic materials, STO-RP_N anisotropy can be controlled by changing the STO-RP_N order N, which leverages flexibility to optimize the material properties depending on the targeted functionality/device design. STO-RP_N thin layers combines the advantages of optical metamaterials in terms of engineering flexibility with the integrability of homogeneous anisotropic materials, bridging the gap between both approaches. They can be epitaxially grown on Si and GaAs platforms thanks STO templates.⁶ by using industry-standard growth processes. This collection of unique properties confers on these materials considerable interest for the design of novel integrated optical devices.

[1] L.H. Nicholls *et al.*, Nat. Photonics **11** 628, (2017)

[2] O. Takayama *et al.*, Nature Nanotechnology **9**, 419 (2014)

[3] X. Xu *et al.*, Nat. Photonics **16**, 698 (2022)

[4] J.D. Caldwell *et al.*, Nanophotonics **4**, 44 (2015)

[5] H. Mei *et al.*, Adv. Mater. **35**, 2303588 (2023)

[6] G. Saint-Girons *et al.*, Chem. Mater. **28**, 5347 (2016), L. Louahadj *et al.*, Appl. Phys. Lett. **103**, 212901 (2013)

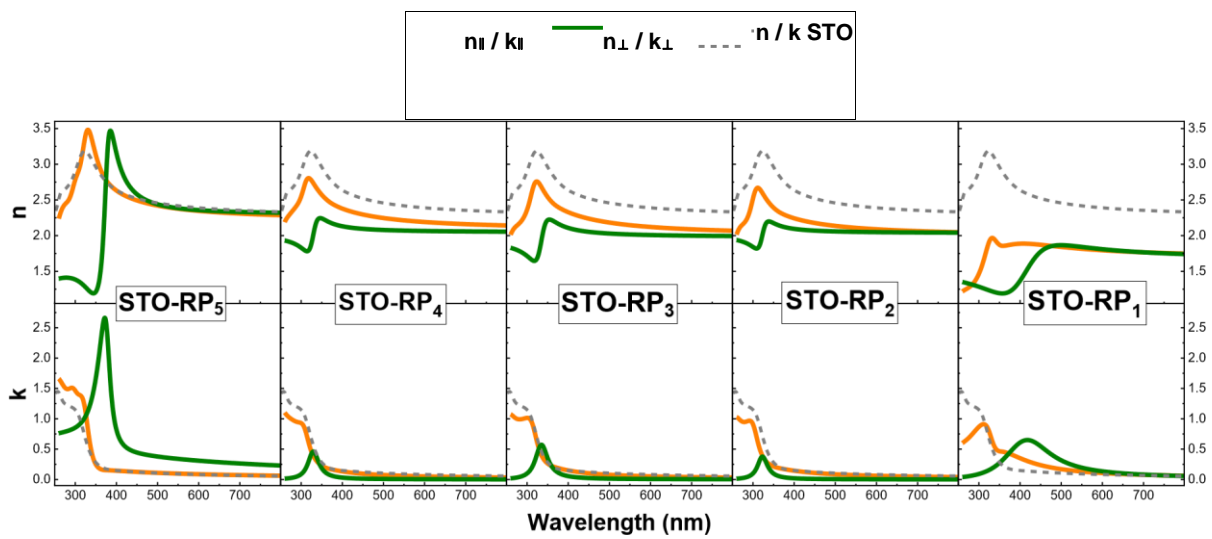


Fig. 1: Refractive indices and extinction coefficients for the five STO -RP_N samples, compared to that of STO.

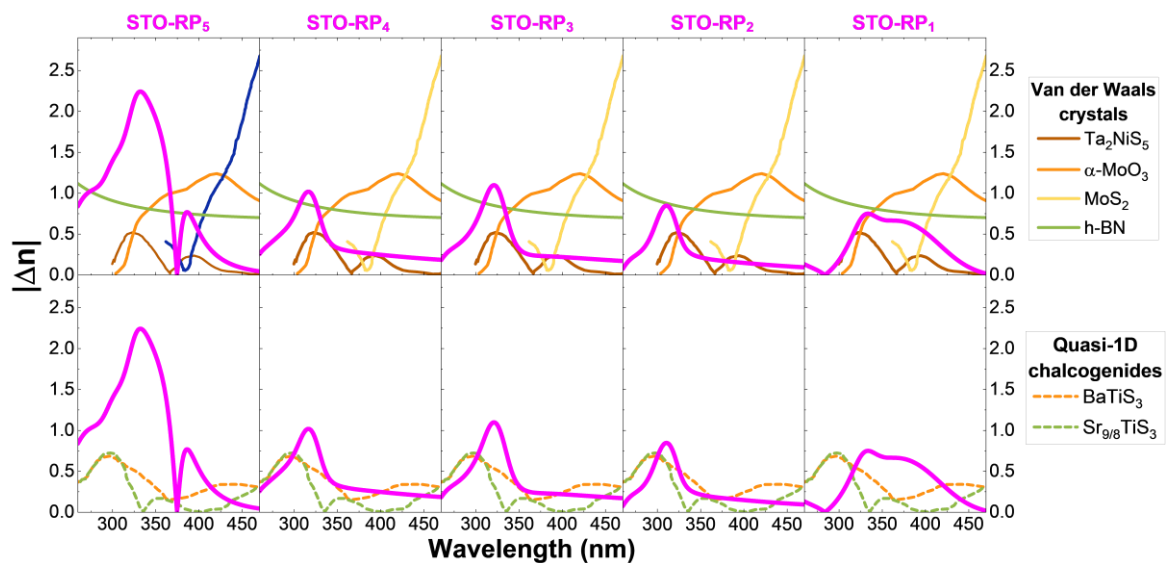


Fig. 2: Birefringence of the STO-RP_N layers (pink) compared to that of materials with the highest anisotropy in the UV -visible spectral range : van der Waals crystals Ta₂NiS₅, α-MoO₃, MoS₂ and h-BN and quasi-1D chalcogenides BaTiS₃ and Sr_{9/8}TiS₃.



Invited talk : 23min + 7min questions
 Oral : 15min + 5min questions

Tuesday, 11.03

08:00	Registration
	Session 4 : Ultra-low temperature, Photonics : chairman Shumin Wang
08:30	Invited talk I4: Group-IV epitaxy at ultra-low temperatures for optoelectronic and quantum photonic applications , <u>Moritz Brehm</u> , <i>Institute of Semiconductor and Solid State Physics, Johannes Kepler University Linz, Austria</i>
09:00	S4.1: Direct MBE growth of GaSb on Ge, Ge-on-Si and Ge-on-SiGe-on-Si platforms for integrated mid-infrared photonics , <u>Milan Silvestre</u> , <i>IES, University of Montpellier, CNRS, F – 34000 Montpellier, France</i>
09:20	S4.2: MBE-grown Ge-rich nanosheets on silicon-on-insulator as a planar platform for nanoelectronic devices , <u>Moritz Brehm</u> , <i>Institute of Semiconductor and Solid State Physics, Johannes Kepler University Linz, Austria</i>
09:40	S4.3: Tunable GaAs_xP_{1-x} Quantum-Dot Emission in Wurtzite GaP Nanowires , <u>Paolo De Vincenzi</u> , <i>Department of Physics, Sapienza University of Rome, P.le A. Moro 5, I-00185 Rome, Italy</i>
10:00	S4.4: Design and growth of GaAsBi and InGaAs based Vertical-External-Cavity Surface-Emitting-Lasers <u>Andrea Zelioli</u>
10:20	break
	Session 5: 2D Materials : Chairman Lutz Geelhaar
10:40	Invited talk I5: Ultra-Thin Semiconductors: From Epitaxy to Band Engineering and UV Photon Sensing , <u>Amalia Patanè</u> , <i>School of Physics and Astronomy University of Nottingham, Nottingham NG7 2RD, UK</i>
11:10	S5.1: Epitaxial 2D HfSe₂ Semiconductor/TaSe₂ Metal van der Waals Heterostructure , <u>Corentin Sthioul</u> , <i>Univ. Lille, CNRS, Centrale Lille, Univ. Polytechnique Hauts-de-France, Junia-ISEN, UMR 8520 - IEMN, Lille, France</i>
11:30	S5.2: Multi-particle Excitonic Systems in WSe₂ Grown on hBN by Molecular Beam Epitaxy , <u>Julia Kucharek</u> , <i>Institute of Experimental Physics, Faculty of Physics, University of Warsaw, 02-093 Warsaw, Poland</i>
11:50	S5.3: Optically active indium selenide crystal phase heterostructures grown by molecular beam epitaxy <u>Piotr Wojnar</u> , <i>Institute of Physics, Polish Academy of Sciences, Warsaw, Poland</i>
12:10	S5.4: High-temperature MBE of hBN for Deep-ultraviolet, Single-photon Emitters and Lateral Heterostructures , <u>Sergei V. Novikov</u> , <i>School of Physics and Astronomy, Univ. of Nottingham, Nottingham, UK</i>
12:30	Lunch Boxes
16:00	Poster session 1
	Session 6: Production : Chairman Jean-Yves Duboz
17:30	Invited talk I6: III-Nitrides NWs based μLEDs: a solution for AR display technology , <u>Benoît Amstatt</u> , <i>ALEDIA, Rue des Lavières ZAC Saut du Moine 38800 Champagnier</i>
18:00	S6.1: Emerging Growth Opportunities for GaN Using Molecular Beam Epitaxy (MBE): From Research to Production , <u>Samuel Matta</u> , <i>RIBER SA, 31 Rue Casimir Périer 95873 Bezons France</i>
18:20	S6.2: GaN Power HEMT with Breakdown Voltage >800 V Grown by MBE , <u>Eason Liao</u> , <i>MASSPHOTON LIMITED, Hong Kong SAR</i>
18:40	
19:30	Debate & Cocktail-buffet "Why and how could be achieved MBE at lower economical costs?"



I4: Group-IV epitaxy at ultra-low temperatures for optoelectronic and quantum photonic applications

M. Karaman,¹ J. Aberl,¹ J. Marböck,¹ E. P. Navarrete,¹ D. Haya Enriquez,¹ C. Wilflingseder,¹
A. Salomon,¹ T. Fromherz,¹ M. Brehm^{1,*}

¹ Institute of Semiconductor and Solid State Physics, Johannes
Kepler University Linz, Austria

*E-mail : moritz.brehm@jku.at

For homo- and heteroepitaxy of group-IV materials like Si and Ge, ultra-low temperature (ULT) growth, (100°C and 350°C), is the key to extending the material properties beyond the state-of-the-art. We highlight that MBE is the suitable choice for ULT growth and stress that the chamber conditions during the growth need to be excellent to limit detrimental point defect formation during epitaxy [1-6].

First, we show that ULT growth can lead to unattainable layer structures for the strained (Si)Ge/Si(001) system. While Ge has successfully entered Si technology, due to the inherent lattice mismatch, high-crystalline and flat SiGe/Si epitaxial layers of a sufficient thickness could only be grown for relatively low Ge concentration (<40%). In turn, planar Ge-rich heterolayers on SOI can be essential for efficient integration and reliable addressing of novel devices [1]. ULT growth can lead to layer that are significantly thicker than their equilibrium thickness [2]. These can be used to demonstrate double heterostructure light-emitting diodes emitting at room temperature and above in the telecom band [3].

Second, we use ULT Si homoepitaxy to obtain Si-color centers within thin carbon-doped Si layers. Such Si telecom emitting color centers, normally generated through ion implantation, can be envisioned as scalable deterministic group-IV-based quantum light sources. However, the resulting ion implantation profiles are broad and lead to a decisive lack of control over the vertical emitter position. This drawback can significantly degrade the coupling efficiency to photonic structures such as resonators or waveguides, and no two SiCC emitters will be located vertically at the same position below the substrate surface. The here presented all-epitaxial approach for fabricating variable SiCCs departs entirely from ion implantation and enables us to restrict the formation of SiCCs to a specific epilayer and control their vertical position in a structure even with sub-nm precision [4,5]. Thereby, the emitter density can be conveniently controlled via the C doping concentration and the Si:C layer thickness [4]. Furthermore, we show the first results for electrically-pumped self-assembled SiCCs by integrating the Si:C nanolayers into ULT-grown p-i-n light-emitting diodes [5].

References

- [1] L. Wind et al. *Small* **18**, 2204178 (2022)
- [2] C. Wilflingseder et al, arXiv preprint arXiv:2410.03295 (2024) ; accepted in *ACS Appl. Electr. Mat.*
- [3] A. Salomon et al., arXiv preprint arXiv:2409.11081 (2024)
- [4] J. Aberl et al., *Advanced Materials* **36**, 2408424 (2024)
- [5] A. Salomon et al., arXiv preprint arXiv:2408.13660 (2024)





S4.1: Direct MBE growth of GaSb on Ge, Ge-on-Si and Ge-on-SiGe-on-Si platforms for integrated mid-infrared photonics

M. Silvestre,^{1,2} S. Lacaze,¹ A. Gilbert,¹ A. De Cerdeira Oliveira,³ D. Impelluso,³ G. Isella,³ J-B. Rodriguez,¹ E. Tournié,^{1,4*}

- 1) IES, University of Montpellier, CNRS, F – 34000 Montpellier, France
- 2) RIBER SA, F – 95870 Bezons, France
- 3) L-NESS, Politecnico di Milano Dipartimento di Fisica, I - 22100 Como Italy
- 4) Institut Universitaire de France (IUF), F-75005 Paris, France

*E-mail: eric.tournie@umontpellier.fr

Monolithically integrated mid-infrared (MIR) photonics is of major interest for free-space communications, bio-sensing, etc. While Si is transparent up to $\sim 7 \mu\text{m}$, longer MIR wavelengths require other materials [1]. Ge being transparent up to $\sim 15 \mu\text{m}$, a variety of photonic integrated circuits (PICs) covering a broad wavelength range from the near-IR to the MIR has recently been developed based on Ge-on-Si and Ge-on-SiGe-on-Si waveguides with various Ge contents and composition profiles [2]. The epitaxial growth of MIR lasers on these PICs is now the missing brick to develop fully integrated active devices.

In this work, we studied the MBE growth of GaSb-based materials on various Ge-based templates grown on silicon wafers by low energy plasma enhanced CVD [3]. Similar to the growth of III-Vs on Si, the main issue is removing anti-phase domains (APDs) delineated by anti-phase boundaries (APBs), a defect detrimental to devices because they create short circuits in lasers [4].

As a preliminary step, we first investigated the growth of GaSb layers on (001) Ge substrates. We will show that the APD burying mechanism previously established for GaSb-on-Si growth, which relies on the substrate surface organization and step-flow growth of GaSb [5], also operates during growth on Ge substrates, but only when they are prepared by UHV annealing in a narrow temperature window.

Next, we studied the growth of GaSb on Ge-on-Si and on Ge-on-SiGe-on-Si relaxed-buffer layers with various Ge-composition profiles. In this case, the cross-hatch pattern on the template surfaces (Fig. 1 c) prevents the proper surface organization prior growth for on axis (001) substrates. However, this effect can be alleviated by using slightly miscut (1°) substrates. By carefully adjusting the surface preparation and GaSb growth conditions, APB-free GaSb layers with a roughness rms as low as 1.0 nm can then be achieved on these templates (Fig. 1 b). Such layers can be used for the direct growth of III-V lasers on germanium-based photonic platforms, and represent a further step in the development of integrated MIR photonics.

Part of this work was sponsored by "France 2030" (Equipex EXTRA, ANR-11-EQPX-0016, Equipex+ HYBAT, ANR-21-ESRE-0026) and the Horizon Europe program (project UNISON, #101128598).

- [1] R. Soref, Nat. Photonics 4, 495 (2010), 10.1038/nphoton.2010.171 .
- [2] D. Marris-Morini, Nanophotonics 7(11), 1781 (2018), 10.1515/nanoph-2018-0113 .
- [3] G. Isella *et al.* , Solid-State Electron. 48, 1317 (2004), 10.1016/j.sse.2004.01.013 .
- [4] H. Kroemer, , J. Cryst. Growth 81, 193 (1987), 10.1016/0022-0248(87)90391-5 .
- [5] M. Rio Calvo *et al.*, Adv. Electron. Mater. 8, 2100777 (2022), 10.1002/aelm.202100777 .

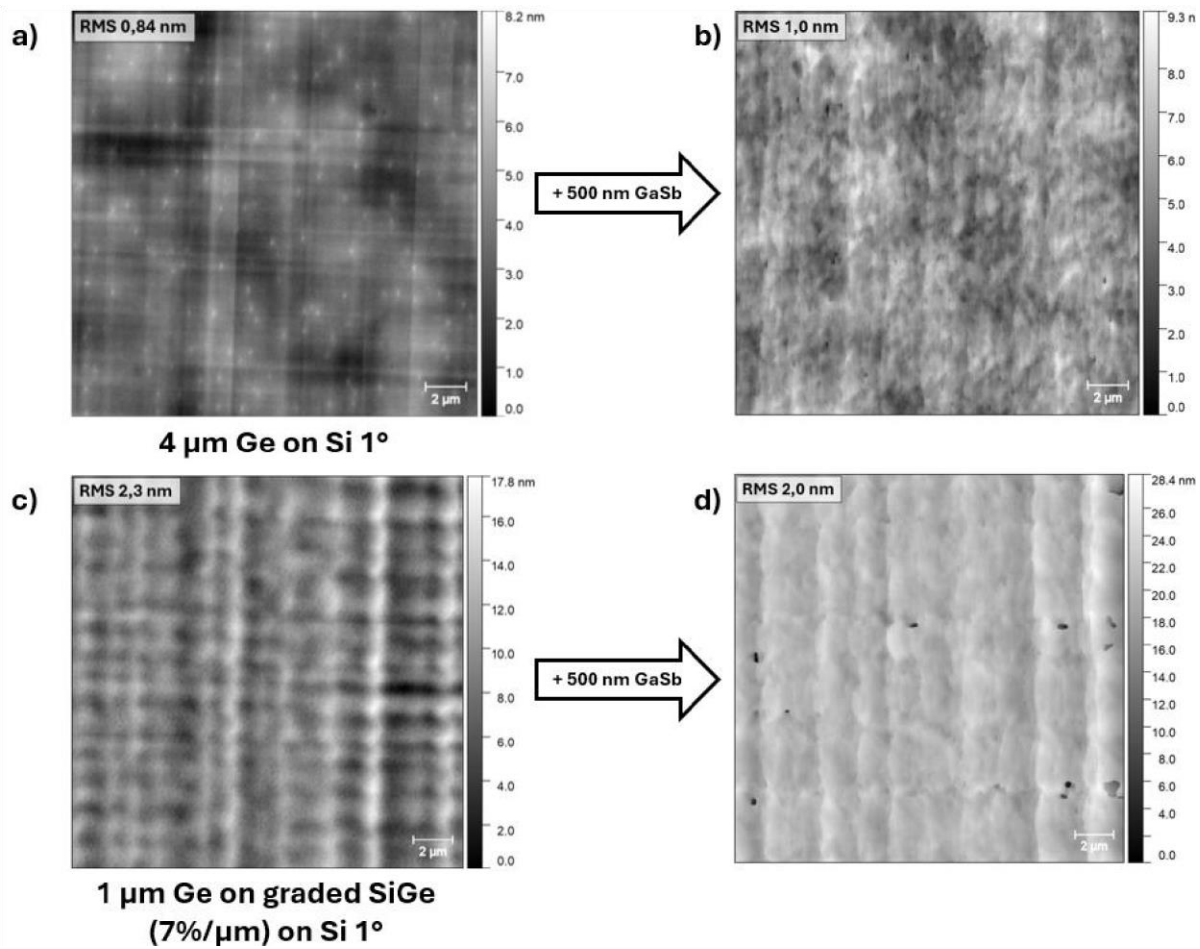


Fig. 1: AFM images of a) 4 μm of Ge template grown on Si with 1° offcut, before GaSb growth. A faint crosshatch is visible. b) Surface after the growth of 500 nm of GaSb on template a). The surface is APB-free. c) Surface of 1 μm Ge grown on graded SiGe buffer on Si with 1° offcut, before GaSb growth. Surface roughness is due to cross-hatch patterns. d) Surface after the growth of 500 nm of GaSb on template c).



S4.2: MBE-grown Ge-rich nanosheets on silicon-on-insulator as a planar platform for nanoelectronic devices

E. Prado-Navarrete¹, J. Aberl¹, J. Marböck¹, C. Wilflingseder¹, A. Fuchsberger², L. Wind², M. Sistani², W.M. Weber², M. Brehm^{1,*}

¹ Institute of Semiconductor and Solid-State Physics, JKU, Linz, Austria

² Institute of Solid-State Electronics, Technische Universität Wien, Vienna, Austria

*E-mail : moritz.brehm@jku.at

Heteroepitaxial layers comprising crystalline stacks of Group-IV alloys, predominantly SiGe, have been employed to enhance the operational efficiency of Si-based devices [1]. However, achieving defect-free pseudomorphic (Si)Ge layers on Si(001) substrates with high Ge compositions ($x \gtrsim 50\%$) poses significant challenges due to strain-induced relaxation beyond a layer thickness of a few monolayers [2].

This study explores molecular beam epitaxy (MBE) growth at ultra-low temperatures (ULT), ranging from 100°C to 350°C, departing from conventional epitaxy temperatures $>500^\circ\text{C}$. Reduced surface kinetics in ULT conditions leads to notable layer supersaturation, allowing for the growth of thicker pseudomorphic layers than previously achieved [3]. We show that maintaining pristine growth pressures at the lower end of the ultra-high-vacuum range ($<3 \cdot 10^{-10}$ mbar) is crucial to minimizing impurities and preserving superior electrical and optical properties of the heterostructures. This is particularly true during ULT growth, where a limited thermal budget hampers efficient gas desorption.

Here, we show that combining ULT and excellent growth pressures enables the fabrication of high-quality, fully strained, defect-free (Si)Ge epitaxial layers directly grown on Si and silicon-on-insulator (SOI) substrates. These layers exhibit remarkable structural qualities, as confirmed by Atomic Force Microscopy (AFM), X-ray diffraction (XRD) and transmission electron microscopy (TEM) experiments [3]. Furthermore, these nanosheets serve as a scalable platform for advanced multifunctional SiGe and Ge-based transistors such as reconfigurable field-effect transistors, capable of runtime switching between n-type and p-type operation, exhibiting outstanding performance for adaptive electronics [4], [5]. For these devices, high-resolution TEM reveals sharp and reproducible interfaces with single-element crystalline Al contacts formed through a thermally induced Al-Si_{1-x}Ge_x exchange reaction [6]. The precisely chosen (Si)Ge channel stoichiometry and abrupt interfaces contribute to exceptional symmetric I-V operability in RFET devices, as observed in their transfer characteristics [4].

References

- [1] I. A. Fischer et al., *APL Photonics*, 7, 050901 (2022).
- [2] M. Brehm and M. Grydlik, *Nanotechnology* 28, 392001 (2017).
- [3] A. Salomon et al., *Phys. status solidi*, 219, 2200154 (2022). [4] A. Fuchsberger et al., *Adv. Electron. Mater.*, 9 1–10 (2023).
- [5] A. Fuchsberger et al., *IEEE J. Electron Devices Soc.* 18, 1–1 (2024).
- [6] L. Wind et al., *Small* 18, 2204178 (2022).





S4.3: Tunable GaAs_xP_{1-x} Quantum-Dot Emission in Wurtzite GaP Nanowires

Robert Andrei Sorodoc¹, Paolo De Vincenzi², Akant Sagar Sharma², Giada Bucci¹, Mario Roggi², Enrico Mugnaioli³, Lucia Sorba^{1,*}, Marta De Luca², and Valentina Zannier¹

1 NEST, Istituto Nanoscienze -CNR and Scuola Normale Superiore, P.zza S. Silvestro12, I34127 Pisa, Italy

2 Department of Physics, Sapienza University of Rome, P.le A. Moro 5, I-00185 Rome, Italy.

3 Department of Earth Sciences, University of Pisa, Via S. Maria 53, I-56126 Pisa, Italy.

*lucia.sorba@nano.cnr.it

Quantum light emitters can be realized by employing semiconductor quantum-dots (QD) for advanced quantum optics and nanophotonic applications. Tunable Gallium Arsenide Phosphide (GaAs_xP_{1-x}) QD in nanowires (NWs) with emission in VIS-NIR wavelength range have a strong technological potential. Here, we synthesized crystal-pure wurtzite Gallium Phosphide (GaP) nanowires (NWs), incorporating single GaAs_xP_{1-x} QDs of various As content with a great degree of control over the shape and composition of the ternary alloy QD. A well-defined confinement of the QD and the tunability of the emission wavelength are confirmed by low-temperature micro-photoluminescence (μ -PL) spectroscopy showing that the QD NW emission is dominated by a narrow peak whose energy shifts according to the As content of the QD: from \sim 650 nm (As = 70%) to \sim 720 nm (As = 90%) (see Fig. 1). Moreover, a localized and efficient carrier recombination mechanism is found by single-NW μ -PL mapping, confirming that this emission arises from the QD. Finally, a power and temperature dependent μ -PL study is performed to characterize the QD excitonic properties and to identify the origins and the nature of the involved energy levels [1].

Acknowledgments This work has been funded by the PRIN Project 20223WZ245 (“Growth and optical studies of tunable QDs and superlattices in semiconductor nanowires”), supported by the Next Generation EU program in the context of the PNRR Italian plan, mission 4 “education and research”. It has also been funded by the European Union (ERC starting grant, NANOWHYR, 101042349).

References

- [1] Robert Andrei Sorodoc, Paolo De Vincenzi, Akant Sagar Sharma,, Giada Bucci, Mario Roggi, Enrico Mugnaioli, Lucia Sorba, Marta De Luca, and Valentina Zannier, Tunable GaAs_xP_{1-x} Quantum-Dot Emission in Wurtzite GaP Nanowires, ACS Applied Materials & Interfaces, in press DOI 10.1021/acsami.4c15343

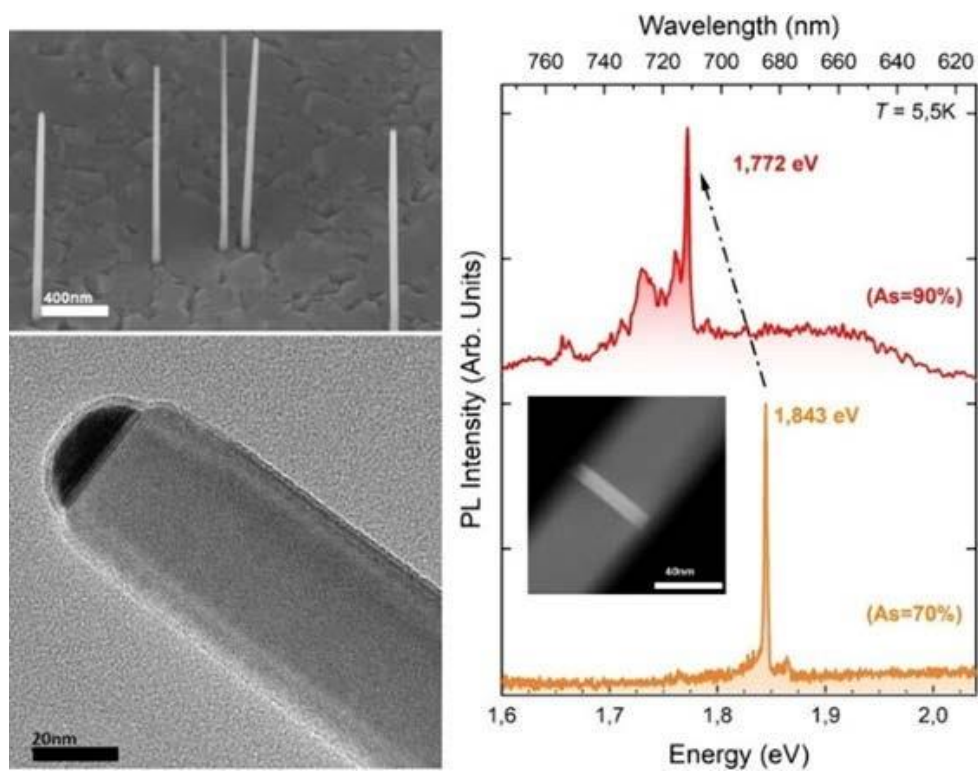


Fig.1 Scanning and transmission electron microscopy images (left side panels) and low-temperature μ -PL spectra (right side panel) of $\text{GaAs}_x\text{P}_{1-x}$ QD NWs with As = 70% and As = 90%.



S4.4: Design and growth of GaAsBi and InGaAs based Vertical-External-Cavity Surface-Emitting-Lasers

A. Zelioli,^{1*} A. Špokas,¹ A. Štaupienė,¹ E. Dudutienė,¹ A. Suchodolskis,¹ B. Čechavičius,¹ M. Talaikis,¹ G. Kontenis,² D. Gailevičius,² and R. Butkutė¹

¹ Center for Physical Sciences and Technology, Saulėtekio av. 3, Vilnius, Lithuania

² Laser research center, Vilnius University, Saulėtekio av. 10, Vilnius, Lithuania

*andrea.zelioli@ftmc.lt

Vertical-External-Cavity Surface-Emitting Lasers (VECSELs) have emerged as a versatile alternative to traditional Vertical-Cavity Surface-Emitting Lasers (VCSELs) by replacing the top Distributed Bragg Reflector (DBR) with an external coupler, enabling efficient optical pumping and cavity access. This design offers higher output power potential, constrained primarily by thermal management challenges [1, 2].

In this work, two VECSEL chips were fabricated, targeting emission wavelengths of 976 nm and 1070 nm. The 976 nm VECSEL employed InGaAs multiple quantum wells (MQW) in the gain region, while the 1070 nm VECSEL utilized GaAsBi MQW. Incorporation of Bi in the GaAs lattice reduces the bandgap faster than In. This also improves bandgap temperature stability, and increases the spin-orbit split-off energy, mitigating non-radiative Auger recombination, and making GaAsBi an attractive material for long-wavelength optoelectronic devices.

Both MQW structures were grown via solid-source Molecular Beam Epitaxy (MBE) using a Veeco GENxplor system. The DBR, comprised 30 AlAs/GaAs periods, was designed to centre the MQW emission within the photonic stopband. A gain region with 12 QWs and alternating barrier thicknesses, shown in Figure 1, was adopted to reduce the chip total thickness and improve thermal management. The thicknesses of the barrier were calculated to align the antinodes of the lasing standing wave with the position of the QWs allowing for coupling of enhancing emission.

In the InGaAs based chip the thickness of the QW was 5.7 nm with an indium content of 20% and barrier of 7 nm. The pairs of QWs were separated by 98 nm thick-barrier. While in the gain region based on GaAsBi the QW thickness was 5.5 nm with a bismuth content of around 8% and alternating barrier thicknesses of 7 nm and 150 nm.

Lasing was successfully demonstrated from the InGaAs/GaAs MQW VECSEL at 976 nm, with emission from a 500 μm diameter region. The lasing from the GaAsBi/GaAs MQW VECSEL was observed at 1070 nm, marking the first reported instance of lasing from a GaAsBi based VECSEL.

Lasing characteristics of bismide VECSEL presented in the Figure 2.

This research was funded by the Research Council of Lithuania (LMTLT), agreement No. [S-LT-TW-24-8].

[1] Muszalski Jan, et al., "VECSELs emitting at 976nm designed for second harmonic generation in the blue wavelength region", Proc. SPIE 8702, Laser Technology 2012: Progress in Lasers, 87020A (2013).

[2] Jacquemet Mathieu, et al., "Single-frequency cw vertical external cavity surface emitting semiconductor laser at 1003 nm and 501 nm by intracavity frequency doubling", Applied Physics B, 86(3), 503-510 (2007).

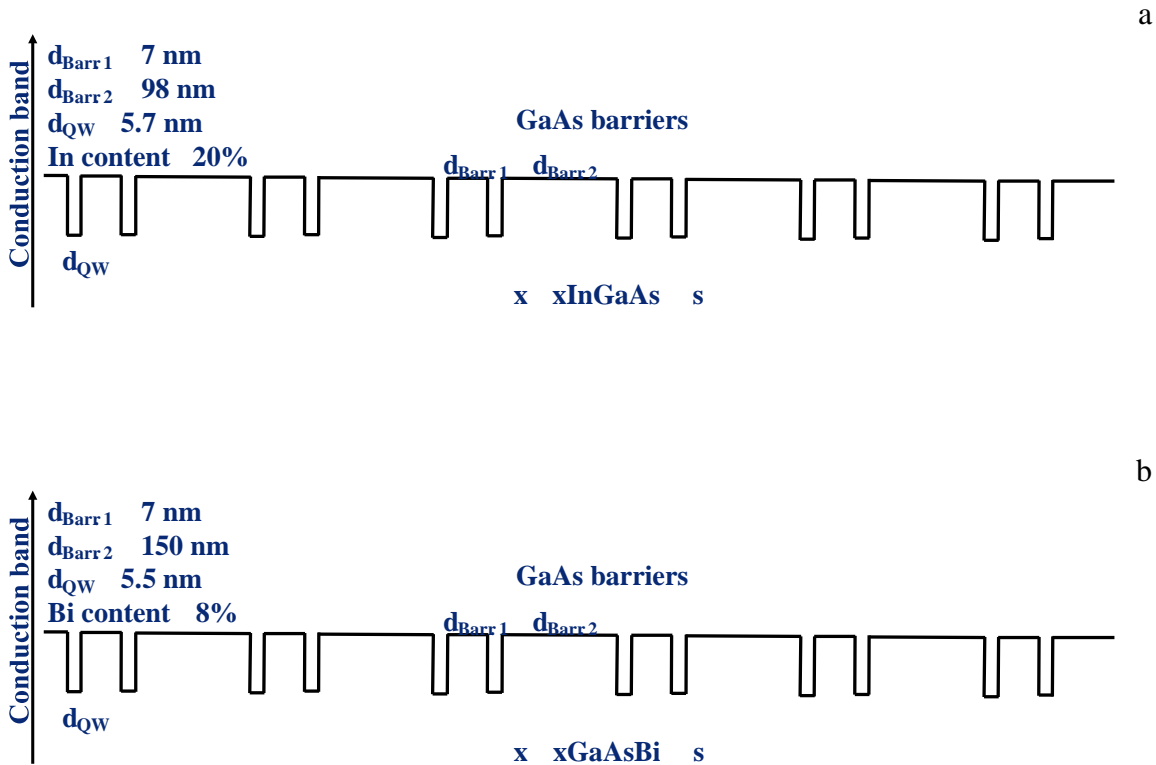


Figure 1: Conduction band scheme of the grown active areas:

a) InGaAs based active area; b) Gain region based on GaAsBi MQW

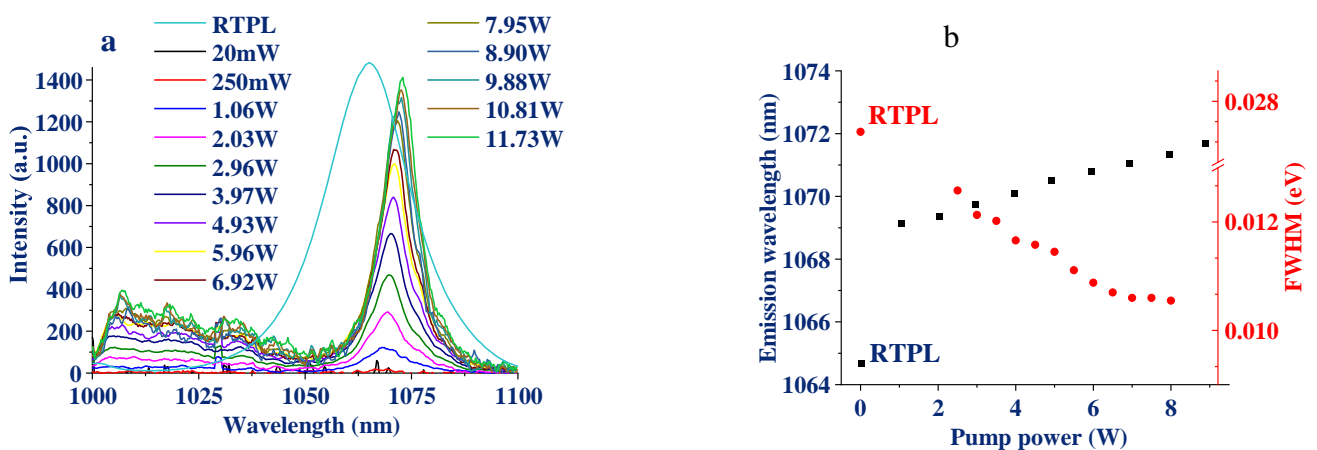


Figure 2: Lasing measurements of the GaAsBi based VECSEL:

a) Lasing spectra at different pumping powers, from PL to lasing;
b) The emission wavelength dependence on pumping power on the left in black,
full width at half maximum (FWHM) in red on the right.



I5: Ultra-Thin Semiconductors: From Epitaxy to Band Engineering and UV Photon Sensing

Amalia Patanè

School of Physics and Astronomy

University of Nottingham, Nottingham NG7 2RD, UK e-mail:

amalia.patane@nottingham.ac.uk

Two-dimensional semiconductors can drive advances in fundamental science and advanced technologies. However, they should be free of any contamination; also, the crystallographic ordering and coupling of adjacent layers, and their electronic properties should be wellcontrolled, tuneable and scalable. Here, these challenges are addressed by a new approach, which combines molecular beam epitaxy and in-situ band engineering in ultra-high vacuum of semiconducting gallium selenide (GaSe) on different platforms [1-2], including graphene to form a heterostructure referred to as 2semgraphene.

In-situ studies by electron diffraction, scanning probe microscopy and angle-resolved photoelectron spectroscopy reveal that atomically-thin layers of GaSe align in the layer plane with the underlying lattice of graphene. The GaSe/graphene heterostructure features a centrosymmetric polymorph of GaSe, a band structure tuneable by the layer thickness, and a charge dipole at the GaSe/graphene interface. Both as-grown and defective GaSe layers are remarkably resilient to oxidation at room temperature. However, a high-temperature annealing of the grown layers in an O-rich environment can promote the chemical transformation and full conversion of GaSe into the crystalline oxide Ga₂O₃ [3]. These features are scalable, as demonstrated experimentally and modelled by density functional theory. The newly-developed 2semgraphene is used to demonstrate ultrathin optical sensors that exploit the photoactive GaSe and the sensitivity of its interface with the graphene channel to photogenerated carriers. Versatile functionalities are demonstrated in GaSe- and oxide-based photon sensors, ranging from electrical insulation to unfiltered deep ultraviolet (UV) optoelectronics [4], unlocking the technological potential of GaSe and its crystalline oxide for a myriad of potential applications.

[1] Shiffa et al. *Small* 20, 2305865 (2024)

[2] Bradford et al. *Small* 20, 2404809 (2024)

[3] Cottam et al. *ACS Applied Nano Materials* 7 (15), 17553 (2024)

[4] Cottam et al. *ACS Photonics* (2025)





S5.1: Epitaxial 2D HfSe₂ Semiconductor/TaSe₂ Metal van der Waals Heterostructure

C. Sthioul,^{1,*} Y. Chernukha,¹ H. Koussir,¹ C. Coinon,¹ G. Patriarche,² L. Thomas,¹ P. Roussel,² B. Grandidier,¹ P. Diener,¹ and X. Wallart¹

¹Univ. Lille, CNRS, Centrale Lille, Univ. Polytechnique Hauts-de-France, Junia-ISEN, UMR 8520 - IEMN, F-59000 Lille, France

² Université Paris-Saclay, CNRS, Centre de Nanosciences et de Nanotechnologies, 91120, Palaiseau, Paris, France

² Unité de Catalyse et de Chimie du Solide (UCCS), Université de Lille, CNRS, Centrale Lille, Université d'Artois, UMR 8181 - UCCS, F-59000 Lille, France

*E-mail: corentin.sthioul@univ-lille.fr

The formation of low resistance electrical contacts on 2D semiconductors remains a challenge and is one of the bottlenecks for their application in devices. Although some successful attempts have been reported [1], the standard contact fabrication by metal deposition often induces defects and damages to the 2D materials, which degrade their intrinsic properties. One way to circumvent that relies on the use of a metallic 2D material allowing a van der Waals interface with the 2D semiconductor. In this work, we focus on such a system involving a metallic (TaSe₂) and a semiconducting (HfSe₂) transition metal dichalcogenide (TMD). HfSe₂ seems promising due to its predicted high carrier mobility [2] whereas TaSe₂ clearly exhibits a metallic character in its 2H phase [3]. Interestingly, a high work function has been reported for both materials and make their association appealing for contact realization [4].

We first optimize the growth of TaSe₂ and HfSe₂ layers on Se-terminated GaP(111)_B substrates. The layers are prepared by MBE under excess Se with a typical growth rate in the 3-4 ML/h range. HfSe₂ crystallizes in the 1T phase whose structural quality is rather independent on the growth temperature within the explored range (250-500°C). By contrast, multilayers TaSe₂ mostly exhibit the 3R and 2H polytypes with an improvement of the film crystallinity with increasing growth temperature and the layers grown between 250°C and 500°C have a resistivity comparable to those reported for bulk TaSe₂. In both cases, diffraction techniques clearly evidence the epitaxial relationships between the GaP substrate and the TMD layer. These latter are preserved during the growth of the HfSe₂/TaSe₂ heterostructure (Fig. 1) and the respective polytypes of each material are clearly identified in the stacking using scanning transmission electron microscopy (Fig. 2). Finally, photoelectron spectroscopy measurements show a n-type doping in HfSe₂ and a small work-function mismatch with TaSe₂ (Fig. 3).

The authors acknowledge the financial support from the Tunne2D (ANR-21-CE24-0030) and ADICT (ANR-22-PEEL-0011) projects, as well as the French technological network RENATECH.

[1] Y. Wang et al., Nature 610, 61 (2022)

[2] W. Zhang et al., Nano Research 7, 1731 (2014)

[3] F. J. Di Salvo et al., Physical Review B 14(4), 1543 (1976).

[4] D. Tsoutsou et al., ACS Appl. Mater. Interfaces 8, 1836–1841 (2016)

- [5] Levinshtein M. et al. (Ed.), *Handbook Series on Semiconductor Parameters*, vol.1, World Scientific, 104-124 (1996)
 [6] Greenaway D. L. et al., *Journal of Physics and Chemistry of Solids* 26(9), 1445-1458 (1965)

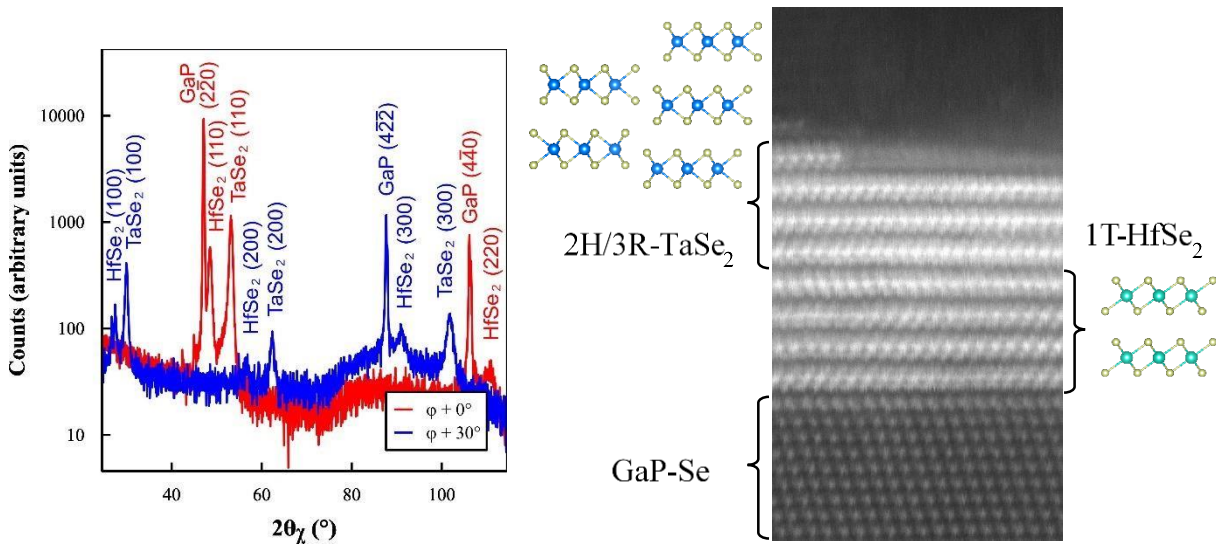


Fig. 1: In-plane grazing incidence X-ray diffraction pattern of a TaSe₂/HfSe₂/GaP heterostructure. The HfSe₂ [1 0 0] // TaSe₂ [1 0 0] // [2-1-1] GaP epitaxial relationship is verified.

Fig. 2: Scanning transmission electron microscopy of a TaSe₂/HfSe₂/GaP heterostructure.

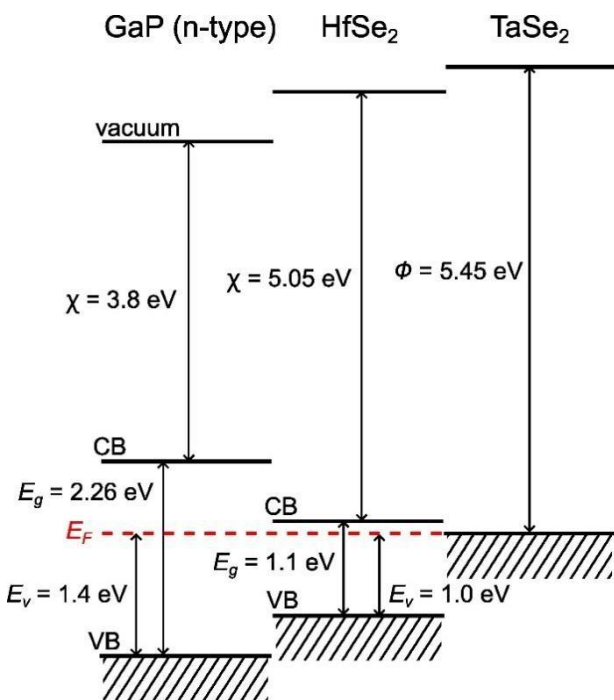


Fig. 3: Band alignments in a TaSe₂/HfSe₂ heterostructure grown on n-type GaP substrates, as derived from X-ray and ultra-violet electron spectroscopy measurements. The GaP electron affinity and band gap energies are from the literature [5,6].



S5.2: Multi-particle Excitonic Systems in WSe₂ Grown on hBN by Molecular Beam Epitaxy

J. Kucharek^{1*}, M. Raczyński¹, R. Bożek¹, A. Kaleta², B. Kurowska², M. Bilaska², S. Kret², T. Taniguchi³, K. Watanabe³, P. Kossacki¹, M. Goryca¹, W. Pacuski¹

¹ *Institute of Experimental Physics, Faculty of Physics, University of Warsaw, 02-093 Warsaw, Poland*

² *National Institute for Materials Science, Tsukuba 305-0047, Ibaraki, Japan* ³ *Institute of Physics, Polish Academy of Sciences, 02-668 Warsaw, Poland*

Monolayer transition-metal dichalcogenides (TMDs) exhibit exceptional optical properties useful for optoelectronic applications. However, for industrial use, large-scale homogeneity optical response is needed. To address this demand we utilize molecular beam epitaxy (MBE). In our previous works, we have achieved super-high quality of MBE grown MoSe₂ on hexagonal boron nitride (hBN) [1] and then we have mixed it with Mn ions and showed that it can lead to the induction of 1T' phase of this material [2]. Here, we report on the WSe₂ grown on hBN by MBE, demonstrating high structural and optical quality on a large-scale. For the first time, multi-particle excitonic systems can be observed in WSe₂ samples fabricated in a bottom-up approach. Monolayers of WSe₂ were grown by MBE on exfoliated hBN flakes that are the best substrate known for TMDs growth. Because of its atomically smooth surface, lack of dangling bonds and uncompensated charges, hBN substrates allows to grow the highest quality monolayers both in terms of optical and structural properties. Before TMD growth, hBN flakes were exfoliated from bulk and deposited on a Si substrate with polycrystalline SiO₂ buffer. Growth has been realised in very easy, two - step process: first deposition at relatively low temperature (300 °C) and then annealing at a high temperature (800 °C) under a high Se flux. WSe₂ was investigated by atomic force microscopy and transmission electron microscopy in crosssection to verify their structural properties. Both techniques confirm that most of the TMD material is observed in the form of one monolayer thin flakes, that covers ~50% of the substrate surface. Both techniques confirm hexagonal structure of the material as well as high crystalline quality. We have used room and low temperature photoluminescence measurements to study optical properties of monolayers. WSe₂ features narrow and resolved spectral lines of neutral and charged exciton as well as wide range of localised excitons present in energies lower than charged exciton. Material exhibits high homogeneity of optical properties within micrometres squared. This is the first MBE grown WSe₂ exhibiting such a high resolution of spectral lines.

[1] *Narrow excitonic lines and large-scale homogeneity of transition metal dichalcogenide monolayer grown by molecular beam epitaxy on hexagonal boron nitride*, W. Pacuski, M. Grzeszczyk, K. Nogajewski, A. Bogucki, K. Oreszczuk, J. Kucharek, K.E. Polczyńska, B. Serebyński, A. Rodek, R. Bożek, T. Taniguchi, K. Watanabe, S. Kret, J. Sadowski, T. Kazimierczuk, M. Potemski, P. Kossacki, *Nano Letters* 20, 3058 (2020).

[2] *Molecular Beam Epitaxy Growth of Transition Metal Dichalcogenide (Mo,Mn)Se₂ on 2D, 3D and polycrystalline substrates*, J. Kucharek, R. Bożek, W. Pacuski, *Materials Science in Semiconductor Processing* 163, 107550 (2023)

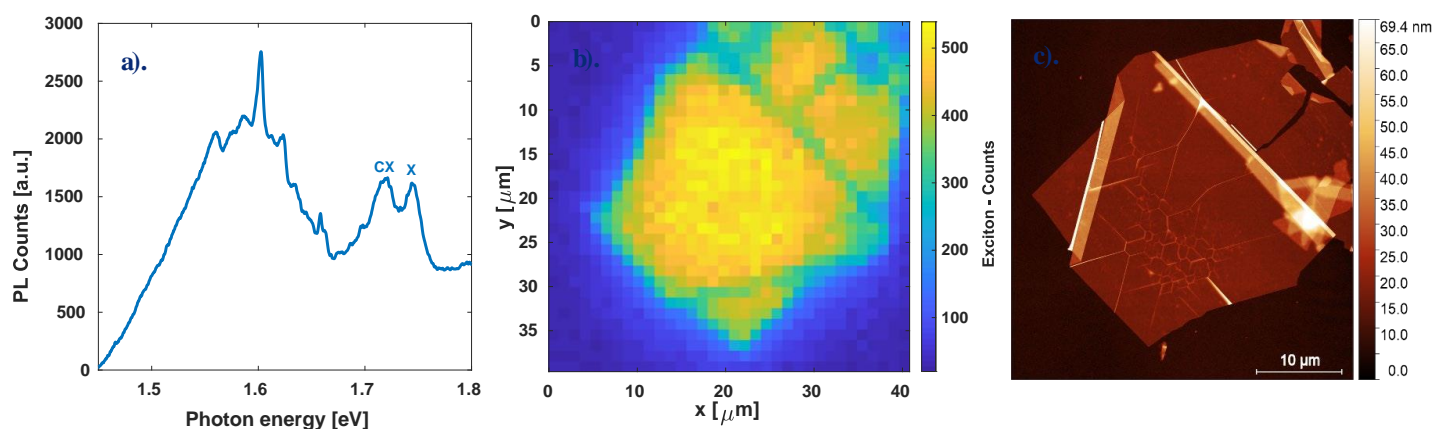


Fig. 1: a). PL spectrum taken in 10 K with 532 nm excitation laser. b). PL map presenting exciton intensity and c). AFM picture mapped in b).



S5.3: Optically active indium selenide crystal phase heterostructures grown by molecular beam epitaxy

P. Wojnar^{1,2*}, M. Wójcik¹, S. Kret¹, P. Baranowski¹, M. Aleszkiewicz¹, J.Z. Domagała¹, S. Chusnutdinow^{1,2}

¹ Institute of Physics, Polish Academy of Sciences, Warsaw, Poland

² International Research Centre MagTop, Institute of Physics, Polish Academy of Sciences, Warsaw, Poland

*E-mail : wojnar@ifpan.edu.pl

Indium selenide attracts the great interest due to its outstanding electronic and photonic properties, such as the excellent photo-responsivity, good electron mobility, robust room temperature ferroelectricity, high Seebeck coefficient and the large band gap tunability depending on the thickness. One of the challenges of fabrication indium selenide is the complexity of its phase diagram. Most of indium selenide crystalline phases belong to the family of two-dimensional (2D) semiconductors which are characterized by strong in-plane covalent bonds and weak interlayer van der Waals forces. Different crystalline phases of indium selenide may be characterized by a significantly different value of the band gap, e.g., the band gap of bulk γ -In₂Se₃ amounts to 2.15 eV and that of bulk γ -InSe to 1.32 eV (at cryogenic temperatures).

In this work we report on the crystal phase control of indium selenide thin layers during a molecular beam epitaxy (MBE) process. It is achieved by changing the growth conditions, such as the growth temperature and the indium to selenium flux ratio, during the growth. In the case of thin layers grown at 350°C on (111)B-GaAs substrate keeping indium to selenium flux ratio of 0.2 an almost perfect γ -In₂Se₃ crystal phase is obtained. This is confirmed by a comprehensive study involving X-ray diffraction and low temperatures photoluminescence which reveals a single emission line at 2.15 eV corresponding well to the bandgap of γ -In₂Se₃. In the next step, the MBE growth is stopped and the indium to selenium flux ratio risen up to 0.5. After the restart of the growth, indium selenide changes its crystal phase which is monitored *in situ* by a distinct change in the reflection of high energy electron diffraction (RHEED) pattern. This observation is consistent with atomic force microscopy, Figure 1, which reveals a remarkable change of the surface morphology: triangular shaped structures with the side lengths of the order of a few μ m and the height of \sim 1.2 nm are characteristic for the growth with the indium to selenium flux ratio of 0.5, while rather oblique structures without any sharp edges - for indium selenide growth with indium to selenium flux ratio of 0.2.

Interestingly, a quite intense optical emission in the near infrared spectral range appears as effect of the growth of the above described indium selenide crystal phase heterostructures, Figure 2. Moreover, it is found that the emission energy exhibits a distinct change depending on the average thickness of the second layer, from 1.1 eV for layers thicker than 20 nm up to 1.2 eV for a layer with the average thickness of 5 nm. This variation is consistent with the quantum size effect influence on the emission energy of thin layers. Furthermore, the photoluminescence lines exhibit a distinct blue shift with increasing excitation fluence. Based on the latter effect the observed optical emission is ascribed to the recombination at the type II interface between the two crystalline phases. Consistent with this interpretation is also the fact that the energy of this transition is lower than both: the bandgap of γ -InSe and the bandgap of γ -In₂Se₃. Inhomogeneity of indium selenide thin layers is investigated by spatially resolved cathodoluminescence revealing changes of max.40 meV of the emission energy depending on the spatial position of the excitation spot.

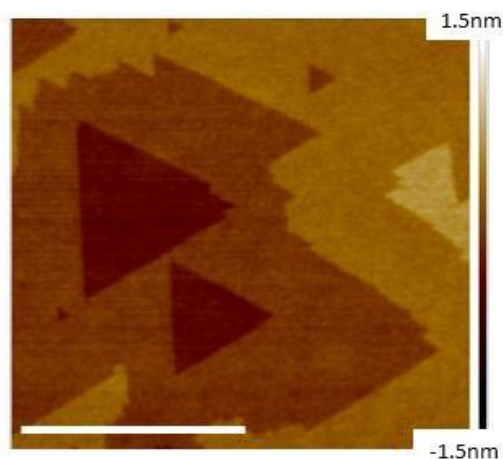


Figure 1 An almost flat surface of an indium selenide layer grown at 450°C with In/Se flux ratio of 0.05 revealed by atomic force microscopy. Atomic steps with the height of 1.2 nm are visible. Scale bar corresponds to 500nm.

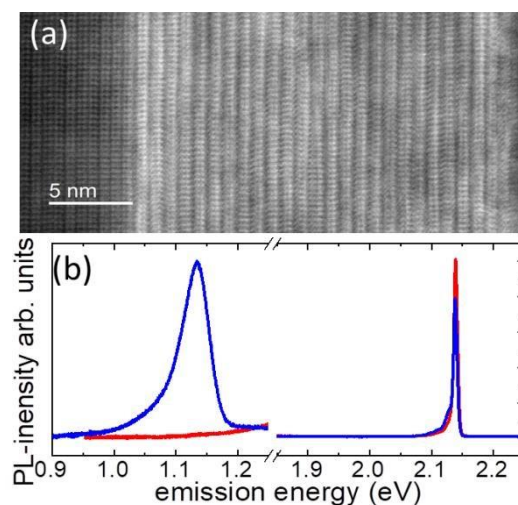


Figure 2 (a) Transmission electron microscopy evidencing the presence of two distinct indium selenide crystalline phases: the γ -In₂Se₃ and γ -InSe on the left and right side of the image, respectively. (b) Photoluminescence spectrum from γ -InSe/ γ -In₂Se₃ heterostructure with the top layer thickness of 17 nm and 60nm, respectively, in blue, compared to the reference γ -In₂Se₃ layer, in red. Temperature of the measurement 10K, excitation 405 nm

This research was partially supported by the Foundation for Polish Science through the IRA Programme “MagTop” no. FENG.02.01-IP.05-0028/23 co-financed by EU from the funds of Priority 2 of the European Funds for a Smart Economy Program 2021–2027 (FENG)



S5.4: High-temperature MBE of hBN for Deep-ultraviolet, Single-photon Emitters and Lateral Heterostructures

T.S. Cheng¹, J. Bradford¹, C.J. Mellor¹, K. Watanabe², T. Taniguchi², I. Aharonovich³, L.F. Zagonel⁴, B. Gil⁵, G. Cassabois⁵, P.H. Beton¹ S.V. Novikov^{1,*}

¹ School of Physics and Astronomy, University of Nottingham, Nottingham, NG7 2RD, UK

² National Institute for Materials Science, 1-1 Namiki, Tsukuba 305-0044, Japan

³ School of Mathematical and Physical Sciences, University of Technology, Sydney, Australia

⁴ Institute of Physics, University of Campinas, UNICAMP, Campinas, 13083-859, Brazil

⁵ Laboratoire Charles Coulomb, CNRS-Université de Montpellier, 34095, Montpellier, France

*E-mail: Sergei.Novikov@nottingham.ac.uk

There has been a surge of interest in hexagonal boron nitride (hBN) due to its technological potential for deep ultraviolet (DUV) photonics, single photon emitters (SPEs) and through its incorporation into van der Waals (vdW) two-dimensional (2D) heterostructures.

We have developed high-temperature molecular beam epitaxy (HT-MBE) of hBN at growth temperatures from 1100°C to 1700°C using high-temperature sublimation and e-beam MBE sources for boron and nitrogen RF-plasma sources. We will discuss our measurements of a direct optical energy gap of ~6.1 eV and electronic band gap of ~6.8 eV in single monolayer hBN. We will demonstrate that the single-photon emitters can be reproducibly produced in hBN layers by C-doping.

Boron has two naturally occurring stable isotopes and the natural mixture contains ¹¹B (80.1%) and ¹⁰B (19.9%). We will explore HT-MBE of h-BN using isotopically enriched (>98%) boron ¹⁰B and ¹¹B with 6N purity.

Recent studies worldwide have focused on the development of novel 2D lateral heterostructures with unique transport and optical properties. Whereas vertical 2D heterostructures can be produced by epitaxy or by exfoliating and stacking of 2D layers, lateral 2D heterostructures can only feasibly be produced by an epitaxial growth process. Sequential HT-MBE growth of hBN, graphene and a second cycle of hBN growth resulted in the formation of lateral hBN-graphene-hBN heterostructures, in which a strip of graphene is laterally embedded between monolayers of hBN.

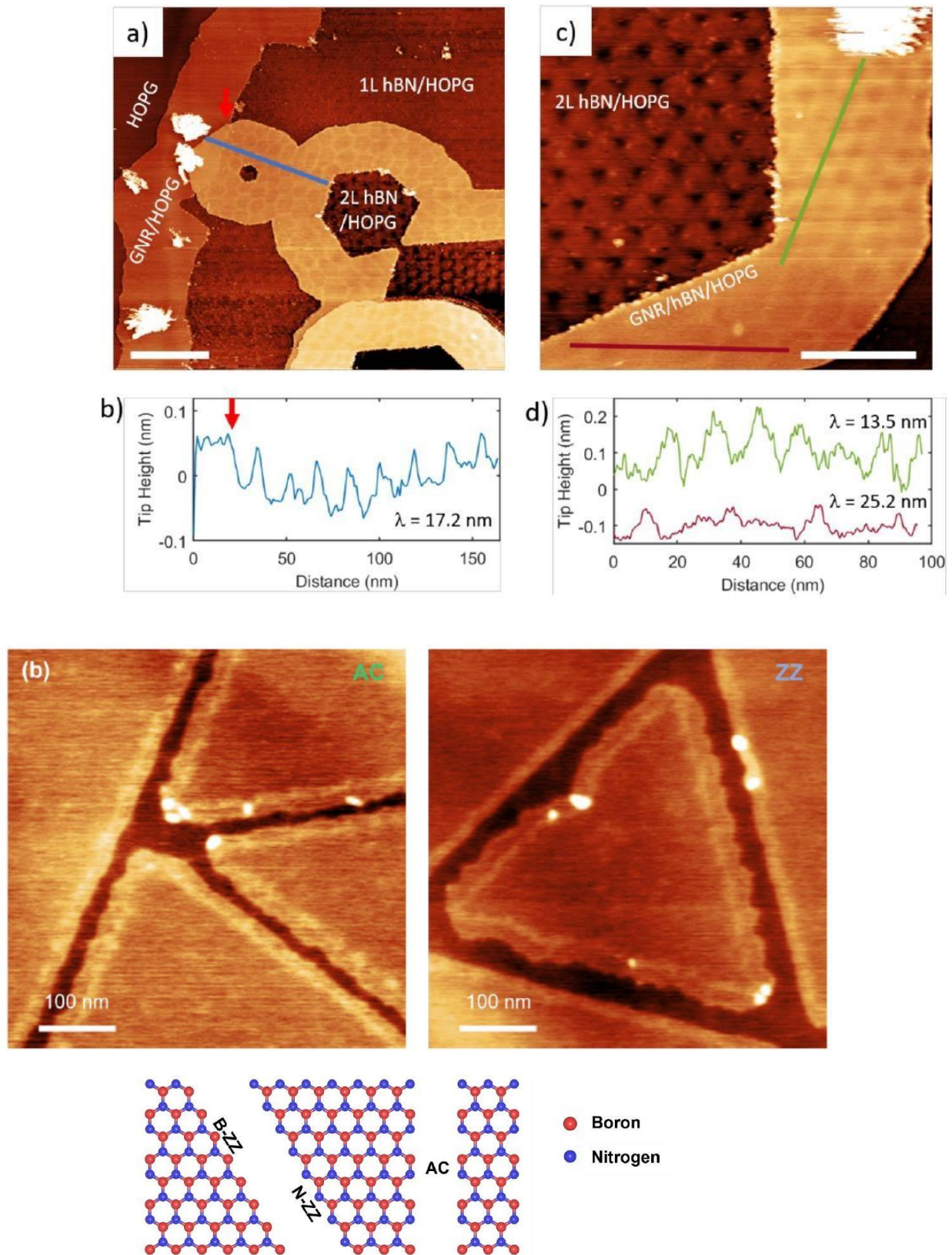


Fig. 1. Graphene (G) - Boron Nitride (hBN) lateral heterostructures.



Tuesday 11.03
Poster session 1



P1.1 AlGaN channel High Electron Mobility Transistors grown by NH₃-MBE on Silicon substrates

Antoine BARBIER-CUEIL, Stephanie RENNESSON, Jash MEHTA, Farid MEDJDOUB and Fabrice SEMOND

*Université Côte d'Azur, CNRS, CRHEA, Rue Bernard Gregory, F-06905 Sophia Antipolis, France
EasyGaN SAS, Rue Bernard Gregory, F-06905 Sophia Antipolis, France,
CNRS-IEMN, Av. Poincaré, F-59650 Villeneuve d'Ascq, France*

P1.3 AlScN alloys as pseudo-substrate for InGaN

J. Schörmann, S.A. Jentsch, M.F. Zscherp, M. Stein, F. Meierhofer, C. Margenfeld, A. Waag, and S. Chatterjee
*Institute of Experimental Physics I and Center for Materials Research, Justus-Liebig-University Giessen, D-35392 Giessen, Germany
Institute of Semiconductor Technology and Nitride Technology Center (NTC), Technische Universität Braunschweig, D-38106 Braunschweig, Germany*

P1.5 Empirical Study of the Impact of Process Deviations on Structure and Performance of MIR-QCL for Volume Production

T. Meyer, R. Aidam, K. Frei, S. Giudicatti, M. Haertelt, S. Hugger, R. Keil, L. Kirste, M. Prescher, R. Trejo-Hernández and Q. Yang

Fraunhofer IAF, Freiburg, Germany

P1.7 Fermi level control by above band gap illumination during molecular beam epitaxy growth of Mg-doped GaN

Brault Julien, Shetty Sankesh, Mitra Sunanda, Ibanez Alexandra, Valvin Pierre, Konczewicz Leszek, Matta Samuel, Chenot Sebastien, Leroux Mathieu, Al Khalfioui Mohamed, Contreras Sylvie, Cassabois Guillaume and Gil Bernard

*Université Côte D'azur, CNRS, CRHEA, France
L2C and Université Montpellier 2, France*

P1.9 GaN/AlGaN quantum wells grown on high-quality GaN substrates in the perspective of indirect exciton diffusion

B. Damilano, R. Aristégui, H. Teisseyre, S. Vézian, V. Guigoz, A. Courville, I. Florea, D. Lefebvre, P. Vennéguès, M. Bockowski, T. Guillet, M. Vladimirova

*Université Côte d'Azur, CNRS, CRHEA, Valbonne, France
Laboratoire Charles Coulomb (L2C), University of Montpellier, CNRS, Montpellier, France
Institute of Physics, Polish Academy of Sciences, Warsaw, Poland
Institute of High-Pressure Physics, Polish Academy of Sciences, Warsaw, Poland*

P1.11 Growth and optimization of N-polar GaN epilayers on silicon substrates using ammonia-MBE and a hybrid NbN/AlN buffer layer

A. Pedeches, H. Rotella, I. Florea, M.P. Chauvat, P. Vennéguès and F. Semond

*Université Côte d'Azur, CNRS, CRHEA, France
CIMAP, ENSICAEN, France*

P1.13 Growth of InAlN/NbN Heterostructures in Indium-rich Conditions by Plasma Assisted MBE

Wolny Paweł, Lachowski Artur, Chlipała Mikołaj, Dybko Krzysztof, Nowakowski-Szkudlarek Krzesimir, Skierbiszewski Czesław

*Institute of High Pressure Physics PAS, Sokolowska 29/37, 01-142 Warsaw, Poland
Institute of Physics PAS, Al. Lotników 32/46, 02-668 Warsaw, Poland*

P1.15 High Resolution Temperature Mapping of Intentionally Induced Thermal Gradients on GaSb Wafers during Growth

Sascha R. Valentin, Timo A. Kurschat, Peter Zajac, Rainer Krage, Arne Ludwig, and Andreas D. Wieck

*Gesellschaft für Gerätebau mbH, Klönnestr. 99, 44143 Dortmund, Germany
Lehrstuhl für Angewandte Festkörperphysik, Ruhr-Universität Bochum, Germany*



P1.17 Influence of growth temperature and scandium concentration on the oxidation of ScAlN films grown by molecular beam epitaxy

V. Gallardo-Mödinger, F. Georgi, C. Elias, Y. Cordier, and M. Hugues

Université Côte d'Azur, CNRS, CRHEA, rue B. Gregory, 06560 Valbonne, France

Mines Paris, PSL University, Center for Material Forming (CEMEF), UMR CNRS, 06904 Sophia Antipolis, France

P1.19 Investigation of the effect of GaAs substrate orientations and doping on the electrical and optical properties of InGaP solar cell structures

S. Alotaibi, M. A. Correa, A. Almalki, S. Alhassan, M. Alhuways, Y. Galvão Gobato, H. Sodabanlu, M. Sugiyama, H. V. A. Galetj, M. Henini

School of Physics and Astronomy, University of Nottingham, Nottingham, UK

Physics Department, Shaqra University, Saudi Arabia *3 Electrical Engineering Department, Federal University of São Carlos, São Carlos-SP, Brazil*

Physics Department, Taibah University-Yanbu, Yanbu El-Bahr, Saudi Arabia

School of Physics, College of Science, Jouf University, Saudi Arabia

Department of physics, Princess Nourah bint Abdulrahman University, Riyadh, Saudi Arabia

Physics Department, Federal University of São Carlos, São Carlos-SP, Brazil

School of Engineering, University of Tokyo, Tokyo, Japan

P1.21 Metal-Modulated Growth of Cubic, Red Emitting InGaN Layers and Self-Assembled InGaN/GaN Quantum Wells by Molecular Beam Epitaxy

Silas A. Jentsch, Mario F. Zscherp, Vitalii Lider, Fabian Winkler, Andreas Beyer, Jürgen Belz, Nicolai M. Gimbel, Markus Stein, Donat J. As, Anja Henss, Kerstin Volz, Sangam Chatterjee, and Jörg Schörmann

Institute of Experimental Physics I and Center for Materials Research, Justus Liebig University Giessen, D-35392 Giessen, Germany

Materials Science Center and Faculty of Physics, Philipps-University Marburg, D-35032 Marburg, Germany

Department of Physics, Paderborn University, D-33098 Paderborn, Germany

P1.23 Photoluminescence investigation of the annealing effects on GaAsBi quantum wells with parabolic AlGaAs barriers

A. Štaupienė, A. Špokas, A. Zelioli, B. Čechavičius, R. Butkutė and E. Dudutienė

SRI Center for Physical Sciences and Technology, Saulėtekio av. 3, Vilnius, Lithuania

P1.25 Production of mm-Wave epiwafers of GaN on Si grown by NH₃-MBE

Abdennacer Benali, Elodie Carneiro, Lyes Ben Hammou, Kathia Harrouche, Etienne Okada, Sebastian Tamariz, Stéphanie Rennesson, Farid Medjdoub and Fabrice Semond

EasyGaN SAS, Rue Bernard Gregory, 06905 Sophia Antipolis, France

CNRS-IEMN, Av. Poincare, F-59650 Villeneuve d'Ascq, France

Université Côte d'Azur, CNRS, CRHEA, Rue Bernard Gregory, F-06905 Sophia Antipolis, France

P1.27 Short wavelength infrared avalanche photodiode beyond 2.0 μm based on InGaAs/GaAsSb superlattice as the absorber

Peng Cao, M. Bentley, Hongling Peng, Yidan Hu, Wanhua Zheng and Q.D. Zhuang,

Laboratory of Solid State Optoelectronics Information technology, Institute of

Semiconductors, Chinese Academy of Sciences, Beijing, China

Physics Department, Lancaster University, Lancaster, UK

P1.29 Silicon epitaxy using trisilane

M. A. Pampillón, M. Martín-Bravo, M. J. Hernández, M. Cervera, B. J. García

Grupo de Electrónica y Semiconductores (ElySe) Dpto. Física Aplicada, Instituto Nicolás Cabrera (INC), Centro de Investigación Avanzada en Física Fundamental (CIAFF)

Universidad Autónoma de Madrid, C/ Francisco Tomás y Valiente 7, 28049, Madrid, Spain

P1.31 Automated growth of DBR supervised by in-situ spectral reflectance measurement

P. Gadrás, K. Ben Saddik, L. Bourdon, Q. Gravelier, A. Arnoult, G. Almuneau

LAAS-CNRS, Toulouse, France



P1.33 Key Points of Compound Semiconductor Material Evaluation by High resolution XRD

S. Ibrahimkuty

Rigaku Europe SE, Hugenotten alle 167, 63263 Neu-Isenburg, Germany

P1.35 Manufacturing of Three Terminal Heterojunction Bipolar Solar Cells based on AlGaAs grown by MBE

I. Artacho, S.A. Svatek, E. Antolín and A. Martí

Instituto de Energía Solar, Universidad Politécnica de Madrid, Madrid, Spain

P1.37 NIR Diode Emitters for Applications in Biophotonics

A. Špokas, A. Zelioli, V. Bukauskas, M. Kamarauskas, E. Dudutienė, B. Čechavičius,
A. Bičiūnas, J. Spigulis, Y-J. Chiu and R. Butkutė

Center for Physical Sciences and Technology, Vilnius, Lithuania

University of Latvia, Riga, Latvia

National Sun Yat-Sen University, Kaohsiung, Taiwan

P1.39 Progress towards closed cycle AI controlled MBE systems

F. Bastiman, H. Karakachian, B. Gerace, K. Strandemar

Scienta Omicron GmbH, Limburger Strasse 75, 65232 Taunusstein, Germany

Scienta Omicron Inc. 3222 E. 1st Ave, #521, Denver, CO 80206 United States

Scienta Omicron AB, Danmarksgratan 22, 75323 Uppsala, Sweden

P1.41 Growth and optical properties of $\text{Al}_{1-x}\text{Ga}_x\text{As}_{0.56}\text{Sb}_{0.44}$ on InGaAs/InP

P. Patil, E. Clarke, T. Fordos, P. Fry, J. Heffernan

EPSRC National Epitaxy Facility, University of Sheffield, Sheffield S3 7HQ, United Kingdom

Nanotechnology Centre, VŠB - Technical University of Ostrava, 17. listopadu 15, 708 00 Ostrava - Poruba, Czech Republic

IT4Innovation, VŠB - Technical University of Ostrava, 17. listopadu 15, 708 00 Ostrava - Poruba, Czech Republic

Department of Electronic and Electrical Engineering, University of Sheffield, Sheffield S1 4DE, United Kingdom

P1.43 In-situ measurement of AlAs growth rate by magnification inferred curvature method

K. Ben Saddik, G. Almuneau, P. Gadras, B. Reig, and A. Arnoult

LAAS-CNRS, Université de Toulouse, CNRS, 31400 Toulouse, France

P1.45 In situ control of GaN growth rate in nitrogen limited regime

Matteo Canciani, Oksana Koplak, Sergio Bietti, Stefano Sanguinetti, Stefano Vichi

University of Milano-Bicocca, Via R. Cozzi, 55, Milano, Italy



I6: III-Nitrides NWs based μ LEDs: a solution for AR display technology

Benoît Amstatt¹, Walf Chikhaoui¹, Marion Gruart¹, Ivan-Christophe Robin, Pierre Tchoulfian¹, Pascal Guénard¹, Mehdi Daanoune¹ and Philippe Gilet¹

¹ALEDIA, Rue des Lavières ZAC Saut du
Moine
38800 Champagnier
Benoit.Amstatt@aledia.com

The major challenges of micro-displays for augmented reality (AR) are to find ways of drastically increasing the amount of lumens provided to the user eyes via an optical system. The projector form factor has to be as small as possible while keeping the power consumption as low as possible.

Micro-LED micro-displays can potentially meet those requirements because the brightness of micro-LEDs can be several orders of magnitude higher than the competitive technologies such as OLED or LCOS, and with an excellent contrast ratio. However, most of the micro-LED technologies experience efficiency loss when reducing the size of the micro-LEDs, provide a lambertian emission, which limits the coupling efficiency with an optical waveguide and need complex processes such as junction stacking or color conversion for RGB array manufacturing. Those issues limit the capability of those micro-LED technologies to produce efficient and cost competitive RGB micro-displays.

Aledia has developed a technology based on the epitaxy of GaN NanoWires (NWs), allowing the growth on 200mm to 300mm Si substrates. By its know-how in epitaxy, Aledia has succeeded in combining two epitaxy worlds, Metal Organic Chemical Vapor Deposition (MOCVD) and Plasma Assisted-Molecular Beam Epitaxy (PA-MBE) to develop this specific technology. Thanks to the unique combination of NWs and PA-MBE characteristics, Aledia is able to grow in the same epitaxy run, Red, Green and Blue active regions of a RGB array. The pixels and subpixels are constituted of array of NWs (Figure 1), which prevents EQE reduction with size, enabling to target subpixels down to 1.25 μ m. This allows to drastically reduce the size of a micro-LED micro display and the RGB light engine.

Moreover, the periodic arrangement of the NWs in the subpixels allow to obtain a photonic crystal effect that greatly increases the directivity of the emission of the subpixels. The amount of lumens emitted in +/- 20° around the normal of the microdisplay can be increased up to a maximum theoretical factor of 8 compared to a Lambertian emission, without the use of micro-lenses.

In this paper we will present RGB devices obtained in a single epitaxy run and show the directional emission of our GaN NWs based LEDs grown on Si wafers. We will emphasize how PA-MBE can revolutionize the RGB Augmented Reality world.

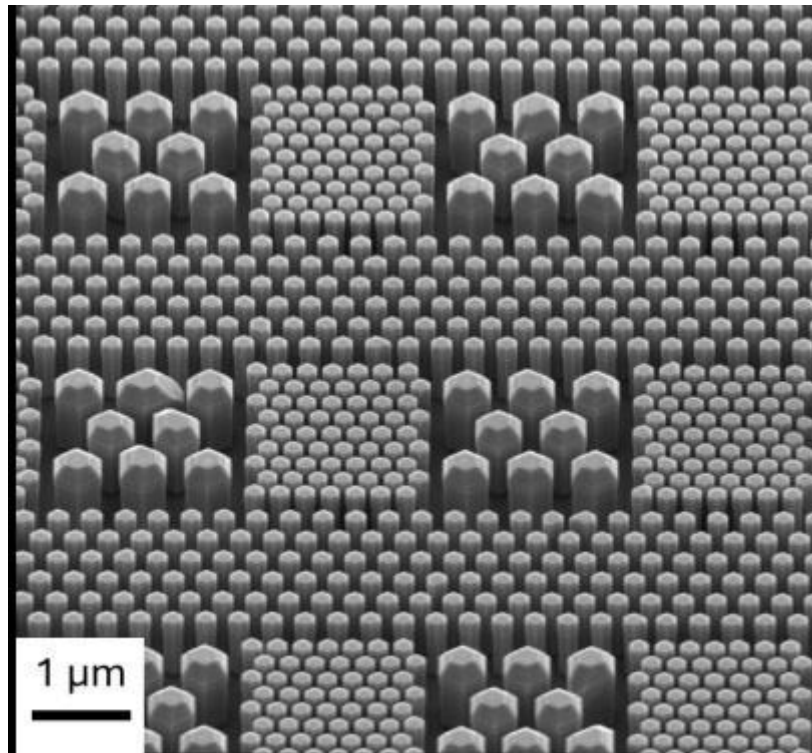


Figure 1: Bird view SEM image of Aledia 2 μm subpixel pitch Native Color NWs grown on Si



S6.1: Emerging Growth Opportunities for GaN Using Molecular Beam Epitaxy (MBE): From Research to Production

S. Matta,^{1,*} R. Roger,¹ S. Rennesson,² F. Semond^{2,3} and J-L. Guyaux¹

¹RIBER SA, 31 Rue Casimir Périer 95873 Bezons France

²EasyGaN SAS, Rue Bernard Grégory, Sophia Antipolis, 06560, France

³Université Côte d'Azur, CNRS, CRHEA, Sophia Antipolis, 06560, France

*E-mail: smatta@riber.fr

Gallium Nitride (GaN) is a wide-bandgap semiconductor with exceptional properties, making it an ideal material for the new generation of optoelectronic and electronic devices such as UV LEDs, micro-LEDs, and RF components [1]. Molecular Beam Epitaxy (MBE) has proven to be an effective method for growing high-quality III-Nitride epilayers [2,3] due to its precise control over layer thickness, composition, purity and low growth temperature. This abstract explores the emerging growth opportunities for Nitride MBE production Machines, with a particular focus on the competitive advantages it offers in the development of next-generation of devices.

We highlight the Riber MBE 49 Nitride Production system (compatible with 1x200 mm and 3x4'' wafers), a fully automated hybrid production platform that is compatible with both ammonia and nitrogen plasma sources [4]. This system facilitates the production of high-quality GaN based layers with exceptional purity, crystal quality and uniformity. Optimizing the new generation of MBE production machines for Nitride applications permit the growth from research to large-scale production, supporting applications in optoelectronics and electronics fields.

Key results from the MBE 49-GaN system demonstrate the potential of this technology. Specifically, we report the dedicated MBE component developed for nitrides production machines, the layer thickness and composition uniformity $\leq \pm 2\%$ (with capabilities to reach uniformity $\leq \pm 1\%$) on 200 mm wafers. Additionally, high-purity GaN films with excellent crystal quality were confirmed through a combination of Secondary Ion Mass Spectrometry (SIMS), X-ray Diffraction (XRD), and Photoluminescence (PL) measurements.

These results confirm the system's ability to produce highly uniform, GaN based layers suitable for advanced applications.

The MBE 49-GaN system can also play a key role in the production of high-quality GaN/AlN based layers on silicon substrates [2], offering improved breakdown voltages, and reduced the RF losses. This makes the MBE 49-GaN system an optimal solution for high-volume production of next-generation GaN-based devices, driving the future of optoelectronic and electronic technologies.

The authors would like to thank CRHEA/CNRS team for the collaboration work on the MBE49-GaN.

[1] Mishra, U.K.; Parikh, P.; Wu, Y.F. AlGaIn/GaN HEMTs—An overview of device operation and applications. Proc. IEEE 2002, 90, 1022–1031.

[2] E. Carneiro et al., Electronics, 12, 2974 (2023) ;

[3] Y. Liao et al., Applied Physics Letters, 98(8),081110, (2011) ;

[4] https://www.semiconductor-today.com/news_items/2023/oct/riber-171023.shtml;

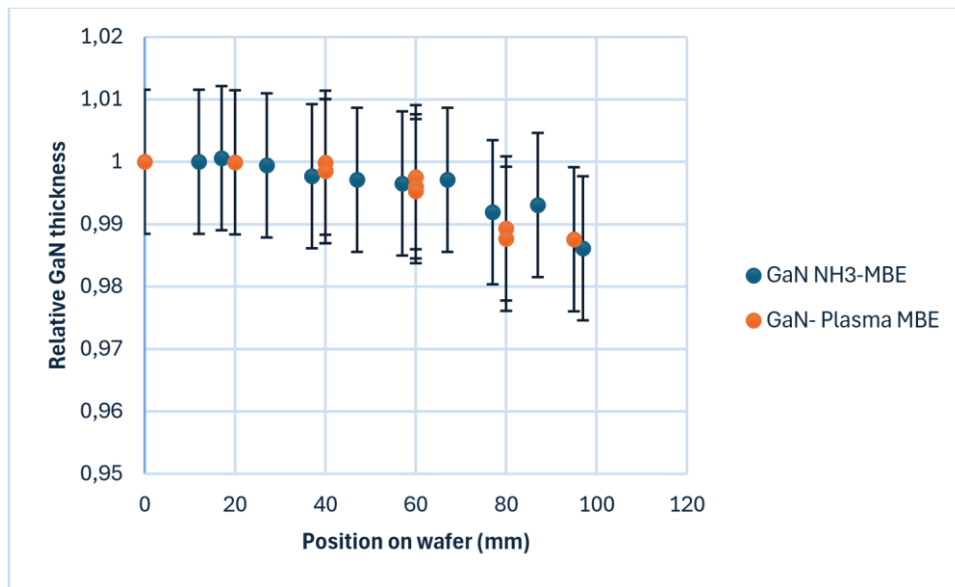


Figure 1. Uniformity of GaN thickness grown by plasma and NH₃ assisted MBE on a 200 mm Si wafer



Figure 2. 200mm GaN grown by MBE

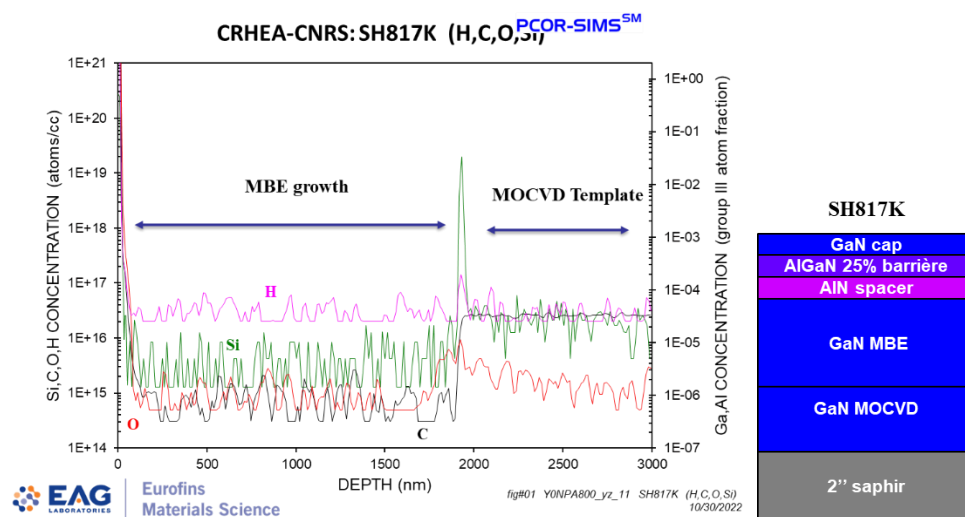


Figure 3. SIMS measurement of a HEMT structure grown by MBE on a GaN template grown by MOCVD



S6.2: GaN Power HEMT with Breakdown Voltage >800 V Grown by MBE

ZC Yang,^{1,*} YQ Wang,¹ JG Zhuang¹, and Eason Liao¹

¹ MASSPHOTON LIMITED, Hong Kong SAR

*zcy@massphoton.com

We report GaN power HEMT with breakdown voltage >800 V grown by MBE on sapphire. High breakdown voltage >800 V is obtained by using ultra-thin AlN buffer grown by MBE and one gate field plate structure technique. MBE technique enables dopant-free buffer layer and pseudomorphic growth of epilayers, which is beneficial to the high reliability of GaN power HEMT. One gate field plate technique helps reduce the total cost of fabrication and also contribute to the high reliability of GaN power HEMT. These merits shows the potential of the reported GaN power HEMT in the applications of high power electronics [1].

The schematic epitaxy structure of GaN power HEMT is shown in Fig. 1 (a). Plasma-assisted MBE was employed to fabricate the complete HEMT structure on a sapphire substrate. 1 μm AlN buffer layer [2], AlGaIn layers with Al compositions of 70%, 50% and 20%, GaN channel layer, 1 nm AlN spacer, 24nm 30% AlGaIn and 10 nm *in-situ* SiN were sequentially grown on the sapphire substrate. The schematic cross section of GaN power HEMT is shown in Fig. 1 (b). Source/drain ohmic contacts with typical contact resistance of 1.2 $\Omega\cdot\text{mm}$ were obtained with Ti/Al/Ni/Au (20/120/30/50 nm) and rapid thermal annealing at 800 $^{\circ}\text{C}$ in N_2 for 30 s. One gate field plate structure (GS and GT) was formed with 120 nm gate recess in the 150nm thick ICP-CVD SiN layer with gate length of ~ 2 μm and gate field plate metal of Ti/Al/Ti (30/500/30 nm) with field plate length of ~ 9 μm . The gate drain spacing Lgd was ~ 22 μm . Interconnection M1 to the ohmic contacts was formed by Ti/Al/Ti (30/1000/30 nm) through via holes V0.

The fabricated normally-on GaN HEMT exhibits an on-state current of ~ 160 mA/mm and a ON-resistance of 44 $\Omega\cdot\text{mm}$ at drain bias $V_{\text{ds}} = 10$ V and gate bias $V_{\text{gs}} = 0$ V, as shown in Fig. 2 (a). The device shows threshold voltage of ~ 30 V and low gate leakage current below 1 $\mu\text{A}/\text{mm}$ at drain bias of ~ 5 V, as shown in Fig. 2 (b). The insitu SiN grown by MBE suppresses the interfacial defects and thus enables the low gate leakage and device operation. The relatively high ON-resistance is due to the thin GaN channel and a back barrier of 8% AlGaIn. Increasing the channel thickness and barrier composition and further optimization of the growth will lead to lower ON-resistance. Off-state characteristics is shown in Fig. 3. Off-state leakage less than 10 $\mu\text{A}/\text{mm}$ was achieved at gate-drain voltage of 800 V, showing a breakdown voltage greater than 800 V. The relatively high breakdown voltage with one gate field plate structure shows the promise of the fabricated GaN HEMT in the applications of high power electronics with low cost.

References

- [1] Zhibo Cheng et al., IEEE Transactions on Electron Devices, vol.71, no.12, pp.7689-7695, 2024.
- [2] Junbo Wang et al., IEEE Transactions on Electron Devices, vol.71, no.11, pp.6609-6615, 2024.

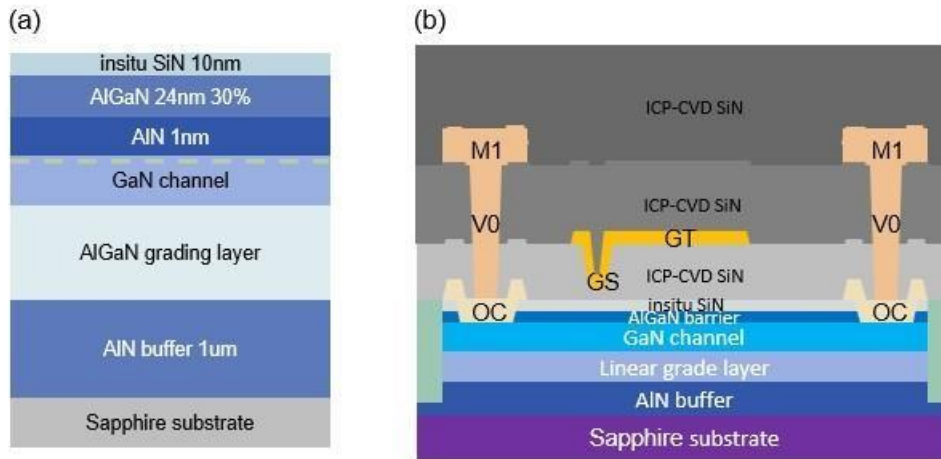


Fig. 1: Schematic (a) epitaxy structure grown by MBE and (b) cross section of GaN power HEMT

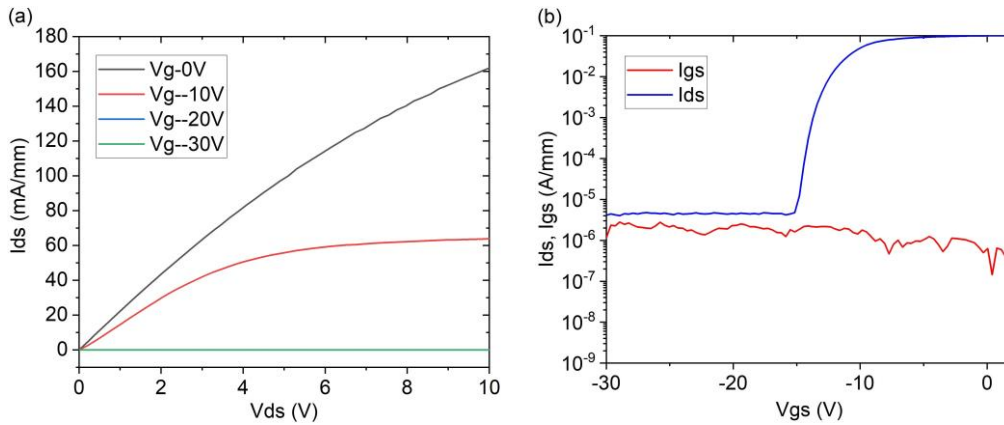


Fig. 2: (a) Output (a) and (b) transfer characteristics of GaN power HEMT grown by MBE

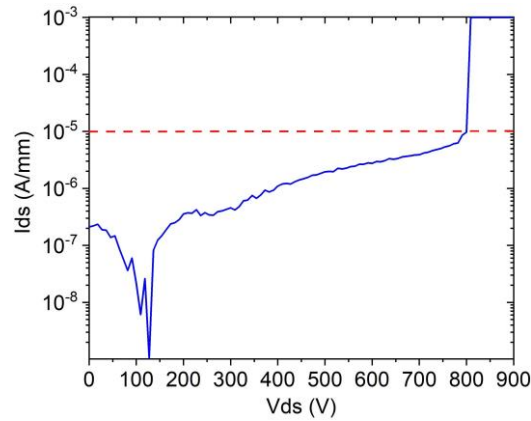


Fig. 3: Breakdown properties of GaN power HEMT grown by MBE



Tuesday 11.03

19h30

DEBATE & COCTAIL-BUFFET

“Why and how could be achieved MBE at lower economic and ecological costs ?”

Movie Theater Le Riounet

Bd Georges Pompidou, 06660 Auron



Invited talk : 23min + 7min questions
 Oral : 15min + 5min questions



Wednesday, 12.03	
08:00	Registration
Session 7 : Quantum: chairman Mark Hopkinson	
08:30	Invited talk I7: Hybrid Josephson junctions (JJs) realized in superconductor - semiconductor heterostructures , <u>Werner Wegscheider</u> , <i>Advanced Semiconductor Quantum Materials Group, Solid State Physics Laboratory and Quantum Center, ETH Zürich, CH-8093 Zürich, Switzerland</i>
09:00	S7.1: Selective area epitaxy of in-plane HgTe nanowires on CdTe(001) substrate , <u>Philippe Ballet</u> , <i>CEA, LETI, Univ. Grenoble Alpes, 38000 Grenoble, France</i>
09:20	S7.2: Superconductor-semiconductor hybrids for quantum technologies: looking for alternatives to Al , <u>Moïra Hocevar</u> , <i>Univ. Grenoble-Alpes, CNRS, Inst. NEEL, 38042 Grenoble, France.</i>
09:40	S7.3: MBE growth of parallel hybrid semiconductor-superconductor nanowires for quantum devices , <u>Raphaël Rousset-Zenou</u> , <i>Univ. Grenoble-Alpes, CNRS, Inst. NEEL, 38042 Grenoble, France.</i>
10:00	S7.4: Metamorphic InAs 2DEGs for quantum computation platforms , <u>Davide Curcio</u> , <i>CNR - Istituto Officina dei Materiali (IOM), 34149 Trieste, Italy</i>
10:20	break
Session 8: Novel materials - Topological : Chairwoman Esperanza Luna	
10:40	Invited talk I8: The birth of ferroelectric topological insulators , <u>Gauthier Krizman</u> , <i>Laboratoire de Physique de l'Ecole normale supérieure, ENS, Université PSL, CNRS, Sorbonne Université, Paris, France</i>
11:10	S8.1: MBE growth of Ge-doped PbSe ferroelectric Rashba semiconductor , <u>Tetiana Zakusylo</u> , <i>Institute of Semiconductor and Solid State Physics, Johannes Kepler University, Linz, Austria</i>
11:30	S8.2: AlN/NbN epitaxial heterostructures on Si: polytypes, strain and polarity , <u>I.Florea</u> , <i>Université Côte d'Azur, CNRS, CRHEA, Valbonne, FRANCE</i>
11:50	S8.3: Mutual Exchange Growth of Zintl Eu₃In₂As₄ and Eu₅In₂As₆ Nanowires by Molecular Beam Epitaxy <u>Man Suk Song</u> , <i>Department of Condensed Matter Physics, Weizmann Institute of Science, Rehovot, Israel</i>
12:10	22nd EuroMBE Group Photo
12:30	Lunch Boxes
16:00	Poster session 2
Session 9: New Concepts : Chairman Sergei Novikov	
17:30	Invited talk I9: Machine Learning for the simulation of strained-film growth: tackling longtime scales with Finite Element Method accuracy , <u>D. Lanzoni</u> , <i>Department of Physics, Università di Genova, Italy</i>
18:00	
18:20	
18:40	
19:00	
20:00	Riber user meeting - Banquet



17: Hybrid Josephson junctions (JJs) realized in superconductor - semiconductor heterostructures

Werner Wegscheider*

*Advanced Semiconductor Quantum Materials Group
Solid State Physics Laboratory and Quantum Center
ETH Zürich, CH-8093 Zürich, Switzerland *werner.wegscheider@phys.ethz.ch*

Semiconductor-superconductor hybrid structures ranging from quasi 1D-nanowires to 2D electron gases (2DEGs) serve as a platform to study interactions between confined electronic states and superconductivity, including phenomena such as Andreev Bound States and Majorana Fermions. Realizing highly transparent interfaces in these systems is essential for the exploration of their physics. Traditionally, hybrid materials like epitaxial Al on InAs have dominated due to their high-quality interfaces achieved through in-situ deposition. However, their relatively small superconducting gap and limited operating range in temperature and magnetic field have motivated exploration of alternative superconductors.

In this work, we present a novel hybrid material platform based on Nb, NbTi and NbTiN as superconductors, leading to a larger superconducting gap and enhanced resilience to magnetic fields. A significant challenge in combining III-V semiconductors with Nb-based superconductors lies in the formation of amorphous interfaces. To address this, we introduced a thin Al interlayer, which provides an epitaxial connection between shallow InAs 2DEGs and the superconducting thin films deposited via magnetron sputtering. Guided by scanning transmission electron microscopy, we optimized the material stack, achieving a highly crystalline interface with a well-defined epitaxial relationship.

Transport measurements of Josephson junctions fabricated from this hybrid material show an induced superconducting gap, nearly five times higher than typical Al-based hybrids and only twice smaller than bulk Nb. This result demonstrates the formation of a highly transparent interface and establishes the potential of Nb-based hybrids as a high-quality material platform for advanced superconducting devices. Furthermore, 2DEG platforms allow for versatile device geometries beyond standard two-terminal designs. Recent advancements in multi-terminal Josephson junctions have revealed rich physics, including spin-splitting effects, ground-state parity transitions, and synthetic Andreev band structures, potentially hosting topological states.

This work highlights the pivotal role of interface engineering in hybrid systems and introduces a robust methodology to maximize the induced superconducting gap, opening pathways for exploring novel quantum phenomena in semiconductor-superconductor platforms.

Work done in collaboration with: Sjoerd Telkamp, Tommaso Antonelli, Clemens Todt, Manuel Hinderling, Marco Coraiola, Peng Zeng, Rüdiger Schott, Erik Cheah, Christian Reichl, Fabrizio Nichele, Filip Křížek and Zijin Lei

Acknowledgements: Stefan Fält for technical support and M. Sousa (IBM) via the Binning and Rohrer Nanotechnology Center (BRNC) for TEM support.

Funding: Swiss National Science Foundation (SNSF) through the National Center of Competence in Research Quantum Science and Technology (QSIT).





S7.1: Selective area epitaxy of in-plane HgTe nanowires on CdTe(001) substrate

P. Ballet^{1,*}, N. Chaize,¹ X. Baudry,¹ P-H. Jouneau², E. Gautier², Y. Deblock³, B. Grandidier³,
L. Desplanque³ and H. Sellier⁴

¹CEA, LETI, Univ. Grenoble Alpes, 38000 Grenoble, France

²Univ. Grenoble Alpes, CEA, INAC-MEM, 38000 Grenoble, France

³Univ. Lille, CNRS, Centrale Lille, Univ. Polytechnique Hauts-de-France, Junia-ISEN, UMR
8520 - IEMN, F-59000 Lille, France

⁴Univ. Grenoble Alpes, CNRS, Institut Néel, 38000 Grenoble, France *E-mail:
philippe.ballet@cea.fr

Topologically protected system as HgTe/CdTe [2] are of great interest for the future of electronic, spintronic and quantum technologies [1]. Nevertheless, its device integration remains challenging. Selective area growth (SAG) of in-plane nanostructures on SiO₂ masked substrate by MBE is a promising technique to address this issue enabling the realization of complex 1D networks, with accurate control of dimensions, geometry and material quality [3]. Thus, we evidence the major levers for SAG of HgTe nanostructures: the growth temperature (GT), the equivalent 2D thickness and the opening geometry. Figure 1 displays several micron long in-plane nanowires (NWs) grown along the three crystal directions ($\langle 110 \rangle$, $\langle \bar{1}10 \rangle$, or $\langle 100 \rangle$) as well as networks and diamond structures with well-defined cross-junctions. A good selectivity is achieved with very little parasitic growth on the mask even for growth temperature as low as 140°C. Figure 2 exhibits the influence of the GT on the growth of a ring structure. The higher the GT the more visible the side faceting, the outer rim turning into an octagon, revealing the morphology anisotropy as function of the in-plane orientation. Indeed, $\langle 110 \rangle$ -oriented ridges show $\{111\}$ A facets with adatoms accumulation on the sides of the top surface as shown in Figure 3. The latter also demonstrates the morphology evolution of NWs as function of the deposited nominal thickness: increasing the thickness enables the formation of a triangular cross-section with smooth $\{111\}$ A facets. The transmission electron microscopy image in Figure 4 reveals the crystalline structure of a $\langle 110 \rangle$ -oriented NW: the center of the nanostructure shows a trapezoidal shape with $\{111\}$ B facets and two grains on the sides made of $\{001\}$ planes but tilted of $\pm 70.5^\circ$, as the symmetry with respect to $\{111\}$ planes. Figure 4 also highlights the continuous epitaxial relation between the CdTe substrate and the HgTe NW. No evidence of misfit dislocations have been found despite the strain in the HgTe lattice. This set of parameters can be used to grow NWs showing a sharp substrate interface and tune their morphology before performing transport electronic measurements.

The authors would like to acknowledge financial support from the national research agency under the INSPIRING project (ANR-21-CE09-0026-01).

[1] S. Das Sarma, M. Freedman, and C. Nayak, npj Quantum Inf., vol. 1, no. 1, 2015.

[2] C. Thomas et al., Phys. Rev. B, vol. 96, no. 24, pp. 1–9, 2017.

[3] P. Aseev et al., Nano Lett., vol. 19, no. 1, pp. 218–227, 2019.

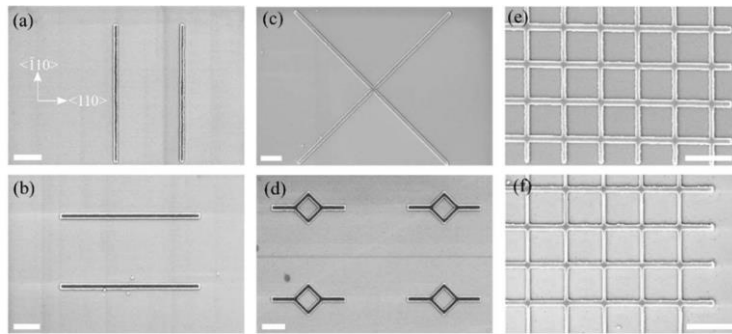


Fig. 1 Top-view SEM images of HgTe nanostructures grown on a patterned CdTe(001) substrate. For images (a)-(d) the opening width is 100 nm and the growth temperature is 140°C. (e)-(f) SEM micrographs of 50 nm-wide $\langle 110 \rangle / \langle \bar{1}10 \rangle$ type NW network grown at, respectively, 140°C and 180°C. The scale bar is 1 μm .

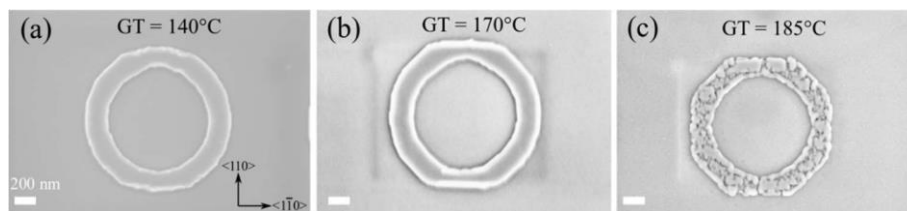


Fig. 2 Top-view SEM images of three HgTe ring nanostructures grown at (a) 140°C, (b) 170°C, (c) 185°C.

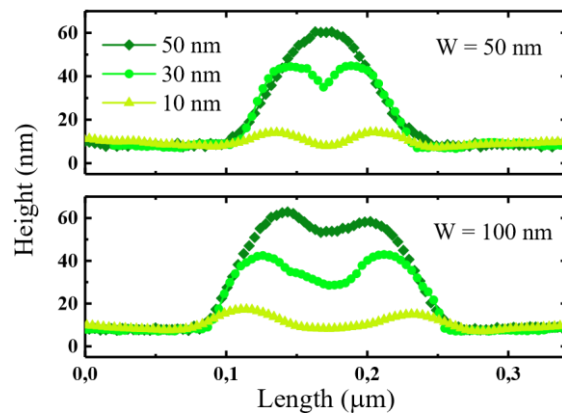


Fig. 3 Change in the NW cross section morphology for three different nominal thicknesses for two $\langle 110 \rangle$ -oriented NWs whose width is 50 nm (top) and 100 nm (bottom)

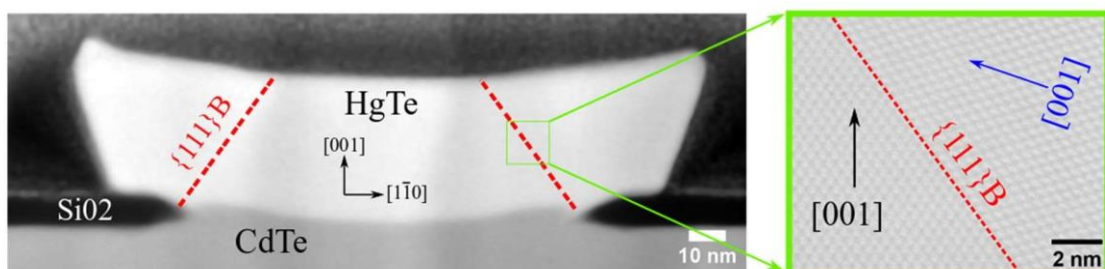


Fig. 4 STEM image of the transversal cross-section of a $[110]$ -oriented NW. The two red dashed 54.7° -tilted lines correspond to grain boundaries of $\{111\}_B$ facets between the center and the side grains. The green outline square is a zoom-in of the grain boundary highlighting the 70.5° -tilted $[001]$ -orientation of the grains.



S7.2: Superconductor-semiconductor hybrids for quantum technologies: looking for alternatives to Al

Ayisha Ferhana¹, An-Hsi Chen², Amrutesh Sharma¹, Amrita Purkayastha¹, Teun van Schijndel³, Edith-Bellet-Amalric⁴, Susheng Tan⁵, Sergey Frolov¹, Christopher Palmstrøm^{3,6,7}, Moira Hocevar^{2,*}

¹*Department of Physics and Astronomy, Univ. of Pittsburgh, Pittsburgh, USA*

²*Univ. Grenoble-Alpes, CNRS, Inst. NEEL, 38042 Grenoble, France.*

³*Electrical and Computer Engineering, University of California, Santa Barbara, Santa Barbara, CA 93106, USA*

⁴*Univ. Grenoble-Alpes, CEA, Grenoble-INP, IRIG, PHELIQS, 38000 Grenoble, France.*

⁵*Department of Electrical and Computer Engineering, Univ. of Pittsburgh, Pittsburgh, USA*

⁶*California NanoSystems Institute, University of California Santa Barbara, Santa Barbara, Santa Barbara, CA 93106, USA*

⁷*Materials Department, University of California Santa Barbara, Santa Barbara, Santa Barbara, CA 93106, USA*

*moira.hocevar@neel.cnrs.fr

The epitaxy community is making significant efforts to develop high-quality superconductor-semiconductor hybrids. These heterostructures hold promise for enabling error-limited quantum computation through qubits with longer coherence times, as well as topologically protected qubits. This effort began with the quest for improved material interfaces for gate tunable Josephson junctions using nanowires, and in particular with the development of in-situ epitaxial aluminum (Al) interfaces. However, Al is limited in terms of critical current, and many other superconductors remain underexplored. Here, we present our efforts to develop expertise in alternative superconductors such as tin (Sn) and tantalum (Ta). Both materials are known for having higher critical temperatures and higher superconducting gap than Al. However, both are allotropes, meaning they can exist in multiple crystalline phases, with only one phase being suitable for quantum bit technologies. Therefore, significant work is needed to control the crystalline phase of Sn and Ta during epitaxy or deposition to favor the desired phase. Additionally, it is critical to ensure that interfaces remain undamaged during the growth process.

Sn, for instance, has a superconducting b-phase, which is tetragonal, while its a-phase is cubic and behaves as a semimetal. Using X-ray diffraction (XRD) and transmission electron microscopy (TEM), we demonstrated that forming the b-phase of Sn on III-V semiconductors is non-trivial, particularly when depositing thin films at cryogenic temperatures. We have shown that b-phase formation depends on surface morphology (planar or nanowire) [1] and on strategies to prevent film dewetting during the return to room temperature [2]. Devices fabricated from Sn/III-V nanowires exhibit high critical currents and strong resilience to magnetic fields [1,3], which are essential properties for quantum devices such as Josephson parametric amplifiers, gatemons, and Majorana-based systems. Yet, one drawback of Sn is that the oxide on its surface causes losses in microwave resonators made from this superconductor. An alternative material could be Ta, as resonators built with tantalum have demonstrated performance comparable to those made with aluminum. The a-phase of Ta is the "holy grail,"

as it exhibits a higher critical temperature. Achieving control over the growth of this phase requires either cryogenic temperatures and the use of titanium sticking layers or very high temperatures incompatible with III-V materials. Preliminary data on the former approach will be presented.

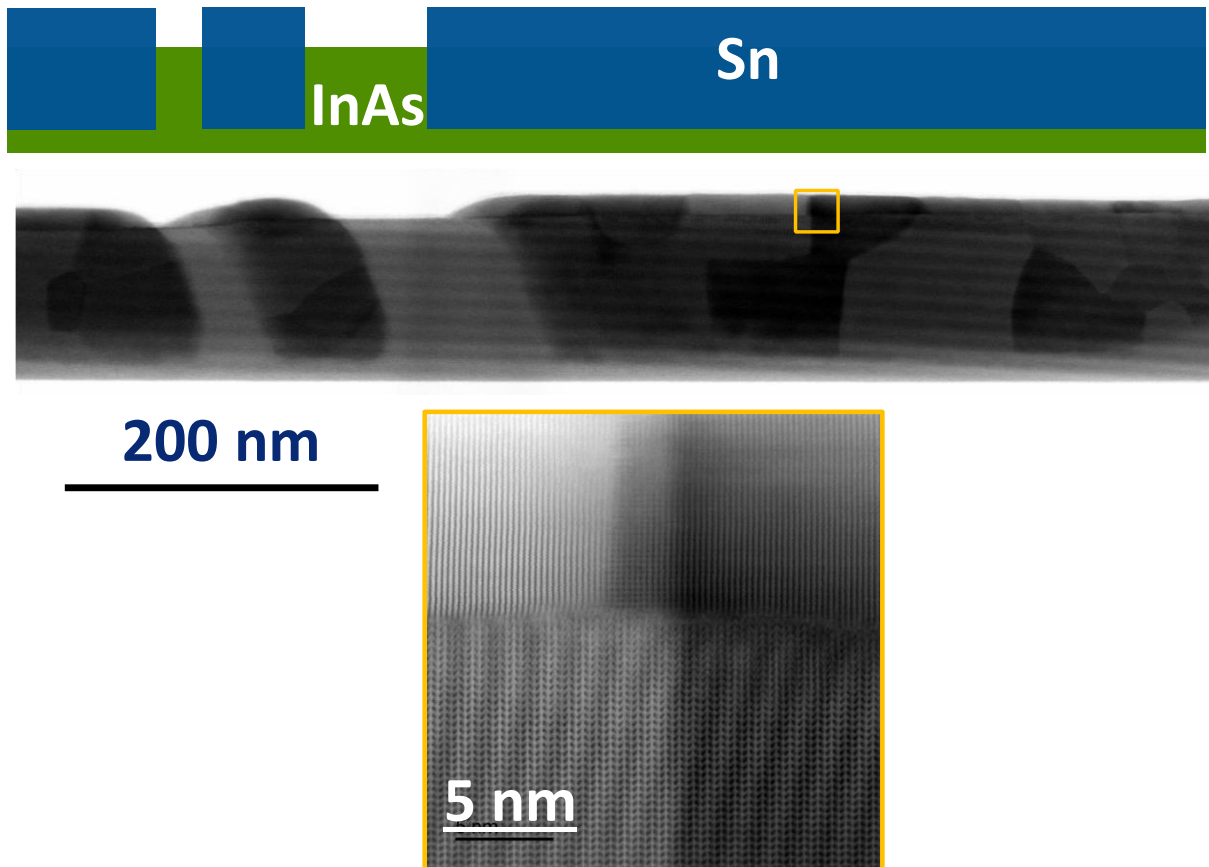


Figure 1: High-resolution bright field transmission electron micrograph of a partial shell of Sn grown on an InAs nanowire. The structural analysis of the shell shows that the grains have the b-phase and are in grain by grain epitaxial relation. Moiré patterns appear by superposition of the InAs and Sn lattices.

References:

- [1] M. Pendharkar et al, Science (2021)
- [2] A. H. Chen et al, Nanotechnology (2023)
- [3] A. Sharma et al, in preparation (2024)

Acknowledgments: This work was supported by ANR HYBRID (ANR-17-PIRE-0001), IRP HYNATOQ and the Transatlantic Research Partnership.



S7.3: MBE growth of parallel hybrid semiconductor-superconductor nanowires for quantum devices

Raphaël Rousset-Zenou^{1,*}, Rasmus D. Sclosser², Martin Bjergfelt²,
Julien Renard¹, Moïra Hocevar¹, Jesper Nygård^{1,2}

¹University Grenoble Alpes, CNRS, Grenoble INP, Institut Néel, 38000 Grenoble, France

²Center for Quantum Devices, Niels Bohr Institute, Univ. of Copenhagen, 2100 Copenhagen, Denmark

*raphael.rousset-zenou@neel.cnrs.fr

Hybrid superconductor-semiconductor materials are attractive for research on several types of gatetunable quantum devices, such as superconducting qubits [1], Andreev qubits, and cryogenic switches. They have also played an important role in fundamental research on bound states in topological superconductors and quantum dots, where superconductor-semiconductor nanowires have been established as an essential platform [2]. Up to now, these platforms have been based on individual nanowires. However, coupling multiple parallel nanowires could open new avenues. Pairs of parallel nanowires match theoretical proposals for quantum devices, such as Cooper pair splitters and Andreev bound state molecules [3,4].

We present our results on the fabrication of multiple (5-10) parallel hybrid nanowires (Figure 1a). The synthesis (Figure 1b) is based on arrays of closely spaced catalyst particles positioned by electron beam lithography, vapor-liquid-solid growth of vertical InAs nanowires by molecular beam epitaxy (1), vaporsolid radius overgrowth (2) and in-situ deposition of superconducting shells on the coupled wires (3). Our study shows that the parallel wires grow aligned with a yield depending on the distance between adjacent catalyst particles. The yield decreases with decreasing pitch (Figure 2a) and we ascribe this to the merging of Au droplets prior to growth. We will discuss the morphology, structural and electrical properties of the nanowire arrays.

Furthermore, by etching away part of the in-situ deposited Aluminum one can form Josephson junctions, a key element in superconducting circuits (Figure 2b). We show that the supercurrent in the parallel wires is an order of magnitude higher than for a single nanowire device. By embedding the parallel wires in a microwave resonator, we fabricate a Josephson parametric amplifier (JPA). This type of ultra-lownoise amplifier requires a large critical current and has been made before using metal tunnel junctions, graphene [5] and planar semiconductors [6]. We demonstrate the first nanowire-based JPA and show the gate-voltage tunability enabled by this new semiconducting platform.

[1] Larsen, T. W. et al. Phys. Rev. Lett. 115, 127001 (2015)

[2] E. Prada et al., Nature Rev. Phys. 2, 575 (2020)

[3] Kürtösy, O. et al. npj Quantum Mater. 7, 88 (2022)

[4] T. Kanne et al., Adv. Func. Mat. 32, 2107926 (2021)

[5] Butseraen, G. et al. Nat. Nanotechnol. 17, 1153–1158 (2022)

[6] Phan, D. et al. Phys. Rev. Applied 19, 064032 (2023)

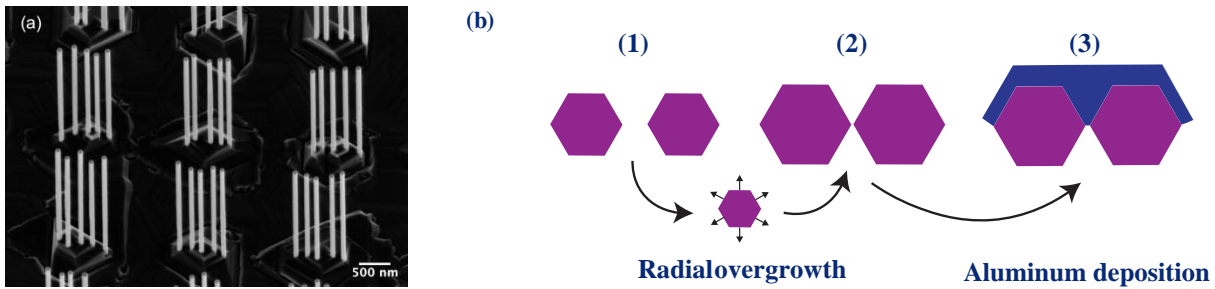


Figure 1: (a) Arrays of InAs nanowires grown by MBE. (b) Schematic representing the three steps growth process for two parallel InAs nanowires (purple, top view) with in situ Aluminum (blue).

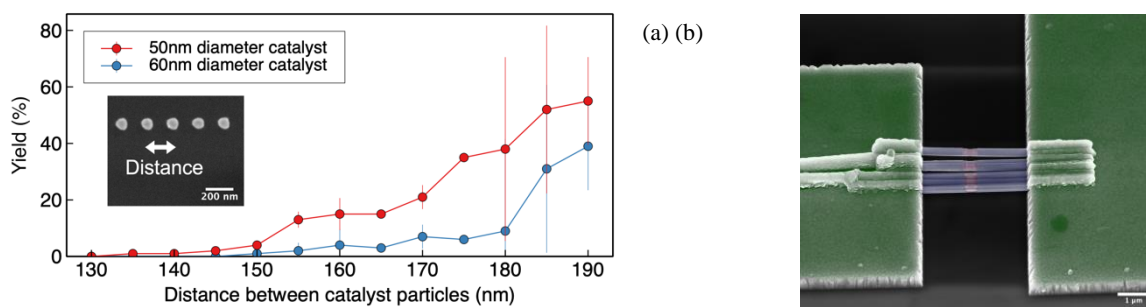


Figure 2: (a) Yield (percentage of successfully grown parallels arrays) with respect to the distance between the catalyst particles in an array before growth for two catalyst diameters (50nm and 60nm). Inset : scanning electron micrograph of gold catalyst particles before growth. White arrow shows the distance between two catalyst particles. (b) Scanning electron micrograph of parallel InAs nanowires (InAs: purple ; in situ Aluminum: blue) Josephson junction contacted with Ti/Al electrodes (green) to perform electronic transport measurements.



S7.4: Metamorphic InAs 2DEGs for quantum computation platforms

D. Curcio^{1*}, O. Batchuluun^{1,2}, L. Sbuelz¹, S. K. Appani¹, M. Kirti^{1,2}, M. Sütő⁴, E. Tóvári³, P. Makk³, T. Prok³, S. Csonka³, G. Biasiol¹

¹CNR - Istituto Officina dei Materiali (IOM), 34149 Trieste, Italy

²Department of Physics, University of Trieste, 34128 Trieste, Italy

³Department of Physics, Budapest University of Technology and Economics and Nanoelectronics “Momentum” Research Group of the Hungarian Academy of Sciences, 1111 Budapest, Hungary

⁴HUN-REN Centre for Energy Research, Institute of Technical Physics and Materials Science, 1121 Budapest, Konkoly Thege Miklós út 29-33.

* curcio@iom.cnr.it

The development of quantum computing still relies on the development of advanced material platforms. Among the most promising candidates are semiconductor-superconductor hybrid systems, such as Andreev quantum bits and Kitaev transmons. These systems are based on high-quality superconducting thin films with transparent interfaces to low-dimensional semiconductors, offering the potential for extended coherence times and robust qubit-qubit coupling [1].

To this end, a metamorphic growth protocol has been employed, and low-temperature electron mobilities up to $8 \times 10^5 \text{cm}^2/\text{Vs}$ have been achieved in undoped deep InAs/In_{0.81}Ga_{0.19}As twodimensional electron gases (2DEGs) grown on GaAs (001) [2]. Additionally, superconducting proximity effects have been observed in Josephson junctions between shallow InAs 2DEGs and epitaxial Al layers [3]. Optimal mobilities were achieved by tuning the thickness t of a strain-relieving

In_{0.84}Al_{0.16}As layer beneath the quantum well (QW) region [2].

Here, discuss the strain relaxation dynamics for varying t and their impact on electron scattering mechanisms in the InAs 2DEGs. Two-dimensional XRD reciprocal space maps of the (004) and (224) reflections (Fig. 1) reveal how increasing t from 50 nm to 300 nm leads to near-complete strain relaxation and a reduction in mosaicity in both the InAs QW and the surrounding barriers. Mobility measurements from gated Hall bars (Fig. 2) reveal striking gains in electron mobility and a reduced anisotropy between the [110] and [-110] orientations as t grows. This improvement stems from diminished anisotropic scattering mechanisms, linked to the cross-hatch roughness pattern—a memory of the buried dislocation network in the buffer layer (see insets of Fig. 2). These features, shaped by strain and composition fluctuations, highlight the interplay between structural engineering and electronic properties.

[1] J. S. Lee et al. Nano Lett. **19**, 3083 (2019)

[2] A. Benali et al., J. Cryst. Growth **593**, 1267681 (2022)

[3] M. Sütő et al. Phys. Rev. B **106**, 235404 (2022)

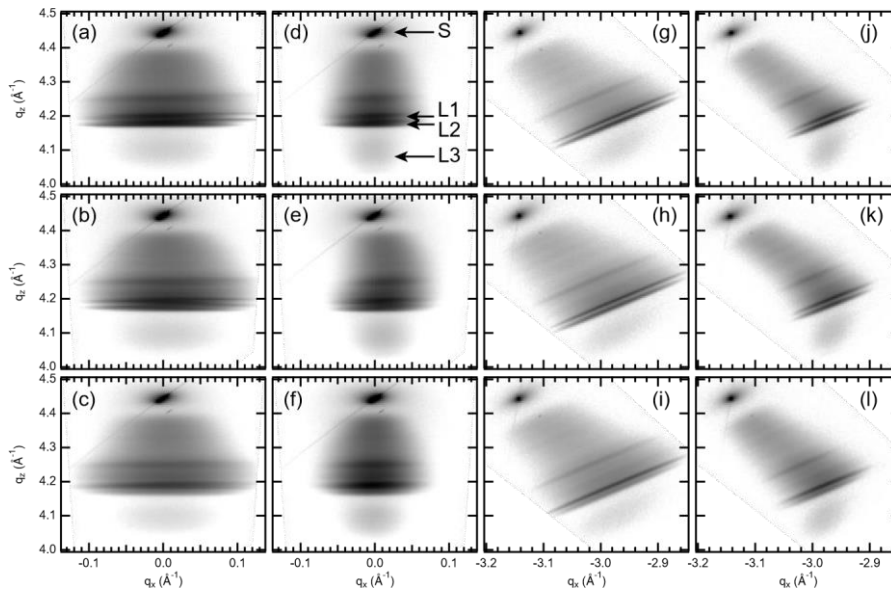


Fig. 11: X ray diffraction reciprocal space maps of (004) (a-f) and (224) reflections (g-l) of InAs QWs along the [110] direction (a-c, g-i) and along the [-110] direction (d-f, j-l) with $t = 300$ nm (a,d,g,j) , 150 nm, (b,e,h,k) and 50 nm (c,f,i,l). Substrate, $\text{In}_{0.81}\text{Al}_{0.19}\text{As}$, $\text{In}_{0.84}\text{Al}_{0.16}\text{As}$, and InAs peaks are labelled as S, L1, L2 and L3, respectively.

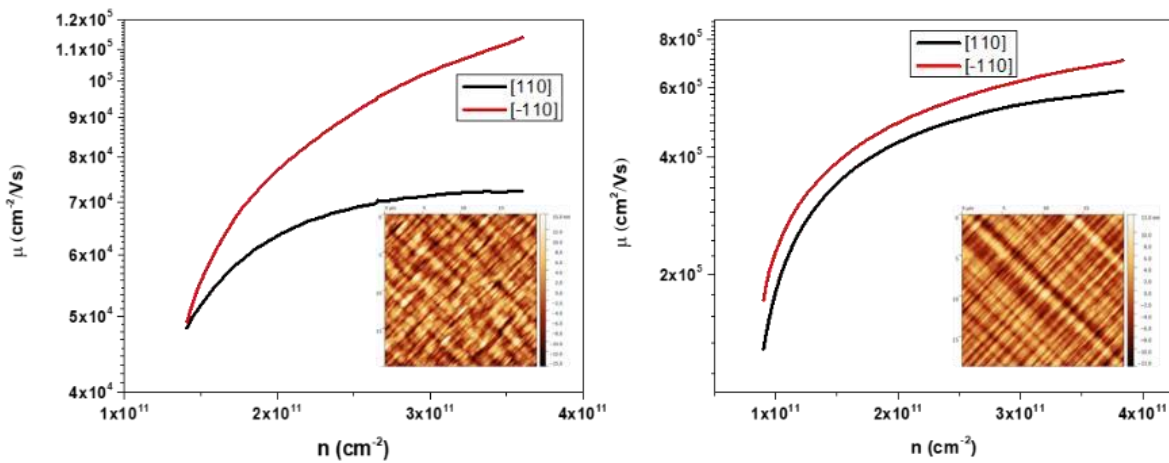


Fig. 22: Mobility vs. charge density along [110] and [-110] for $t = 50$ nm (left) and 300 nm (right). Inset: corresponding AFM images of top surfaces.



I8: The birth of ferroelectric topological insulators

Gauthier Krizman^{1,2}, Tetiana Zakusylo², Lakshmi Sajeev³, Joaquin Bermejo-Ortiz¹, Takuya Takashiro², Mahdi Hajlaoui², Günther Bauer², Yves Guldner¹, Ondrej Caha³, Louis-Anne de Vaultchier¹ and Gunther Springholz²

¹ *Laboratoire de Physique de l'Ecole normale supérieure, ENS, Université PSL, CNRS, Sorbonne Université, 24 rue Lhomond 75005 Paris, France*

² *Institute of Semiconductor Physics, Johannes Kepler University Linz, Altenbergerstrasse 69, A-4040 Linz, Austria*

³ *Department of Condensed Matter Physics, Masaryk University, Kotlářská 2, Brno 61137, Czech Republic*

Breaking internal material symmetries like time reversal with magnetism or gauge with superconductivity has always been of primary interest in the perspective of discovering novel states of matter. When combined with the recently discovered Dirac matter with non-trivial band topology, these symmetry breakings have allowed the recent breakthrough of the quantum anomalous Hall phase in magnetically-doped topological insulator; whereas topological superconductors are leading materials to evidence Majorana quasi-particles.

In this work, we initiate the case of *ferroelectric topological insulators* and see how 3D and 2D topological band structures evolve under a ferroelectric distortion. In particular, marrying topology and ferroelectricity allows to unravel the emergence of novel quasiparticles that mimic Weyl fermions, a gapless state with left or right-handed chirality, i.e., massless electrons with spin parallel or antiparallel to their momentum. The search of Weyl fermions in condensed-matter is motivated by their numerous specific properties highlighting their fundamental chiral nature.

To disclose the Weyl fermions in ferroelectric topological matter, we rely on lead salt materials such as PbSe and PbTe that have shown both non-trivial topology when Sn is added and ferroelectricity when Ge atoms are incorporated. Both concepts will be tackled in this talk, showing the possibility to reach topological and ferroelectricity at the same time. The growth of Ge-doped lead salts by molecular beam epitaxy is developed and will be discussed in a first place. Secondly, the resulting topological ferroelectric materials will be characterized using magneto-optical spectroscopy, X-ray diffraction and Angle-resolved Photoemission spectroscopy (ARPES). The combination of these three techniques allows us to have a complete overview on both the structural and electronic properties of such novel material system.





S8.1: MBE growth of Ge-doped PbSe ferroelectric Rashba semiconductor

T. Zakusylo,^{1,*} M. Hajlaoui¹, T. Takashiro¹, L. Sajeev², O. Caha², M. Rosmus³, N.

Olszowska³, G. Krizman⁴, and G. Springholz¹

¹Institute of Semiconductor and Solid State Physics, Johannes Kepler University, Linz, Austria

²Department of Condensed Matter Physics, Masaryk University, Brno, Czech Republic

³Solaris National Synchrotron Radiation Centre, Jagiellonian University, Kraków, Poland

⁴Laboratoire de Physique, ENS, Paris, France

*tetiana.zakusylo@jku.at

Ferroelectric Rashba semiconductors (FERSC) are a new class of multifunctional materials combining Rashba physics and ferroelectricity, hence, promising for semiconductor spintronics [1-2]. Although vast variety of materials have been theoretically predicted as FERSC, the experimental realization is, however, still limited to a few (mainly Telluride) compounds: GeTe [3], PbGeTe [4], SnTe [5]. Hereby we report low temperature epitaxial growth of a new ferroelectric Rashba semiconductor $\text{Pb}_{1-x}\text{Ge}_x\text{Se}$, thus providing a new material system for FERSC.

High-quality epitaxial films of $\text{Pb}_{1-x}\text{Ge}_x\text{Se}$ were grown by molecular beam epitaxy (MBE) on (111)oriented BaF_2 substrates with $1\mu\text{m}$ PbSe buffer layers using elemental sources of PbSe and GeSe. To ensure Ge incorporation in the host material, a very low growth temperature is required to suppress GeSe reevaporation. Despite the remarkably low-temperature growth window, which is more than 100°C below the standard growth temperature of PbSe-based compounds, the epilayers of $\text{Pb}_{1-x}\text{Ge}_x\text{Se}$ demonstrate high quality pseudomorphic layer-by-layer 2D growth and atomically smooth surfaces exhibiting only monoatomic steps (Fig. 1). Ge incorporation in PbSe is extremely temperature-dependent and it saturates at lower growth temperatures below 160°C (Fig. 2,a). Due to Ge incorporation, the cubic rock-salt PbSe lattice undergoes a ferroelectric lattice distortion below the ferroelectric Curie temperature T_C , that is determined by the observation of a resistivity anomaly at the T_C .

The effect of Ge incorporation on the band structure of $\text{Pb}_{1-x}\text{Ge}_x\text{Se}$ quantum wells was determined by angle resolved photoemission spectroscopy (ARPES) performed at the SOLARIS Synchrotron with the samples transported in a battery operated vacuum suitcase. The ARPES measurements reveal a temperature-dependent ferroelectric Rashba spin splitting in the ferroelectric phase below the T_C (Fig.2.b) with a very large Rashba coupling constant. This makes the system very promising for spintronic device applications.

[1] Picozzi, S. *Front. Phys.* **2**, 10 (2014).

[2] Di Sante, D., Barone, P., Bertacco, R., Picozzi, S. *Adv. Mater.* **25**, 509 (2013).

[3] Kremer, G., Maklar, J., Nicolai, L. et al. *Nat. Commun.* **13**, 6396 (2022).

[4] Chassot, F., Pulkkinen, A., Kremer, G., Zakusylo, T. et al. *Nano Lett* **24**, 82 (2024).

[5] Krizman, G., Zakusylo, T., Sajeev, L., Hajlaoui, M., et al. *Adv. Mater.* **36**, 2310278 (2024).

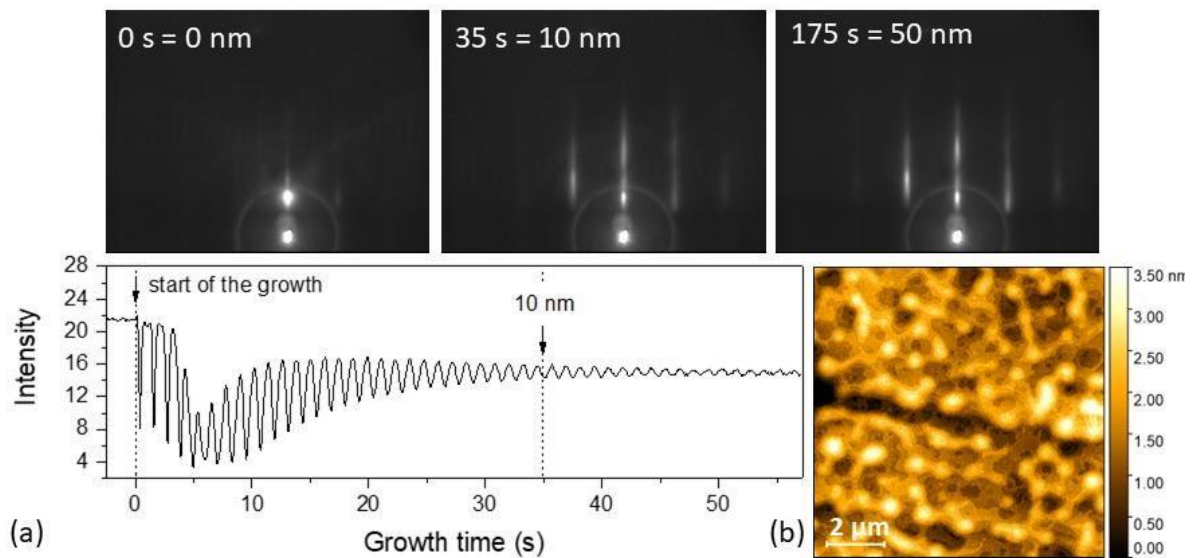


Fig. 1: Low-temperature high-quality epitaxial growth of $\text{Pb}_{1-x}\text{Ge}_x\text{Se}$: (a) RHEED intensity oscillations, signifying layer-by-layer growth and selected RHEED patterns, evidencing the pseudomorphic 2D growth of $\text{Pb}_{1-x}\text{Ge}_x\text{Se}$. (b) AFM image of 50 nm – thick $\text{Pb}_{1-x}\text{Ge}_x\text{Se}$, showing atomically smooth surface.

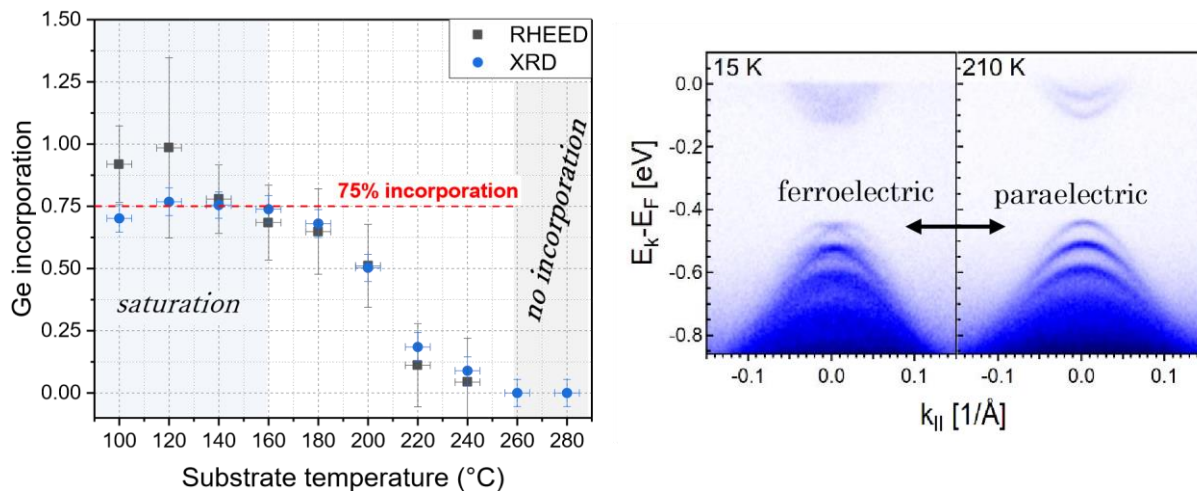


Fig. 2: (a) Ge incorporation in PbSe vs temperature, as determined from RHEED intensity oscillations and x-ray diffraction patterns. (b) Demonstration of ferroelectric-driven Rashba effect in 10 nm – thick $\text{Pb}_{1-x}\text{Ge}_x\text{Se}$ by temperature-dependent angle resolved photoemission spectroscopy recorded along the M–K direction at a photon energy $h\nu = 18$ eV at the URANOS beamline of SOLARIS.

S8.2: AlN/NbN epitaxial heterostructures on Si: polytypes, strain and polarity

I.Florea,^{1*} A. Pedeches¹, H. Rotella¹, M.P. Chauvat², F. Semond¹, and P. Vennéguès¹

¹ Université Côte d'Azur (UniCA), CNRS, CRHEA, France

² CIMAP, ENSICAEN, France ileana.florea@crhea.cnrs.fr

The combination of metal/superconductor NbN with III-N semiconductors opens the way to a wide range of innovative applications. Notably, it is possible to epitaxially integrate NbN and III-N. NbN can exist in different crystalline structures, commonly referred as polytypes. We found that by a fine-tuning of the growth conditions, a precise control of the NbN polytype formed on AlN can be obtained. This work focuses on a detailed analysis through advanced scanning transmission electron microscopy (STEM) of AlN/NbN/AlN heterostructures epitaxially-grown on Si (111) substrates by NH₃-molecular beam epitaxy (MBE).

Figure 1 (a) show a high angle annular dark field (HAADF) image of a δ -NbN layer viewed along the AlN_[11-20] zone axis where the ABC cubic stacking is clearly observed. The epitaxial relationship is

AlN_{<11-20>} | | δ -NbN_{<1-10>} and AlN_{<0001>} | | δ -NbN_{<111>}. Conversely, it is also possible to achieve a predominantly ϵ -NbN layer. Figure 2(a) show a HAADF image of such a layer observed along the AlN_[11-20] zone axis. While the first monolayers adopt the δ -polytype, the majority of the NbN layer exhibit the AA-BB stacking corresponding to the ϵ -polytype. The observed epitaxial relationship is

AlN_{<11-20>} | | ϵ -NbN_{<11-20>} and AlN_{<0001>} | | ϵ -NbN_{<0001>}.

The lattice mismatches between AlN and NbN depends on the NbN polytype. Specifically, the inplane lattice mismatches are -0.7% and -4.7% for δ - and ϵ -NbN respectively. Figure 1(b) and 2(b) show strain maps obtained using the geometrical phase analysis (GPA) method for both heterostructures, with the AlN lattice distance used as reference. These maps reveal that, due to the low mismatch, δ -NbN is fully strained on AlN without introduction of misfit dislocations. For the NbN layer consisting of δ polytype at the bottom and ϵ -polytype at the top, the δ -region is strained on AlN whereas the ϵ -region is fully relaxed.

A key distinction between wurtzite III-N and NbN is that III-N are polar materials whereas NbN is non-polar. Our observations using integrated differential phase contrast (iDPC) (figure (3)) confirm previous results: adding a thin epitaxial NbN layer reverses the polarity of AlN from Al-Polar to N-Polar.

Our STEM study demonstrates that is possible to control the NbN polytype by adjusting the growth conditions. Whatever the polytype, the introduction of a thin NbN layer consistently reverses the polarity of the AlN top layer. Another interesting finding obtained from our analyses is that the AlN/ δ -NbN/AlN heterostructures are pseudomorphic with no misfit dislocations paving the way for the realization of high crystalline quality hybrid semiconductor/superconductor heterostructures and also hybrid Al-

Polar/N Polar AlN layers.

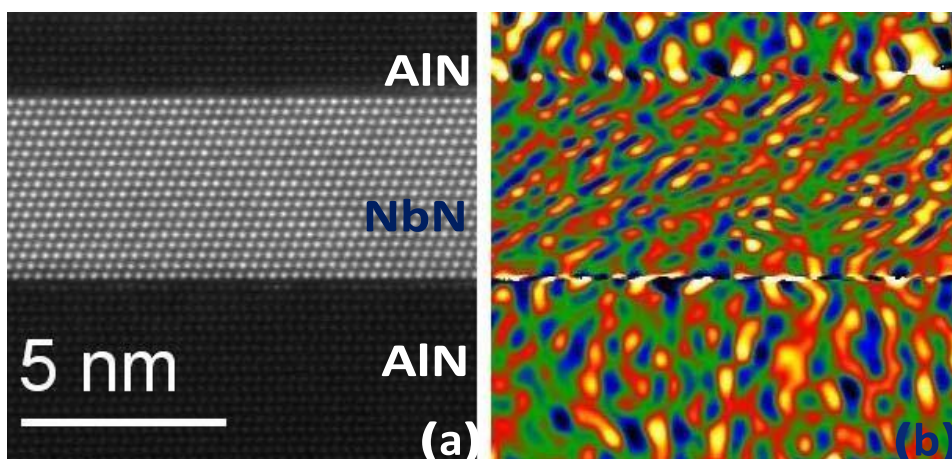


Figure 1: HAADF image of a δ -NbN layer (a) and corresponding GPA strain map for in plane distances (b).

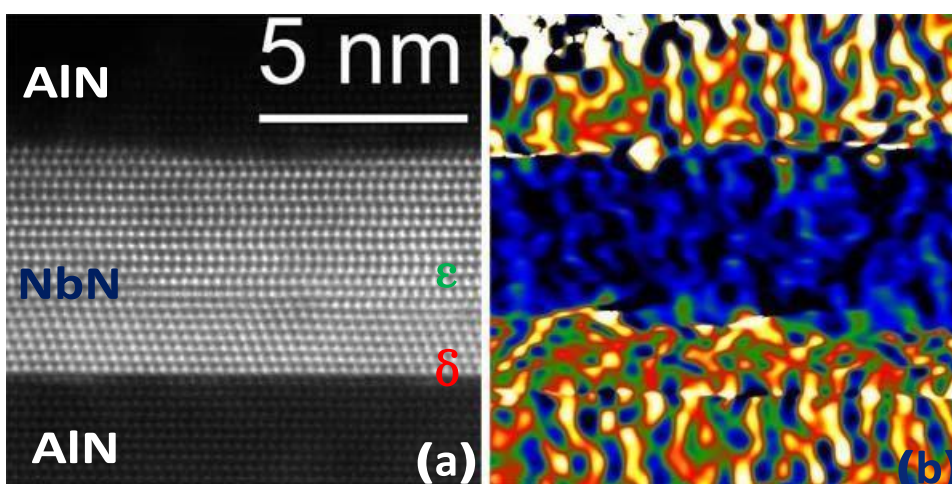


Figure 2: STEM-HAADF image of a mixed δ -NbN/ ϵ -NbN layer (a) and corresponding GPA strain map for in plane distances (b).

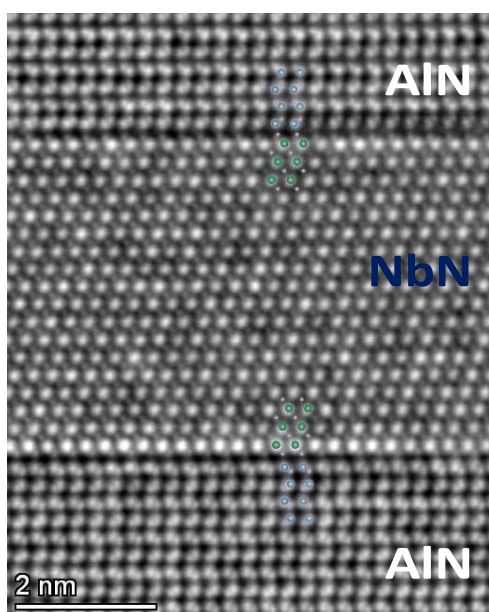


Figure 3: STEM-iDPC image of a δ -NbN layer. Both heavy (Nb, Al) and light (N) elements, are observed revealing the polarity reversal between the bottom and top AlN layers. Ball-and-stick model is superimposed on the experimental image with Nb in green, Al in blue and N in grey.



S8.3: Mutual Exchange Growth of Zintl $\text{Eu}_3\text{In}_2\text{As}_4$ and $\text{Eu}_5\text{In}_2\text{As}_6$ Nanowires by Molecular Beam Epitaxy

Man Suk Song,^{1,*} Lothar Houben,² Yufei Zhao,¹ Nadav Rothem,³ Ambikesh Gupta,¹ Binghai Yan,¹ Beena Kalisky,³ Haim Beidenkopf, and Hadas Shtrikman¹

¹Department of Condensed Matter Physics, Weizmann Institute of Science, Rehovot, Israel

²Department of Chemical Research Support, Weizmann Institute of Science, Rehovot, Israel

³Department of Physics and Institute of Nanotechnology and Advanced Materials, Bar-Ilan University, Ramat Gan, Israel.

*E-mail : man-suk.song@weizmann.ac.il

Eu-based Zintl compounds have emerged as magnetic topological materials due to their antiferromagnetic (AFM) order and strong spin-orbit coupling [1]. To harness these properties and realize quantum devices, atomic-scale precision and extremely low defect densities in crystal growth are a prerequisite. We report the successful synthesis of Zintl-phase $\text{Eu}_3\text{In}_2\text{As}_4$ and $\text{Eu}_5\text{In}_2\text{As}_6$ nanowires (NWs) using molecular beam epitaxy (MBE) through a mutual cation exchange mechanism [2]. Starting with wurtzite (WZ) InAs and zincblende (ZB) InAsSb NWs grown on InAs substrates, we introduced Eu and As flux during MBE growth, which facilitated the exchange of In atoms with Eu atoms within the InAs lattice. This process resulted in the formation of single-crystalline $\text{Eu}_3\text{In}_2\text{As}_4$ and $\text{Eu}_5\text{In}_2\text{As}_6$ along the core NWs. High-resolution transmission electron microscopy (HRTEM) and energy-dispersive X-ray spectroscopy (EDS) analyses provided information on their atomic coordination and composition, confirming the structural transformation within the NWs (Figure 1). The morphology of $\text{Eu}_3\text{In}_2\text{As}_4$ grains originates from two distinctive orientational relationships between the orthorhombic $\text{Eu}_3\text{In}_2\text{As}_4$ and the underlying InAs. In contrast, $\text{Eu}_5\text{In}_2\text{As}_6$ grains extend in four directions corresponding to the tetrahedral faces of the ZB core, exhibiting an anisotropic growth preference along the *c*-axis of their orthorhombic crystal structure. Both $\text{Eu}_3\text{In}_2\text{As}_4$ and $\text{Eu}_5\text{In}_2\text{As}_6$ NWs exhibited AFM ordering, as evidenced by magnetic susceptibility measurements such as a magnetic property measurement system (MPMS) and a scanning superconducting quantum interference device (SQUID). The ability to convert InAs NWs into different Zintl phases by selecting the crystal structure of core demonstrates the versatility of this mutual exchange growth method. This study contributes to the fundamental understanding of topotactic reactions in nanostructures and highlights the potential of MBE in fabricating complex nanomaterials with precise control over composition and structure.

References

- [1] Zhao, Y. *et al.* Hybrid-order topology in unconventional magnets of Eu-based Zintl compounds with surface dependent quantum geometry. *Phys. Rev. B* 110, 205111 (2024).
- [2] Song, M.S., *et al.* Topotaxial mutual-exchange growth of magnetic Zintl $\text{Eu}_3\text{In}_2\text{As}_4$ nanowires with axion insulator classification. *Nature Nanotechnology* 1–8 (2024).

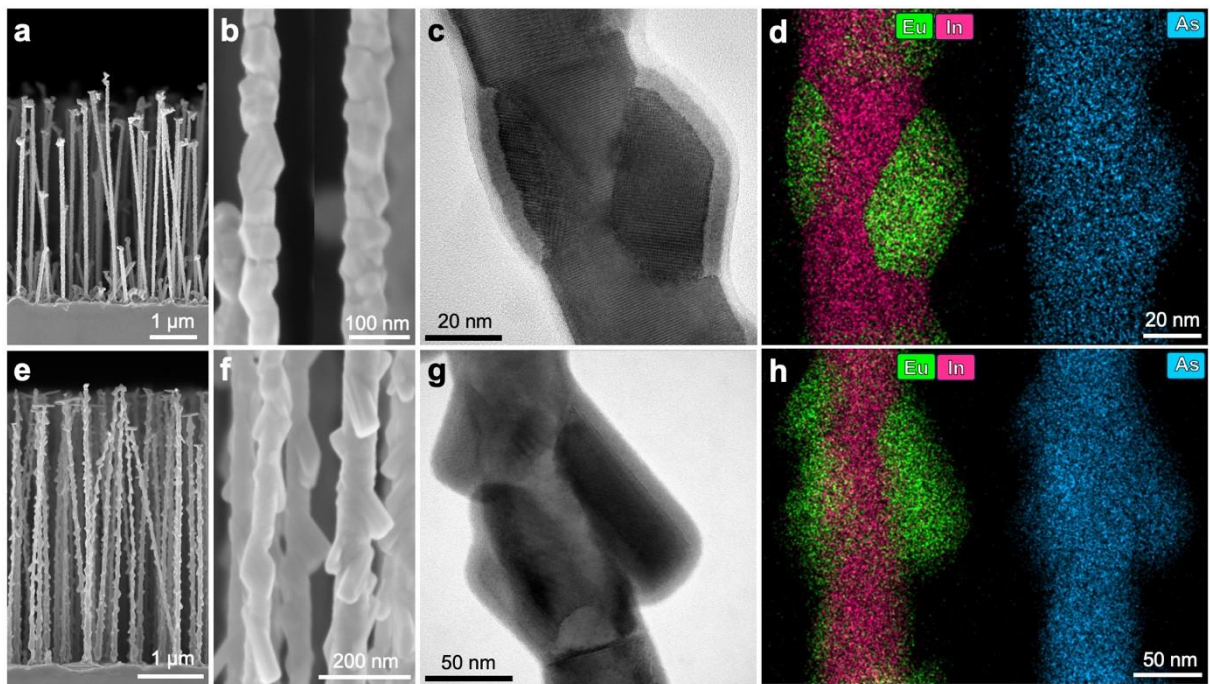


Fig. 1: (a) SEM image of as-grown $\text{Eu}_3\text{In}_2\text{As}_4$ along WZ InAs NWs. (b) The unique facets characterize the Zintl-phase $\text{Eu}_3\text{In}_2\text{As}_4$. (c) TEM image of $\text{Eu}_3\text{In}_2\text{As}_4$ grains on a WZ InAs core. (d) EDS elemental maps of Eu, In, and As (green, magenta, and blue respectively), corresponding to the area in (c). The map shows Eu and In distributed on opposite sides of the core boundary, while As is uniformly distributed throughout the core and shell. (e) SEM image of as-grown $\text{Eu}_5\text{In}_2\text{As}_6$ along ZB InAsSb NWs. (f) The Zintl-phase $\text{Eu}_5\text{In}_2\text{As}_6$ exhibits anisotropic growth direction preferences. (g) TEM image of $\text{Eu}_5\text{In}_2\text{As}_6$ grains on a ZB InAsSb core. (h) EDS elemental maps of Eu, In, and As (green, magenta, and blue respectively), corresponding to the area in (g). As in (d), Eu and In are located on opposite sides of the core boundary, with As uniformly distributed across both core and shell.



Wednesday 12.03
Poster session 2



P2.2: Epitaxial growth of LaCoO₃ thin films by MBE.

T. Zhu, A. D. Lamirand, C. Furgeaud, C. Botella, A. Benamrouche, P. Regreny, G. Saint-Girons, R. Bachelet
Institut des Nanotechnologies de Lyon, INL-UMR5270, CNRS, Ecole Centrale de Lyon, Ecully, France

P2.6: Growth and analysis of InAs/ZnTe core-shell nanowires for superconductivity applications.

D. Mosiats, C. W. Shum, Y. Genuist, S. Tan, J. Cibert, E. Bellet-Amalric, S. M. Frolov, M. Hocevar
University Grenoble-Alpes, CNRS, Grenoble INP, Institut Néel, Grenoble, 38000, France
Department of Physics and Astronomy, University of Pittsburgh, Pittsburgh, USA
NanoScale Fabrication and Characterization Facility, Petersen Institute of NanoScience and Engineering, University of Pittsburgh, Pittsburgh, USA
Department of Electrical and Computer Engineering, University of Pittsburgh, Pittsburgh, USA
University Grenoble-Alpes, Grenoble INP, CEA-IRIG, PHELIQS, Grenoble, 38000, France.

P2.8: Growth of MoS₂ on GaN/Sapphire Substrates Using Molecular Beam Epitaxy.

Z. Bouyid, M. T. Dau, I. Florea, P. Vennéguès, J. Brault, S. Vézian, A. Michon, Y. Cordier, P. Boucaud, M. Al Khalfioui
Université Côte d'Azur, CNRS, CRHEA, Valbonne, 06560, France

P2.10: High electron mobility in in-plane InAs/GaSb core-shell nanowires: growth, characterization, and magneto-transport properties.

W. Khelifi, C. Coinon, M. Berthe, G. Patriarche, H. Sellier, X. Wallart, B. Grandidier and L. Desplanque
Univ. Lille, CNRS, Centrale Lille, Univ. Polytechnique Hauts-de-France, Junia-ISEN, UMR 8520 - IEMN, F-59000 Lille, France
Univ Rennes, CNRS, IPR (Institut de Physique de Rennes), UMR 6251, F-35042 Rennes, France
Université Paris-Saclay, CNRS, Centre de Nanosciences et de Nanotechnologies, F-91120, Palaiseau, France
University Grenoble Alpes, CNRS, Institut Néel, 38000 Grenoble, France

P2.12: Hysteresis $\beta \Leftrightarrow \beta'$ phase transition in the In₂Se₃ film.

S. Ponomarev, D. Rogilo, N. Kurus, V. Golyashov, A. Mironov, A. Milekhin, D. Sheglov, A. Latyshev
Rzhanov Institute of Semiconductor Physics SB RAS, Novosibirsk, Russia
Novosibirsk State University, Novosibirsk, Russia

P2.14: InAs/GaAs Heterostructure Nanowires with Phase-Change Materials for Single-Photon Sources.

B. Viollet, J. Bleuse, H. Tlili, L. Cagnon, J. Claudon and M. Hocevar
Univ. Grenoble Alpes, 38000 Grenoble, France
Univ. Grenoble Alpes, CNRS, Inst. NEEL, NPSC group, 38000 Grenoble, France
Univ. Grenoble Alpes, CEA, IRIG, PHELIQS, NPSC group, 38000 Grenoble, France
Univ. Grenoble Alpes, CNRS, Inst. NEEL, MNM group, 38000 Grenoble, France

P2.16: MBE-grown AlN nanowires for 235 nm LEDs realization.

C. Guérin, F. Jourdan, J. L. Rouvière, G. Jacopin and B. Daudin
Univ. Grenoble Alpes, CEA, Grenoble INP, IRIG, PHELIQS, NPSC, 17 av. des Martyrs, 38000 Grenoble, France
Univ. Grenoble Alpes, Grenoble INP, Institut Néel, SC2G, CNRS, 38000 Grenoble, France.
Univ. Grenoble Alpes, Grenoble INP, CEA, IRIG, MEM, LEMMA, 17 av. des Martyrs, 38000, Grenoble, France

P2.18: Optimizing Zincblende InP nanowires morphology with embedded InAs_xP_{1-x} QDs for high emission extraction efficiency at telecom wavelengths.

G. Bucci, T. Gzyl, P. Mrowiński, A. Musiał, V. Zannier, W. Rudno-Rudziński, F. Beltram, G. Sęk and L. Sorba
Scuola Normale Superiore, 56127 Pisa, Italy
Department of Experimental Physics, Faculty of Fundamental Problems of technology, Wrocław University of Science and Technology, Wrocław, Poland



NEST Istituto Nanoscienze CNR and Scuola Normale Superiore, 56127 Pisa, Italy

P2.20: RHEED oscillation decay and signal recovery in nucleation and step flow growth.

Magnus Quaade Oddershede and Peter Krogstrup

Quantum Foundry Copenhagen

NNF Quantum Computing Programme, Niels Bohr Institute, University of Copenhagen, Denmark

P2.22: Threading and misfit dislocations study by Electron Channeling Contrast Imaging.

A. Gilbert, A. Meguekam, E. Tournié and J.-B. Rodriguez

IES, University of Montpellier, CNRS, F – 34000 Montpellier, France

Institut Universitaire de France (IUF), F-75005 Paris, France

P2.24: A Surface X-Ray Diffraction Investigation on the 2×1 Surface Reconstruction of Bismuth on GaAs (001).

D. A. Crackett, G. R. Bell, D. Sterland, P. J. Mousley, H. Hussain and R. D. Richards

Department of Electronic and Electrical Engineering, University of Sheffield, Sheffield, UK

Department of Physics, University of Warwick, Coventry, UK

Diamond Light Source, Harwell Science and Innovation Campus, Didcot, UK

P2.26: Anomalous growth of epitaxial silicene on graphene : a kinetic Monte-Carlo approach.

K. Wang, M. Abel, M. Koudia, F. Fabbri, A. Michon, A. H. Denawi, H. Vach, I.

Berbezier, and J.-N. Aqua

Sorbonne Université, Centre National de la Recherche Scientifique,

Institut des NanoSciences de Paris, Paris, France

Aix Marseille Université, Centre National de la Recherche Scientifique, Université de Toulon, IM2NP, Marseille, France

NEST, Istituto Nanoscienze – CNR, Scuola Normale Superiore, Pisa, Italy

CRHEA, Université Côte d'Azur, CNRS, Valbonne, France

LPICM, CNRS, École Polytechnique, Palaiseau, France

P2.28: Controllable Branching of Self-Catalysed AlGaAs Nanowires Synthesised via Molecular Beam Epitaxy.

Giorgos Boras, Haotian Zeng, Raghavendra Juluri, Stephen Church, Huiwen Deng, Hui Jia, Anton Velychko,

Chong Chen, Ziyue Yin, Mingchu Tang, David Mowbray, Patrick Parkinson, Ana M. Sanchez, Huiyun Liu

Department of Electronic and Electrical Engineering, University College London, WC1E 7J, United Kingdom

Department of Physics, University of Warwick, Coventry CV4 7AL, United Kingdom

Department of Physics and Astronomy and the Photon Science Institute, University of Manchester, M13 9PL, United Kingdom

Department of Physics and Astronomy, University of Sheffield, S3 7RH, United Kingdom

P2.30: Drastic enhancement of the internal quantum efficiency of thick (In,Ga)N layers by thermal annealing.

J. Kang, A. Campbell, J. Lähnemann, L. Geelhaar, and O. Brandt

Paul-Drude-Institut für Festkörperelektronik, Leibniz-Institut im Forschungsverbund Berlin e.V., Hausvogteiplatz 5–7, 10117 Berlin,

Germany

P2.32: Influence of High-temperature annealing on MBE-grown AlN thin film layers.

S. Mitra, J. Brault, M. Nemoz, A. Courville, and J.-V. Duboz

Université Côte d'Azur, CNRS, CRHEA, 06560 Valbonne, France

P2.34: Kinetic monte carlo simulation of GaAs growth on (001) silicon.

M. Silvestre, A. Gilbert, J.-N. Aqua, E. Tournié, J.-B. Rodriguez

IES, University of Montpellier, CNRS, F – 34000 Montpellier, France

RIBER SA, F – 95870 Bezons, France

Sorbonne Univ, CNRS, Inst. Nanosci. Paris, INSP, F-75005 Paris, France

Institut Universitaire de France (IUF), F-75005 Paris, France



P2.36: Segregation-Driven Formation of Bismuth Quantum Dots in GaAsBi Layers and Quantum Structures.

Butkutė Renata, Špokas Aivaras, Zelioli Andrea, Vaitkevičius Augustas , Bičiūnas Andrius , Dudutienė Evelina , Čechavičius Bronislovas, Skapas Martynas , Čerškus Aurimas, Talaikis Martynas, Baranowski Piotr, Wojnar Piotr
Center for Physical Sciences and Technology, Vilnius, Lithuania
Institute of Photonics and Nanotechnology, Vilnius University, Vilnius, Lithuania
Institute of Physics, Polish Academy of Sciences, Warsaw, Poland

P2.38: Surface processes on Bi₂Se₃(0001) during indium deposition studied by in situ reflection electron microscopy.

D. Rogilo, S. Ponomarev, D. Nasimov, K. Kokh, A. Ryabishchenkova, V. Golyashov, D. Sheglov, A. Latyshev
Rzhanov Institute of Semiconductor Physics SB RAS, Novosibirsk, Russia
Novosibirsk State University, Novosibirsk, Russia
Sobolev Institute of Geology and Mineralogy SB RAS, Novosibirsk, Russia

P2.40: Tuning the Diameter of GaAs Nanowires by Wet Chemical Etching. J.Pelenc , P. Regreny, C. Botella, N. Blanchard, N. Chauvin, and J. Penuelas,

Ecole Centrale de Lyon, CNRS, INSA Lyon, Université Claude Bernard Lyon 1, CPE Lyon, INL, UMR 5270, 69130 Ecully, France
University of Lyon – CNRS, ILM, UMR 5306, Université Lyon I, Bât. A. Kastler, 10 rue A.Byron, 69622 Villeurbanne, France

P2.42: Growth of Superconducting Sr₂RuO₄ Thin Films via Thermal Laser Epitaxy.

Faeth Brendan, Harbola Varun, Hensling Felix, Majer Lena, Schwaigert Tobias, Wu Yu-Mi, Van Aken Peter, Suyolcu Eren, Braun Wolfgang, Mannhart Jochen
Max Planck Institute for Solid State Research, Germany
Epiray GmbH, Germany
Cornell University, New York, United States

P2.44: Optimizing thermal management of equipment used in MBE/PVD-processes via simulation.

T. Stiller, I. Nitsche, S. Krinke, A. Ludwig, and A. Wieck
CreaTec Fischer & Co. GmbH, Erligheim, Baden-Württemberg, Germany
Ruhr Universität Bochum, Bochum, Nordrhein-Westfalen, Germany





I9: Machine Learning for the simulation of strained-film growth: tackling longtime scales with Finite Element Method accuracy.

D. Lanzoni,^{1,2,*}, L. Martìn-Encinar³, R. Bergamaschini², F. Rovaris,² A. Fantasia² and F. Montalenti²

¹Department of Physics, Università di Genova, Italy

² Department of Materials Science, Università di Milano-Bicocca, Italy

³ Dpto. de Electricidad y Electrónica, E.T.S.I. de Telecomunicación, Universidad de Valladolid, Spain

*daniele.lanzoni@unimib.it ; daniele.lanzoni@edu.unige.it

In recent years Machine Learning (ML) has proven to be an effective tool to approximate computationally expensive tasks in materials simulations while retaining a high degree of accuracy [1]. Here we present an application of Neural Networks (NNs) to continuum models describing the morphological evolution of thin heteroepitaxial films. The dynamics of this class of system is determined, through Partial Differential Equations [2], by the (generalized) chemical potential. This, in turns, contains surface energy, strain effects and interactions with the underlying substrate. From a computational study perspective, elastic contributions due to the possible mismatch between the film and substrate lattice are the most expensive ones to calculate, as closed form analytical expressions are available only in the small-slope limit [3]. For a generic free surface profile, however, the elastic equilibrium problem should be solved, e.g. through Finite Element Method (FEM). This is the principal computational bottleneck, as a single full evolution may require several hundreds of thousands of FEM calls [4], hindering the study of large systems over long timescales. We show that an accurate and efficient NN model can be trained to surrogate the full FEM solution, with a speed up of ~ 4 orders of magnitude for simulations. Importantly, building the dataset required for the training procedure has a computational cost which is comparable to a single, small computational cell evolution.

For simplicity, the 2D, isotropic case will be discussed, using Ge on Si(001) as a prototypical system [5], although the method generalize to more complex scenarios. Once the NN is trained, it may be used to run simulations involving coarsening and growth with a several orders of magnitude reduction in the computational costs, pushing forward the limits of tractable systems both in terms of time and spatial scales.

[1] P. Mehta et al., *Physics Reports* vol. 810 (2019), p. 1-124

[2] W. W. Mullins, *J. Appl. Phys.* 28 (3), (1957): 333–339.

[3] D. Srolovitz, *Acta Metallurgica*, vol. 37, no. 2, (1989): 621–625

[4] F. Rovaris et al, *Physical Review B* 94.20 (2016): 205304.

[5] D. Lanzoni et al., *APL Mach. Learn.* 2 (3) (2024): 036108

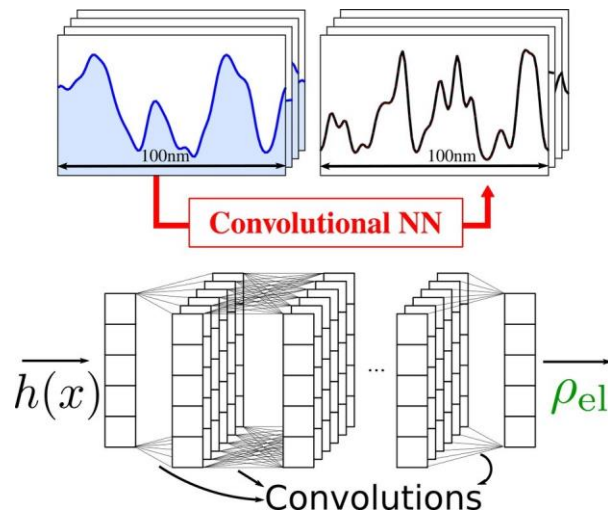


Figure 1: Neural Network (NN) scheme. The NN is used to approximate the mapping between the free surface profile $h(x)$ and the elastic energy density ρ

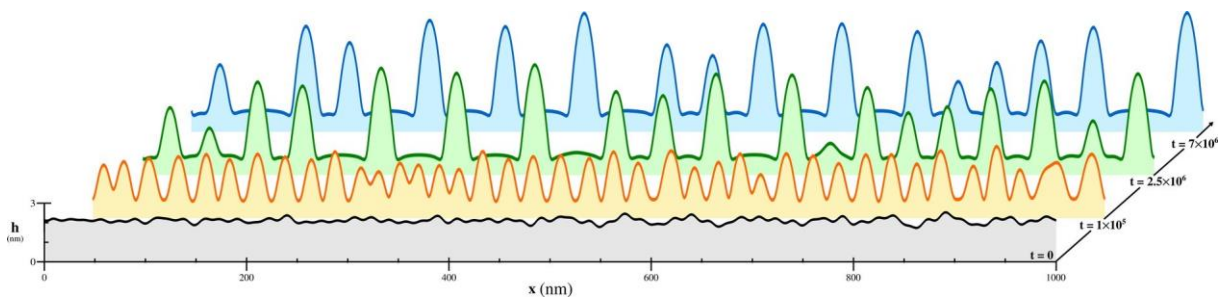


Figure 2: Once the NN is trained, it can be used to perform simulations over larger computational cells at a reduced computational cost, reaching longer time scales



S9.1: Dual-atom diffusion-limited growth model for compound nanowires: Application to InAs nanowires

Danylo Mosiits, Yann Genuist, Joël Cibert, Edith Bellet-Amalric, and Moira Hocevar

¹Univ. Grenoble Alpes, CNRS, Grenoble INP, Institut Néel, 38000 Grenoble, France

²Univ. Grenoble Alpes, CEA, Grenoble INP, IRIG, PHELIQS, 38000 Grenoble, France

*joel.cibert@neel.cnrs.fr

The diffusion-limited model of the growth of nanowires by molecular beam epitaxy, initially developed for silicon nanowires, has been continuously improved over years and extensively applied to describe not only elemental semiconductors, but also compound semiconductors [1]. In the latter case, it assumes either that the growth is limited by one of the constituents (for instance, by arsenic in the case of selfseeded growth of GaAs), or the existence of an “average species” which tries to combine the properties of the two constituents. However, these two constituents may have very different characteristics: A good example is InAs, where arsenic is highly volatile with no or short-ranged diffusion, while indium is not volatile and features a micrometer-sized diffusion length. In the present approach [2], we calculate the current of adatoms which can reach the nanodroplet and contribute to the growth. Then we assume that the instantaneous growth rate is determined by the minority current. As the current depends not only on the flux from the cell, but also on the nanowire radius and length, the two currents must be calculated for each nanowire of the sample (with its radius) and at each time of the growth (with its instantaneous length). This approach allows us to satisfactorily reproduce the final length of InAs nanowires as a function of the radius (Fig. 1), without changing the material parameters (such as the diffusion lengths) when changing the indium or arsenic flux. It also reveals several aspects of the growth of compound nanowires, which are expected to apply as soon as the adatoms of the two constituents feature different behaviors - as well-established for III-V compounds, well beyond InAs, and probably true for other, less-known compounds.

- When describing the growth conditions, the flux ratio is not a sufficient criterion. In Fig. 1, the growth of thin nanowires is limited by the arsenic current (due to arsenic evaporation as a result of the Kelvin effect on a volatile species), see Fig. 2a; the growth of thick nanowires is limited by the indium current (due to the strong diffusion of indium adatoms), see Fig. 2c.
- For nanowires with an intermediate radius value, the limiting current switches during growth (Fig. 2b). The switch is abrupt.
- Under steady-state flux conditions, the two maximum currents strongly differ at all times, except for very short periods of time during the growth of certain nanowires, such as at the switching in Fig. 2b. Stoichiometric growth conditions do not exist for a whole nanowire.

[1] V. G. Dubrovskii, N. V. Sibirev, R. A. Suris, G. É. Cirlin and V. M. Ustinov, M. Tchernysheva, and J. C.

Harmand, *Semiconductors* **40**, 1075 (2006).

[2] D. Mosiits, Y. Genuist, J. Cibert, E. Bellet-Amalric and M. Hocevar, *Cryst. Growth Des.* **24**, 3888 (2024).

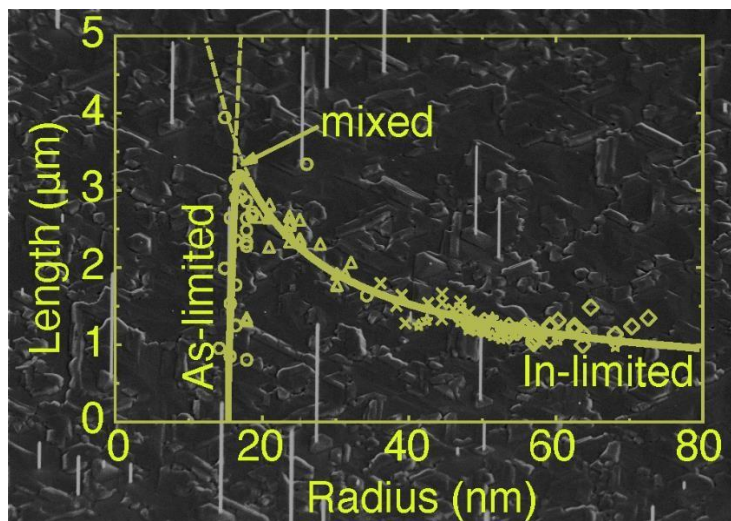


Fig. 1: InAs nanowires: scanning emission microscopy image (background) and length-radius plot. Symbols are experimental, thin dashed lines correspond to the calculated maximum currents of each type, the thick line is calculated using the instantaneous minority currents.

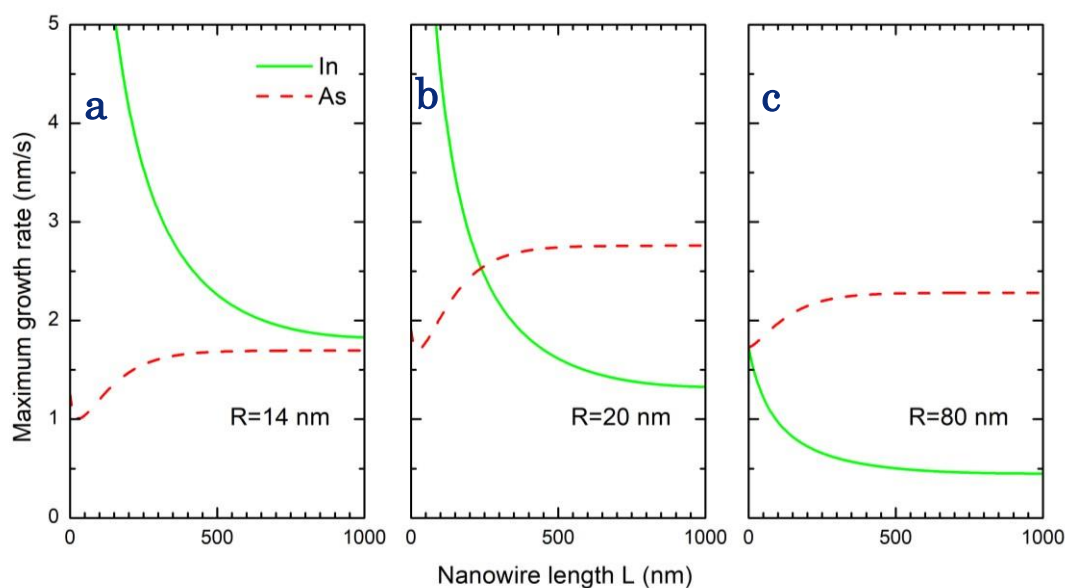


Fig. 2: Calculated indium and arsenic currents (expressed in maximum growth rates of an InAs nanowire), for the growth conditions and fitting parameters used in Fig. 1, as a function of the instantaneous nanowire radius. The arsenic flux impinging the substrate is four times larger than the indium flux. The growth is limited by the arsenic current for a small radius (a, $R=14$ nm), and by the indium current for a large radius (c, $R=80$ nm). At intermediate radius value (b, $R=20$ nm), the growth is limited by arsenic at the beginning of the growth, and by indium as the length increases.



S9.2: Bottom gated in-plane selective area grown InSb nanowires on GaAs(111)B

C. Barbot¹, C. Coinon¹, M. Berthe¹, Y. Deblock¹, Q. Lan², E. Okada¹, L. Thomas¹, P. Capiod¹, P. Ebert²,
B. Grandidier¹ and L. Desplanque^{1,*}

¹ Univ. Lille, CNRS, UMR 8520 – IEMN- F-59000 Lille, France

² Ernst-Ruska Centrum (ER-C-1), Forschungszentrum Jülich GmbH, 52425 Jülich, Germany

*ludovic.desplanque@univ-lille.fr

The selective area growth (SAG) of a semiconductor inside a dielectric mask fabricated by e-beam lithography enables the design of in-plane nanostructures with an arbitrary shape and a deterministic position. This scalable process applied to strong spin-orbit semiconductors such as InSb or InAs is very interesting for the fabrication of quantum devices involving branched NW or nano-resonators exploiting coherent electron transport [1, 2]. However, in this configuration, tuning the charge density in the NW is generally achieved with a top gate, limiting the possibility to adjust the Fermi level inside semiconductor/superconductor hybrid nanostructures that aim to demonstrate Majorana Zero mode [2]. In this work, we investigate (i) the growth of in-plane InSb NWs on a GaAs(111) substrate by atomic hydrogen assisted Selective Area Molecular Beam Epitaxy (SAMBE) and (ii) the possibility to tune the charge density and the conductivity inside the NW by adding a GaInP top barrier on the substrate before the mask fabrication.

An InSb thin film is first grown on a 100 nm Ga_{0.5}In_{0.5}P barrier deposited on a n-doped ($n=3 \times 10^{18} \text{ cm}^{-3}$) GaAs (111)_B substrate (figure 1a). To ensure a quasi-two dimensional growth of InSb despite the 14.6% lattice mismatch between InSb and GaAs, a very large Sb/In flux ratio of 120 is used. As shown in figure 1b, a quite smooth surface with a low density of nano-holes is achieved after a 100nm-thick InSb growth. After processing Van der Pauw and TLM devices from this layer, we measure a 300K Hall mobility of $11000 \text{ cm}^2 \cdot \text{V}^{-1} \cdot \text{s}^{-1}$ and evidence an efficient command of the source-drain current with the bottom gate. We used the same growth conditions for the SAMBE of InSb NWs on patterned GaInP/GaAs:n+ substrates (figure 2a). Scanning Electron Microscopy reveals that quite good morphology can be obtained for the NWs (figure 2b) after 50 nm deposition. Using Transmission Electron Microscopy, we evidence that most of the mismatch between InSb and GaInP is accommodated with an array of misfit dislocations at the interface together with some stacking faults within the InSb nanostructures. A variation of the resistance of 100nm-wide NWs with bottom gate bias is demonstrated using 4P-STM measurements at room temperature (figure 2d). More details about the structure of the NWs and their electrical measurements will be given during the conference.

Acknowledgments and References

This study was financially supported by the French National Research agency under the program Equipex EXCELSIOR, INSPIRING ANR project (ANR-21-CE09-0026-01), PHC PROCOPE project (N°50795SA), the French Technological Network Renatech, and the Région Hauts de France.

[1] Vaitiekėnas et al. Phys. Rev. Lett. 121, 147701 (2018) <https://doi.org/10.1103/PhysRevLett.121.147701>

[2] Op het Veld et al. Commun Phys 3, 59 (2020). <https://doi.org/10.1038/s42005-020-0324-4>

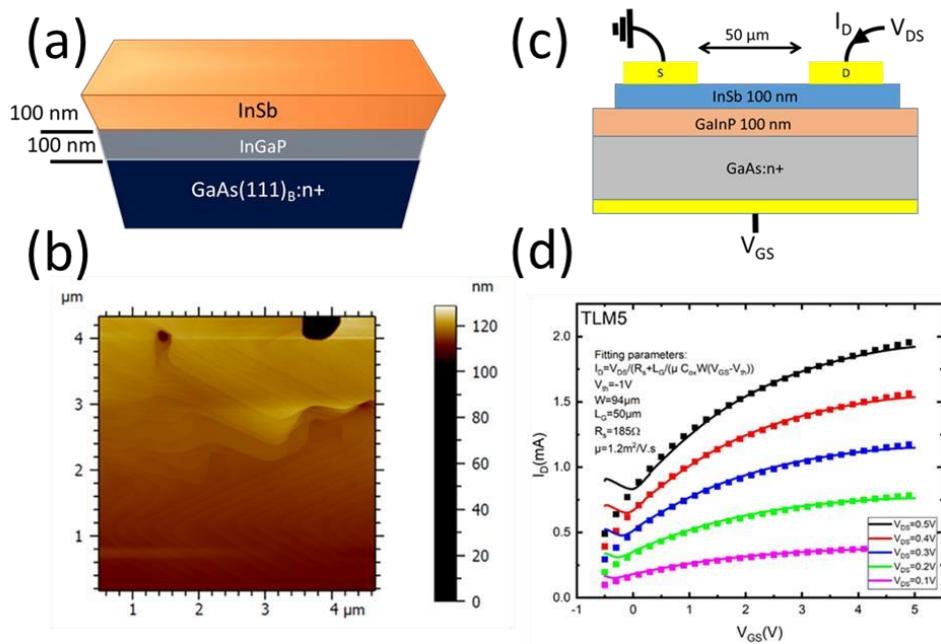


Fig. 1: Structure of the stack of two dimensional InSb/GaInP/GaAs sample (a). AFM image of the surface of the sample (b), Schematics of the device used for the transfer measurements displayed in (d) for different drain voltage. Solid line corresponds to the measurements and dot line to the fit.

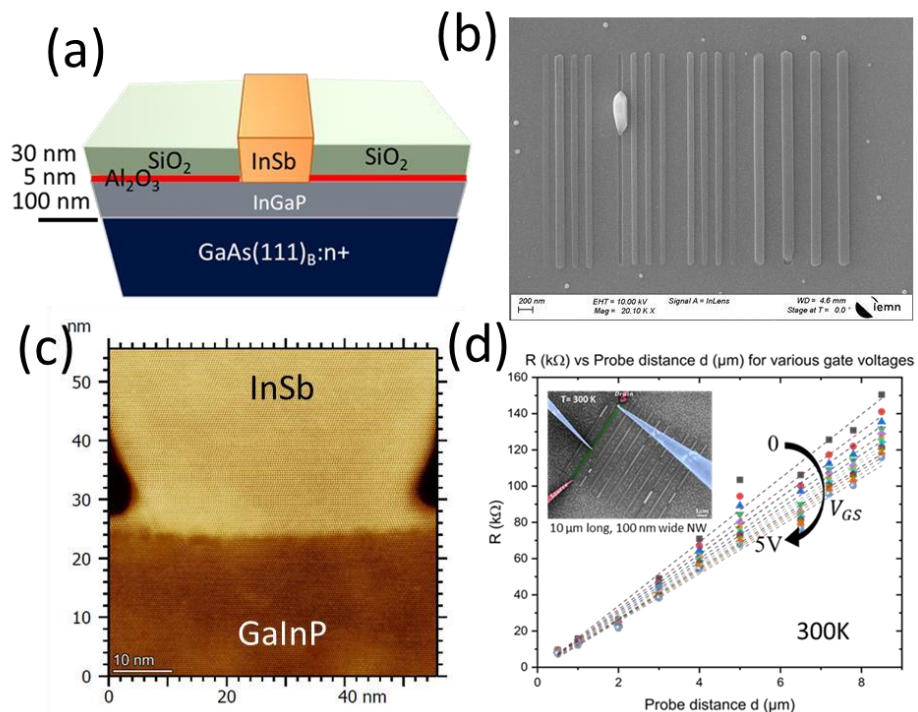


Fig. 2: Structure of the NWs grown by SAMBE (a). SEM image of an array of NWs after 50 nm deposition (b). Cross section TEM image of the interface between InSb NW and GaInP buffer layer (c). Resistance of the NW versus the inner probe distance measured on single 100nm wide InSb NW.



S9.3: High-mobility InAs-AlSb core-shell nanowire heterostructures for thermoelectric energy conversion

G. B. Hirpessa^{*}, S. Fust, R. Maier, F. Del Giudice, J. J. Finley and G. Koblmüller

Walter Schottky Institut and Physics Department, School of Natural Sciences, Technical University of Munich, Am Coulombwall 4, 85748 Garching, Germany

*E-mail : Genetbacha.Hirpessa@tum.de

Thermoelectric energy conversion offers widespread applications in waste heat recovery for power generation and requires suitable materials with large thermoelectric conversion efficiency. To maximize figure-of-merit $ZT = \sigma S^2 T / \kappa$ relevant parameters such as electrical conductivity (σ), thermoelectric power factor (σS^2), and thermal conductivity (κ) need to be optimized for a given operating temperature T . Due to the interdependence between thermal and electrical properties, and Seebeck coefficient S , the optimization of parameters for high ZT is limited in bulk materials, but in nanostructures, the properties can be decoupled [1]. The aim of our work is to experimentally realize independent control of the Seebeck coefficient and electrical conductivity by exploiting the 1D density of states in very high mobility MBE grown III-V nanowires (NWs). First proof-of-principle studies demonstrating these effects were performed recently on modulation-doped GaAs-AlGaAs core-shell NWs, where enhanced σS^2 , and strongly reduced κ were found [2]. While these initial studies were limited to low temperature, studying other III-V materials with lower electron effective mass is more appealing, in order to explore thermoelectric 1D-transport properties at higher temperatures with improved thermoelectric performance.

Here, we propose InAs-AlSb core-shell NW heterostructures as promising materials and show the first results on the growth using solid-source MBE on lithographically pre-patterned Si (111) substrates [3]. Creating high-mobility n-type (Si) modulated doped heterostructures is, however, particularly challenging in this system, since typical Si dopants are amphoteric and induce p-type behavior in AlSb. To mitigate this, two strategies are demonstrated: (i) Si-delta doping of a thin InAs QW embedded in the coaxial AlSb shell, and (ii) doping of a quaternary InAlAsSb shell lattice-matched to the InAs core (Figure 1). Correlated simulations of the band profiles and electron density distribution show clear formation of a high-mobility electron gas that is confined solely to the core InAs region when choosing InAs QW thickness of up to 5.5 nm and Si dopants (10^{19} cm^{-3}) placed in the center of the QW. For quaternary InAlAsSb with group-III and -V molar fractions in the mid-compositional range, Si δ -doping can be achieved directly in the shell without the need of an InAs QW (Figure 1). To realize InAs-QW based NW heterostructures, growth temperature optimization was necessary to induce highly symmetric growth of coaxial InAs QWs on the hexagonal NW sidewall facets, as found from cross-sectional He-ion microscopy. Likewise, we show the growth optimization routine for achieving InAlAsSb shell layers with composition tuned towards the midcomposition, and support these findings by STEM-EDX analysis (Figure 2). Finally, first examples of NW field effect transistor (NWFET) test devices are shown, where both contact formation was established and gate-bias dependent electrical characterization was performed. 1-D sub-band quantization is found in InAsAlSb core-shell NWs for temperatures up to 110K, which is about 40 K higher as in unpassivated InAs reference NWs (Figure 3), and much higher as in Si delta-doped GaAs-AlGaAs NWs.

[1] H. J. Goldsmid, Springer Series in Materials Science Vol. 121, pp 45-66 (2016)

[2] S. Fust, et al., Advanced Materials Vol. 32, No. 4 pp 1905458 (2020)

[3] F. del Giudice, et al., Applied Physics Letters Vol. 119 No. 19, pp 193102 (2021) [4] G. B. Hirpessa, in preparation (2024).

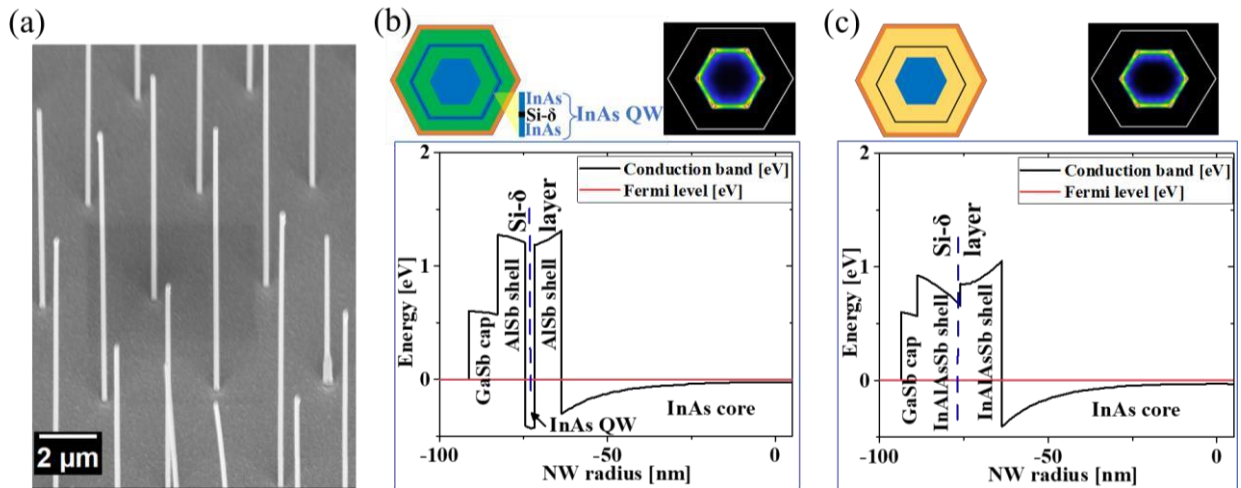


Fig. 1: MBE grown core-shell NWs and simulation data for different modulation doped structures; (a) InAs-AlSb core-shell NWs obtained by selective area epitaxy on prepatterned SiO₂/Si (111) substrate; (b,c) Schematic crosssection, band profiles, and corresponding electron density maps of (b) InAs-AlSb core-shell NW with InAs QW hosting a Si- δ layer, and (c) InAs-InAlAsSb core-shell NW with Si- δ doping layer at the center of the shell.

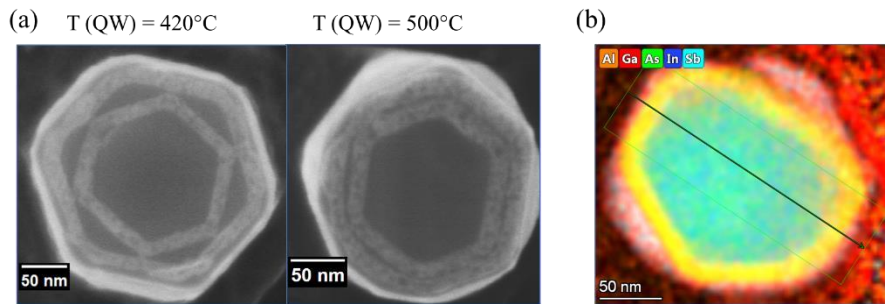


Fig. 2: (a) Helium ion microscopy (HIM) images of InAs-AlSb core-shell NWs with InAs QW embedded in the shell, for QW growth temperature of 420 °C (left, asymmetric growth) and 500 °C (right, symmetric growth); (b) STEMEDX compositional map of the elemental distribution within an InAs-InAlAsSb core-shell NW.

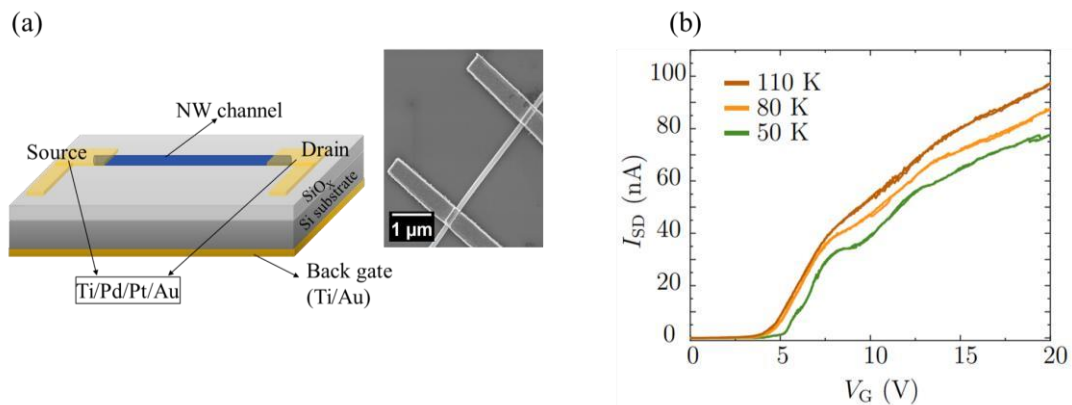


Fig. 3. (a) Schematic (left) and SEM image (right) of a NW field effect transistor (FET) with metallization profile used for InAs-AlSb core-shell NWs with GaSb cap; (b) temperature-dependent transfer characteristic of the NWFET at varying temperatures of 50 K, 80 K and 100 K.



Wednesday 12.03
20h00
Workshop Banquet
Hotel Restaurant Bataclan
Plateau, Rte de Nabinas, 06660

Sponsored by :



There will be a shuttle that brings you from Room « Rovery » to the restaurant.

Pick-up point: room « Rovery »

- 1st departure: 19h20

- 2nd departure: 19h45



It is recommended to take multi-purpose shoes with you.

There is a few hundred meters of walking on the snow from the shuttle drop-off to the restaurant.



Invited talk : 23min + 7min questions
 Oral : 15min + 5min questions



Thursday, 13.03	
08:00	Registration
Session 10 : Quantum dots : chairman Werner Wegscheider	
08:30	Invited talk I10: GaSb-based quantum dot emitters for telecom wavelengths , <u>Teemu Hakkarainen</u> , Optoelectronics Research Centre, Tampere University, Tampere, Finland
09:00	S10.1: Droplet etched InxGa1-xAs quantum dots embedded in In0.52Al0.48As for optical C-band emission , <u>Dennis Deutsch</u> , Department of Physics, Paderborn University, 33098 Paderborn, Germany
09:20	S10.2: Investigations of C-band InAs/InP Quantum Dots Grown by Molecular Beam Epitaxy Using Indium Flush Technology , <u>Hui Jia</u> , Dep. of Electronic and Electrical Engineering, Univ. College London, London, UK
09:40	S10.3: Wafer scale quantum dot growth control for scalable multi single photon sources technology , <u>Arne Ludwig</u> , Lehrstuhl für Angewandte Festkörperphysik, Ruhr-Universität Bochum, 44801, Germany
10:00	S10.4: Electrically tunable orbital couplings in MBE grown InAs/InGaAs QDmolecules emitting in O-band , <u>Pavel Avdienko</u> , Walter Schottky Inst., Phys. Dep., School of Nat. Sciences, TUM, Garching b. München, Germany
10:20	break
Session 11: Novel materials - Photovoltaic : Chairwoman Hélène Rotella	
10:40	Invited talk I11: Interface properties of (Al)GaAs/GaAsBi quantum wells grown by MBE , <u>Esperanza Luna</u> , Paul-Drude-Institut für Festkörperelektronik, Leibniz-Institut im Forschungsverbund Berlin, Germany
11:10	S11.1: GaAs growth on graphene covered substrates towards substrate recycling , <u>Amaury Delamarre</u> , C2N, CNRS, Univ. Paris-Saclay, 10 Boulevard Thomas Gobert, 91120 Palaiseau, France
11:30	S11.2: Earth abundant oxynitrides alloys for tandem solar cells , <u>Khiem Tu Tran</u> , Université Côte d'Azur, CNRS, CRHEA, Valbonne, FRANCE
11:50	S11.3: The correlation between the microstructure and the optoelectronic properties of Zn3P2 grown by Selective Area Epitaxy , <u>Raphaël Lemerle</u> , Lab. of Semicond. Mat., Ecole Polytechnique Fédérale de Lausanne,
12:10	S11.4: Remote epitaxy of III-V films on a universal template , <u>Tobias Henksmeier</u> , Paderborn University, Department of Physics, Warburger Str. 100, 33089 Paderborn
12:30	Closing Remarks
13:00	Lunch Boxes

Meet us at the Movie theater “le Rouret”



I10: GaSb-based quantum dot emitters for telecom wavelengths

T. Hakkarainen

¹Optoelectronics Research Centre, Tampere University, Tampere, Finland

*teemu.hakkarainen@tuni.fi

Solid-state single and entangled photon emitters linked coherently over long distances with optical fibers enable a new generation of quantum-based communications networks. Currently, epitaxial semiconductor quantum dots (QDs) pave the way as a scalable approach for fabricating deterministic non-classical light sources that can be integrated with other photonic or electronic components in miniaturized form. Here, we present a new quantum material system based on GaSb-based QDs formed by filling droplet-etched nanoholes [1,2], a technique which has been previously used for the state-of-the-art single- and entangled-photon sources in the GaAs-based materials emitting at wavelengths shorter than 800 nm [3-6].

This presentation covers the development steps and the current state-of-the-art of (In)GaSb QDs grown by filling droplet-etched nanoholes in AlGaSb. It is demonstrated that, while the GaSb QDs exhibit high homogeneity and small fine structure splitting similarly to their GaAs counterparts, they also enable single-photon emission in the 3rd telecom window [7] with prospects for extending towards 2 μ m. Furthermore, by employing quasi-resonant excitation or LO-phonon-assisted excitation of a single QD, it is possible to achieve spectrally clean emission from a single exciton line and high-quality single-photon emission [8]. These properties make GaSb-based QDs ideal candidates for quantum photonic applications requiring compatibility with Si-photonics and fiber-based telecom.

[1] J. Hilska et al. *Cryst. Growth Des.* 21 1917–1923, 2021

[2] A. Chellu et al. *APL Materials* 9, pp. 051116, 2021 [3] J. Liu et al. *Nature Nanotechnology* 14, 586 (2019).

[4] D. Huber et al. *Nature Communications* 8, 15506 (2017).

[5] E. Schoöll, et al. *Nano Letters* 19, 2404 (2019).

[6] D. Huber et al. *Phys. Rev. Lett.* 121, 033902 (2018).

[7] J. Michl et al, *Adv Quantum Technol.* 6, 2300180 (2023).

[8] T. Hakkarainen et al. <https://doi.org/10.48550/arXiv.2404.06083>



S10.1: Droplet etched $\text{In}_x\text{Ga}_{1-x}\text{As}$ quantum dots embedded in $\text{In}_{0.52}\text{Al}_{0.48}\text{As}$ for optical C-band emission

D. Deutsch,^{1,*} C. Buchholz,¹ V. Zolatanosha,^{1,3} K. D. Jöns,^{1,2,3} D. Reuter^{1,2,3}

¹Department of Physics, Paderborn University, 33098 Paderborn, Germany

²Center for Optoelectronics and Photonics Paderborn (CeOPP), Paderborn University, 33098, Germany

³Institute for Photonic Quantum Systems (PhoQS), Paderborn University, 33098 Paderborn, Germany

*E-mail: ddeutsch@mail.uni-paderborn.de

Semiconductor quantum dots (QDs) have been established as promising sources for on-demand single photon and entangled photon pair generation for quantum communication applications [1]. In the case of polarization entangled photon pairs, it is possible to utilize the biexciton-exciton cascade of a QD system. Here $\text{GaAs}/\text{Al}_x\text{Ga}_{1-x}\text{As}$ QDs grown via local droplet etching (LDE) have been proven to be the current gold standard, as they exhibit very low fine-structure splitting (fss) due to good in-plane symmetry and their negligible strain [2]. However, for the $\text{GaAs}/\text{Al}_x\text{Ga}_{1-x}\text{As}$ system one is limited to photon emission around 780 nm. In this contribution, we present the adaptation of the LDE technique to the $\text{InP}/\text{In}_y\text{Al}_{1-y}\text{As}/\text{In}_x\text{Ga}_{1-x}\text{As}$ system for photon emission in the optical C-band. We show that we can produce nanoholes that display very good in-plane symmetry when utilizing optimized process parameters for the etching process. This we could conclude from atomic force microscopy (AFM) measurements. We investigated the influence of the etching material (In, Al, InAl), the etching temperature and the amount of etching material on the resulting nanohole geometry. When In is included in the etching material we found that the nanoholes start to degrade after the As_2 flux is resumed following the etching step (see Fig. 1). We however found that the nanoholes can be conserved by overgrowing them with a thin $\text{In}_{0.52}\text{Al}_{0.48}\text{As}$ layer directly after resuming the As_2 flux. Etching temperatures of $T_{etch} = 410$ °C and 435 °C proved to be optimum regarding hole depth and in-plane symmetry. Fig. 2 summarized our finding for varying amounts of etching material \square_{InAl} for an exemplary $T_{etch} = 435$ °C. For larger amounts of etching material, we observe a bi-modal distribution of hole sizes. For $\square_{\text{InAl}} = 2.7$ ML and $\square_{\text{InAl}} = 1.4$ ML only one type of nanoholes is found. The hole depth stays constant at ca. 30 nm but the hole diameter decreases with decreasing \square_{InAl} . Reducing \square_{InAl} to 0.7 ML decreases the hole depth to less than 20 nm and for $\square_{\text{InAl}} = 0.3$ ML no holes at all have been observed. Further experiments have shown that these nanoholes can be filled with $\text{In}_x\text{Ga}_{1-x}\text{As}$ and that the filling works better when utilizing an As_4 environment instead of As_2 . Finally, we demonstrate that the filled nanoholes emit light when embedded in an $\text{In}_{0.52}\text{Al}_{0.48}\text{As}$ matrix. The emission wavelength can be tuned to the optical C-band by adjusting filling level and In-content (see Fig. 3). μ -photoluminescence spectroscopy reveals sharp emission line typical for individual semiconductor QDs.

[1] S. F. C. da Silva et al., App. Phys. Lett. 119, 120502 (2021).

[2] Y. Li et al., Chinese Physics B 27, 020307 (2018).

Fig. 1: AFM surface scans of nanoholes produced by In droplet etching after different time lengths of As₂ exposure. After the step the As valve was opened for 0 (a)), 1 (c)) and 5 min (d)) before cooling down the a rate of 30 K/min. Etching on all samples performed at $p_{As_2} = 2 \times 10^{-7}$ mbar with $\theta_{In} =$ and at $T_{etch} = 435$ °C

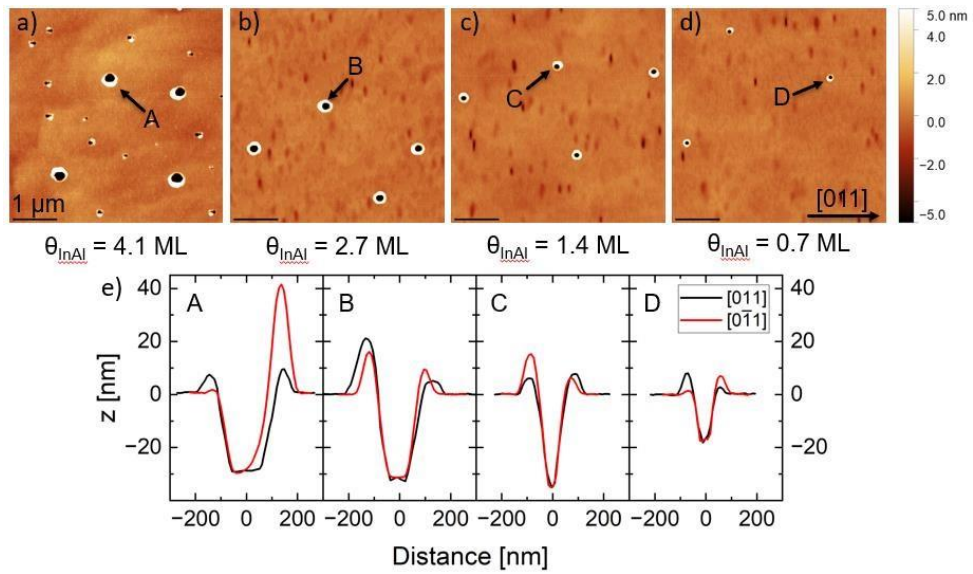
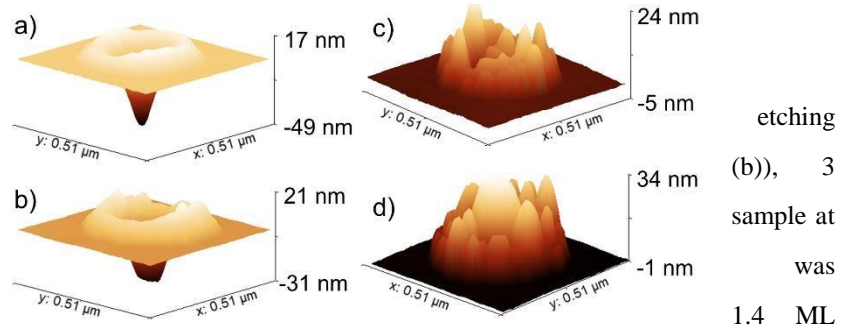


Fig. 2: a) - d) AFM measurement series of samples produced by varying the amount of the etching material (InAl) at a fixed etching temperature of $T_{etch} = 435$ °C, residual As₂ pressure of $p_{As_2} = 2 \times 10^{-7}$ mbar, annealing time of 3 min and heating the samples to 505 °C after the LDE process. e) Corresponding line scans for the two highsymmetry directions of selected nanoholes indicated in the AFM images. $\theta_{InAl} = 0.3$ ML was tested as well and resulted in a nanohole-free surface.

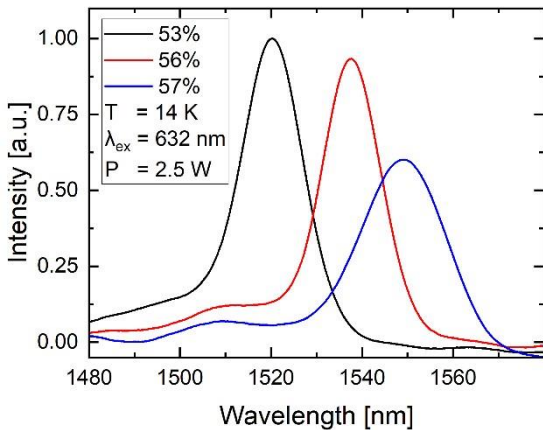


Fig. 3: Ensemble PL spectra of droplet etched In_xGa_{1-x}As QDs embedded in an In_{0.52}Al_{0.48}As matrix. The nanoholes were etched at $T_{etch} = 435$ °C, with $\theta_{InAl} = 1.4$ ML and $p_{As_2} = 2 \times 10^{-7}$ mbar residual As₂ pressure producing ~33 nm deep holes. These nanoholes were completely filled with In_xGa_{1-x}As and then overgrown with In_{0.52}Al_{0.48}As.



S10.2: Investigations of C-band InAs/InP Quantum Dots Grown by Molecular Beam Epitaxy Using Indium Flush Technology

J. Yuan¹, C. Dear¹, H. Jia¹, * J. Park¹, *, Y. Hou², K. El. Hajraoui^{3,4}, H. Zeng¹, H. Deng¹, J.

Yang¹, M. Tang¹, S. Chen¹, Q. M. Ramasse^{3,5}, Q. Li⁶, A. Seeds¹, and H. Liu¹

¹*Department of Electronic and Electrical Engineering, University College London, London, WC1E 7JE, United Kingdom*

²*Department of Electronic and Electrical Engineering, Bay Campus, Swansea University, Swansea, SA1 8EN, United Kingdom*

³*SuperSTEM, SciTech Daresbury Science and Innovation Campus, Block J, Keckwick Lane, Daresbury, WA4 4AD, United Kingdom*

⁴*York NanoCentre & Department of Physics, University of York, York, YO10 5DD, United Kingdom*

⁵*School of Chemical and Process Engineering and School of Physics and Astronomy, University of Leeds, Leeds, LS2 9JT, United Kingdom*

⁶*School of Physics and Astronomy, Cardiff University, Cardiff, CF24 3AA, United Kingdom*

*E-mails : hui.jia@ucl.ac.uk and jae-seong.park@ucl.ac.uk

High-quality InAs/InP quantum dots (QDs) emitting at 1550 nm are indispensable to achieve highperformance telecom C-band lasers. In general, a longer emission (>1550 nm) with broad spectral character has been obtained with InAs/InP QDs. Here, we investigate the use of the indium-flush (IF) method to shorten the emission wavelength and improve the optical properties of InAs/InP QDs. By exploiting IF, the full-width at half-maximum of the room-temperature QD photoluminescence spectra was narrowed from 89.2 meV to 47.9 meV, with a blue shift of 300 nm (from 1824 nm to 1522 nm). The scanning transmission electron microscopy and electron energy loss spectroscopy results reveal the atomic-level mechanism of the IF method which uniformly modify the height of InAs/InP QDs in a controlled manner and form distinct Al-rich and In-rich regions. A slight reduction of the strain at the QD/capping layer interface has also been found for the sample with indium flush. Finally, InAs/InP (001) QD lasers with the IF method have been demonstrated with a low threshold current density per QD layer of 106 A/cm². We demonstrated both in terms of mechanism model and device performance that the IF method could serve as a robust strategy for the growth of high-performance C-band InAs/InP QD lasers via molecular beam epitaxy.

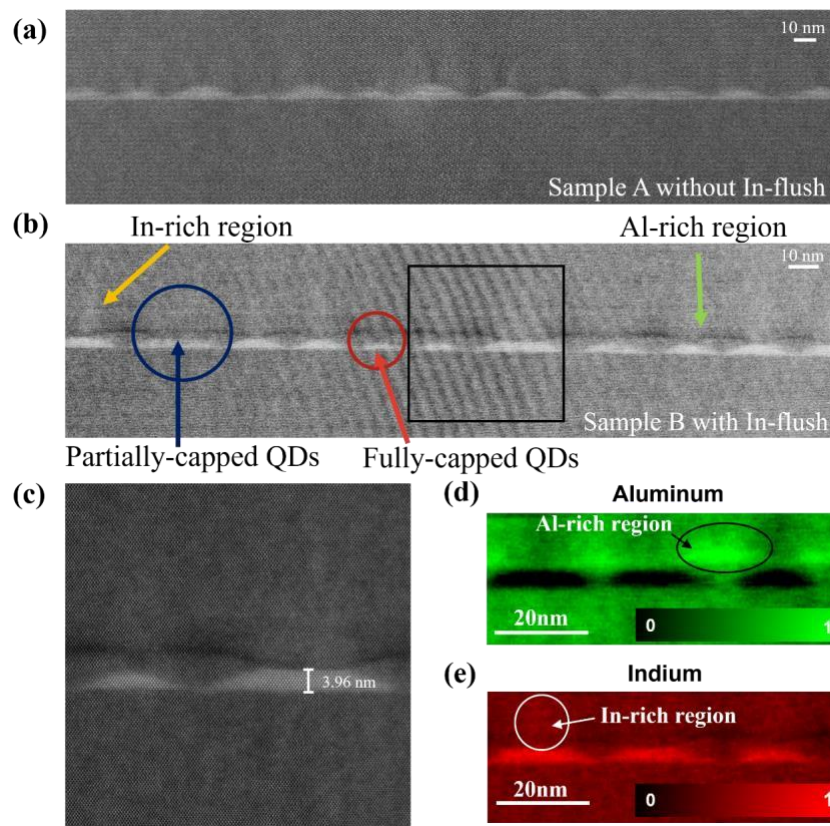


Figure 1. HAADF images of QD morphologies and adjacent layers of the sample A (without IF) in (a) and the sample B (with IF) in (b). (c) High-resolution HAADF image of the area highlighted by a black box in *b*, showing fully-capped and partially-capped QDs. Individual electron energy loss spectroscopy maps of the sample with IF, showing the relative distribution of (d) Al (green intensity channel) and (e) In (red intensity channel).

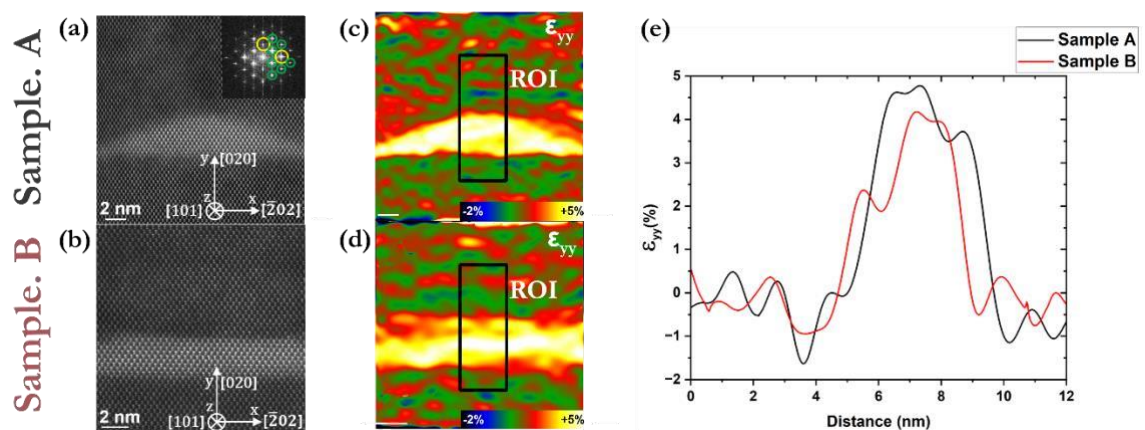


Figure 2. High-resolution high angle annular dark field images of the InAlGaAs/InAs QD/InAlGaAs interface along the [101] axis, as depicted in the Fourier transform (FFT) inset (a), in (a) sample A and (b) sample B. The vertical ϵ_{yy} strain maps calculated using geometrical phase analysis from the FFTs of the experimental images in (c) sample A and (d) sample B (e) The vertical ϵ_{yy} strain profiles for sample A and sample B along the (200) growth direction of the InAs (QD) on the InAlGaAs matrix averaged along the region of interest highlighted by a rectangle box in (c) and (d), respectively.



S10.3: Wafer scale quantum dot growth control for scalable multi single photon sources technology

Elias Kersting, Hans-Georg Babin, Nikolai Spitzer, Severin Krüger, Peter Zajac, Meret Grell, Timo Kruck, Nikolai Bart, Marcel Schmidt, Andreas Wieck, and Arne Ludwig*

Lehrstuhl für Angewandte Festkörperphysik, Ruhr-Universität Bochum, 44801, Germany *E-mail: arne.ludwig@rub.de

A key component for photonic quantum devices is a high-fidelity single photon source. Semiconductor quantum dots (QDs) in photonic cavities offer a promising route to create such devices. However, noise processes can hamper solid-state emitters [1]. Major contributors to decoherence and low efficiency include random charge rearrangements in the semiconductor environment or the QD itself [2], caused by processes such as Meitner-Auger recombination [3] or photoionization [4]. Therefore, it is crucial to meticulously control the molecular beam epitaxy (MBE) machine's vacuum and effusion cells to grow wafers of the highest possible quality. Another important aspect is heterostructure design:

embedding quantum emitters in a diode can stabilize the charge state and shield against fluctuations [5].

Even for ternary matrix material local droplet etched QDs [6,7], we demonstrate that this approach can lead to blinking-free, transform-limited emission [8]. To make QDs a scalable technology, even more demanding requirements must be met:

1. The QD density must range from 0.1 to 10 QDs/ μm^2 across the whole wafer, which is extremely challenging for strain-driven self-assembly [9,10].
2. The emission wavelength of a substantial portion of the QDs must be within the tuning range of the design wavelength.

Wafer rotation stop enables material gradient growth. Newly discovered implications of this wellknown method, such as periodic modulation of QD density [10] and QD emission wavelength [11], will be presented. The gradient growth method is also the basis for identifying ideal growth parameters [11,12] for wafer-scale production of homogeneous QD density and QD wavelength material. Figures 1 and 2 show photoluminescence results of our wafer-scale attempts to homogenize these parameters for LDE-grown GaAs QDs and LDE-grown InAs O-band QDs [12,13].

References:

- [1] A.V. Kuhlmann et al., Nat Phys **9**, 570 (2013).
- [2] G. Gillard et al., npj Quantum Inf **7**, 43 (2021).
- [3] A. Kurzmann et al., Nano Lett **16**, 3367 (2016).
- [4] P. Lochner et al., Phys. Rev. B **103**, 075426 (2021).
- [5] A. Ludwig et al. Journal of Crystal Growth **477**, 193 (2017).
- [6] C. Heyn, et al., Appl. Phys. Lett. **94**, 183113 (2009).
- [7] M. Gurioli et al., Nat. Mater. **18**, 799 (2019).
- [8] L. Zhai et al., Nat Commun **11**, 4745 (2020).
- [9] A.K. Verma et al., Journal of Crystal Growth **592**, 126715 (2022).
- [10] N. Bart, C. Dangel et al., Nat Commun **13**, 1633 (2022).
- [11] H.G. Babin et al., Journal of Crystal Growth **591**, 126713 (2022).
- [12] N. Spitzer et al., Crystals **14**, 1014 (2024). [13] E. Kersting et al., in preparation

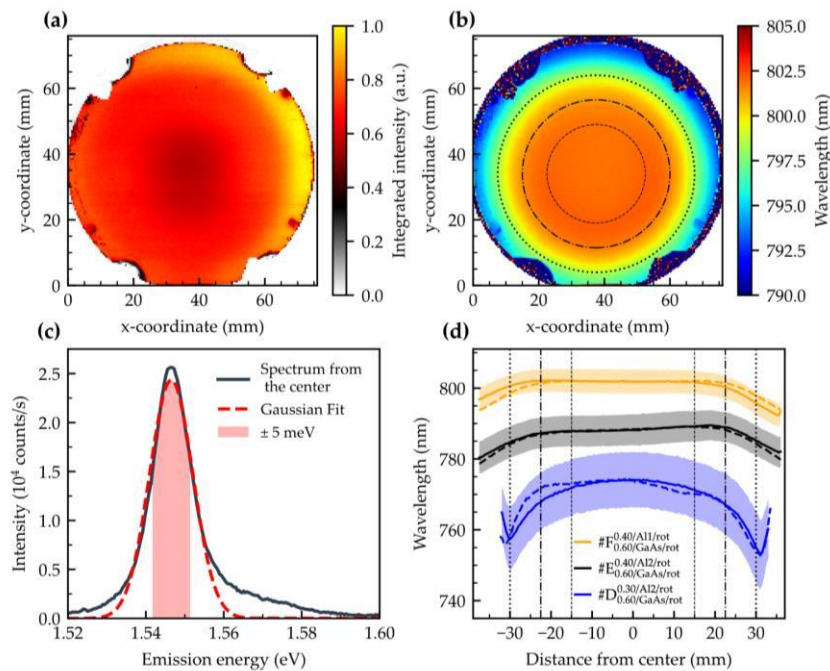


Figure 1: Wafer map photoluminescence of LDE-grown GaAs QDs. (a) A homogeneous intensity of QD luminescence indicates a uniform QD density. (b) The emission wavelength shows minimal variation across the wafer. (c) Photoluminescence (PL) spectrum at the centre of the wafer. (d) Wavelength as a function of position for three different wafers. The orange line corresponds to the wafer shown in (a). The black and blue line are from wafer growth attempts that yield less ideal wavelength distribution. The shaded area indicates the FWHM distribution.

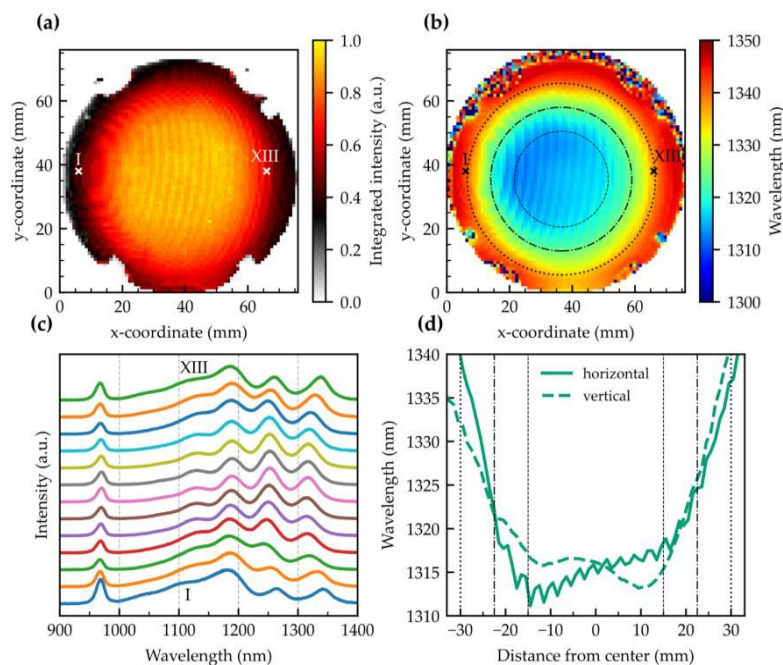


Figure 2: Wafer map photoluminescence of LDE-grown InAs QDs. (a) Intensity map. (b) The wavelength map shows O-band emission around the wafer centre. (c) PL spectra at points I to XIII in (a). A clear shell structure is visible indicating good homogeneity. (d) Wavelength as a function of position. A central region with a diameter of 45 mm yields O-band QDs.



S10.4: Electrically tunable orbital couplings in MBE grown InAs/InGaAs QDmolecules emitting in O-band

P. Avdienko,^{1,*} L. Hanschke,² Q. Buchinger,³ I. Lubianskii,⁴ H. Riedl,¹ A. Pfenning,³ T. HuberLoyola,³ S. Höfling,³ K. Müller,² and J.J. Finley^{1*}

¹Walter Schottky Institute, Physics Department, School of Natural Sciences, TUM, Am Coulombwall 4, 85748, Garching b. München, Germany

²ZEIT Lab, School of Computation, Information and Technology, TUM, Hans-Piloty-Straße 1, 85748, Garching b. München, Germany

³Lehrstuhl für Technische Physik, Physikalisches Institut, Julius-Maximilians-Universität Würzburg, Am Hubland, 97074 Würzburg, Germany

⁴Walter Schottky Institute, Technical University of Munich, Am Coulombwall 4, 85748 Garching, Germany

[*pavel.avdienko@tum.de](mailto:pavel.avdienko@tum.de) and jj.finley@tum.de

Epitaxially grown semiconductor quantum dots (QDs) and QD-molecules are a basis for modern photonic quantum technologies. Compared to spin qubits in III-V QDs, singlet-triplet logical qubits in optically active QD-molecules have been recently shown to have enhanced coherence times, due to suppressed coupling to magnetic noise [1]. Recently, excellent single photon source properties have been demonstrated for the InAs/GaAs QD-molecule devices emitting around 930 nm [2]. Nevertheless, precise control of optical and structural properties of QD-molecules is still a critical task for quantum photonics, especially in the telecommunication O- and C-bands (~1.3- and ~1.5- μm , respectively).

We present the first direct experimental observation of electrically tunable quantum orbital couplings in individual vertically stacked InAs/InGaAs QD-molecules emitting in the O-band at $T = 10\text{K}$. Individual InAs QD layers were grown by MBE on GaAs(001) substrates in Stranski–Krastanov growth mode and overgrown by 7 nm $\text{In}_{0.25}\text{Ga}_{0.75}\text{As}$ strain-reducing layer. The InAs/InGaAs QD layers, separated by 2–5 nm GaAs barriers, were symmetrically positioned near the center of the intrinsic region of a p-i-n diode, enabling tuning of excitonic transition energies and orbital couplings. The first QD layer was deposited 5 nm above a 68 nm short-period superlattice (SPSL) equivalent to $\text{Al}_{0.75}\text{Ga}_{0.25}\text{As}$ [3], while the second QD layer was capped with a 5 nm GaAs and second similar SPSL. The 90-nm-thick intrinsic GaAs layers were situated between p- and n-GaAs layers and the SPSLs (Fig.1). We observed wide tunability of the emission wavelength exceeding ~20 nm via the quantum-confined Stark in the QD structures with SPSL barriers (Fig.2a). By tuning the internal electric field in the samples containing InAs/InGaAs QD-molecules emitting in the O-band, we observe clear anticrossings of different charge state transitions (Fig.2b). Comparison with theoretical predictions reveals that the excitonic anticrossings arise from tunnel coupling of different orbital states in the molecule and the multiplicity of lines arises from optically induced charging of the molecule.

[1] K. X. Tran et al., Phys. Rev. Lett. 129, 027403, (2022)

- [2] J. Schall, et al. Adv. Quantum Technol. 4(6), 2100002 (2021)
 [3] A.J. Bennett, et al. Appl. Phys. Lett. 97(3), 031104 (2010)

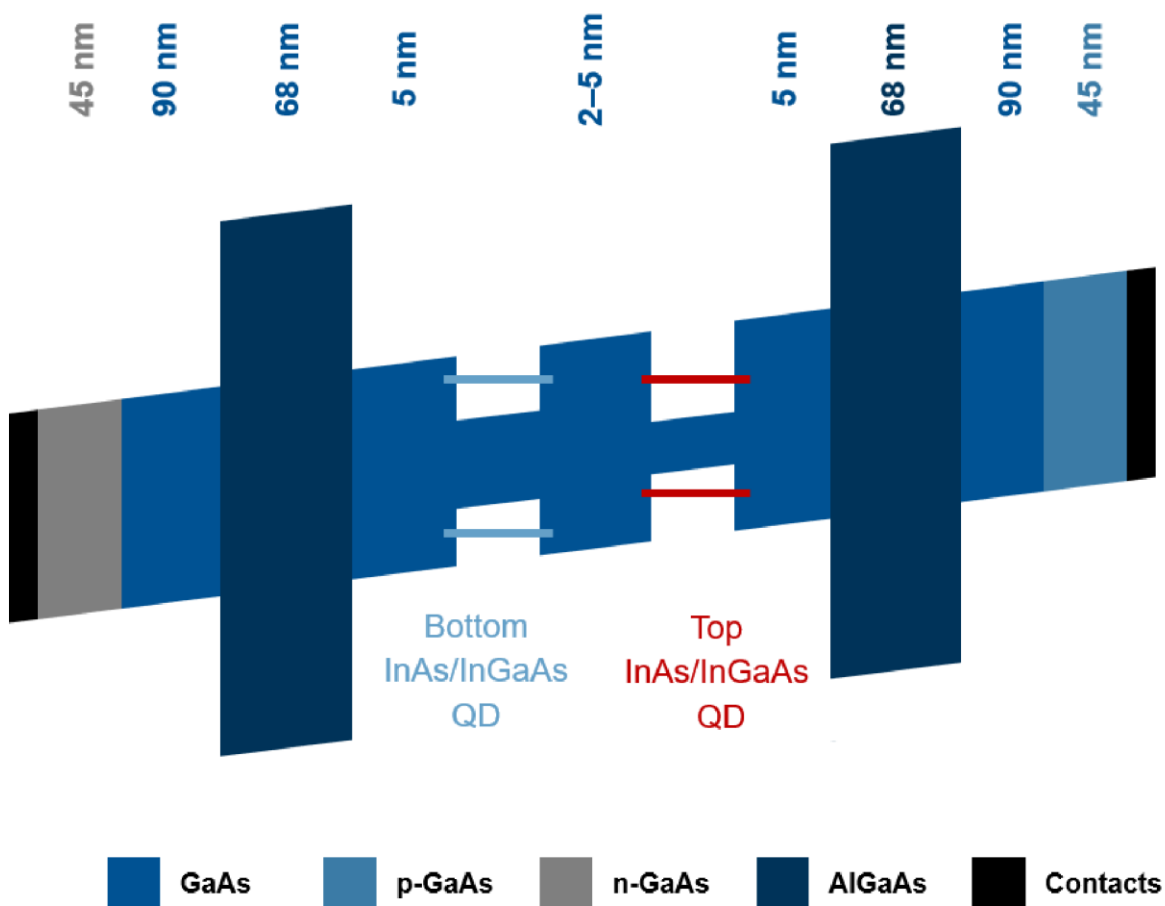


Fig. 1: Schematic of p-i-n diode band diagram with InAs/InGaAs QD-molecule.

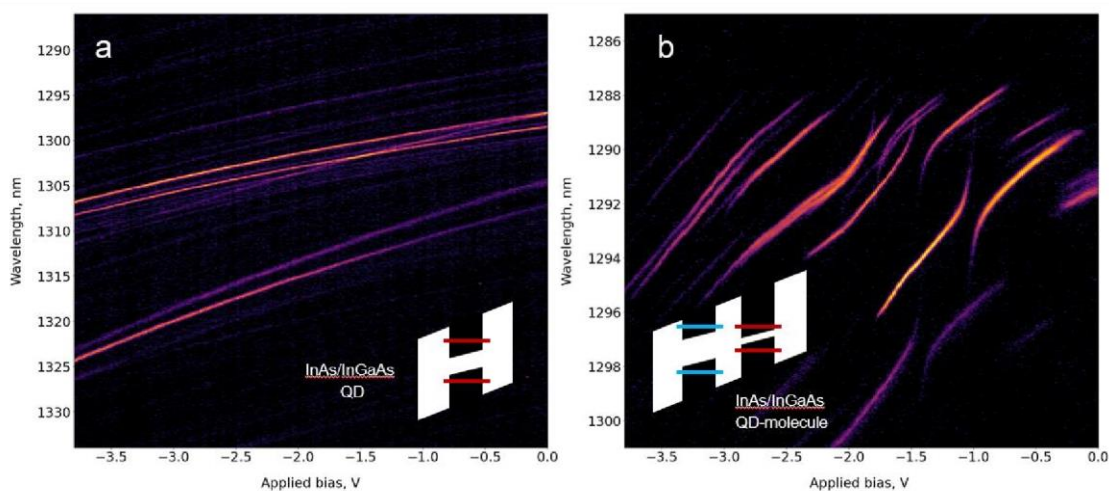


Fig. 2: Voltage-dependent μ PL spectra of InAs/InGaAs QD (a) and QD-molecule (b) under continuous-wave 895 nm excitation with a nominal excitation power of 5 μ W.



I11: Interface properties of (Al)GaAs/GaAsBi quantum wells grown by MBE

E. Luna^{*1}, J. Puustinen², J. Hilska² and M. Guina²

¹Paul-Drude-Institut für Festkörperelektronik, Leibniz-Institut im Forschungsverbund Berlin e.V., Berlin 10117, Germany

²Optoelectronics Research Centre, Tampere University, Tampere 33720, Finland

*luna@pdi-berlin.de

Dilute bismide alloys, such as Ga(As,Bi), represent a novel class of materials that have garnered significant attention due to their unique properties and potential applications in various fields, such as in infrared optoelectronic devices and high-efficiency solar cells. Despite their immense potential, the precise understanding of Bi incorporation into the lattice has remained challenging yet essential for optimizing material quality and harnessing their full functionality.

In this work, we focus on the investigation using (Scanning) Transmission Electron Microscopy (S)TEM of the interface properties and segregation effects in (Al,Ga)As/Ga(As,Bi) quantum well (QW) structures grown by molecular beam epitaxy (MBE).

We find that the interfaces of GaAs/Ga(As,Bi) QWs are dramatically broadened by Bi segregation, as clearly observed in elemental composition profiles directly obtained from the analysis of chemically sensitive g_{002} dark-field TEM (DFTEM) micrographs. Evaluation of segregation effects is possible via quantification of the interface width using a combination of Muraki's phenomenological segregation model with a sigmoidal function defining the intrinsic interfacial width. We discuss how the use of innovative growth procedures/strategies at the interfaces of GaAs/Ga(As,Bi) QWs is very successful in reducing Bi segregation. In particular, the use of a two-temperature growth procedure [1] or the most recent strategy of replacing GaAs barriers with (Al,Ga)As [2,3] significantly reduce Bi segregation.

On the other hand, our detailed TEM investigations of (Al,Ga)As/Ga(As,Bi) QWs disclose the presence of Bi_{Ga} hetero-antisites, a highly anticipated defect yet challenging to detect in dilute bismides, at the interfaces of (Al,Ga)As/Ga(As,Bi) QWs [4]. Detection is made by employing the above mentioned diffraction-based g_{002} DFTEM technique. The spatial resolution associated with TEM enables the precise determination of the location of the defects, in this case at the interfaces of the (Al,Ga)As/Ga(As,Bi) QWs. This discovery significantly advances the ability to identify point defects in novel materials based on III-V semiconductors with zincblende structure, a crucial step in enhancing material quality and facilitating practical applications. The formation of Bi_{Ga} hetero-antisites is discussed in the context of some specific procedures during MBE growth. This highlights the relevance of combined TEM and MBE investigations in advancing materials science.

[1] P. K. Patil, E. Luna, T. Matsuda, K. Yamada, K. Kamiya, F. Ishikawa, S. Shimomura, *Nanotechnology* **28**, 105702 (2017).

[2] R. Butkutė, M. Skapas, A. Selskis, V. Bukauskas, S. Stanionytė, G. Niaura, *Lithuanian J. Phys.* **57**, 29 (2017).

[3] W. Pan, L. Wang, Y. Zhang, W. Lei, and S. Wang, *Appl. Phys. Lett.* **114**, 152102 (2019).

[4] E. Luna, J. Puustinen, J. Hilska, and M. Guina, *J. Appl. Phys.* **135**, 125303 (2024).

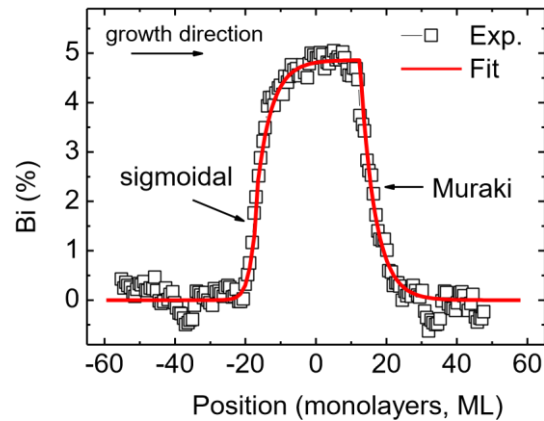


Fig 1. Experimental Bi composition profile obtained from the analysis of g_{002} DFTEM images of GaAs/Ga(As,Bi) QWs grown using a two-temperature growth procedure [1], a successful strategy to reduce Bi segregation.

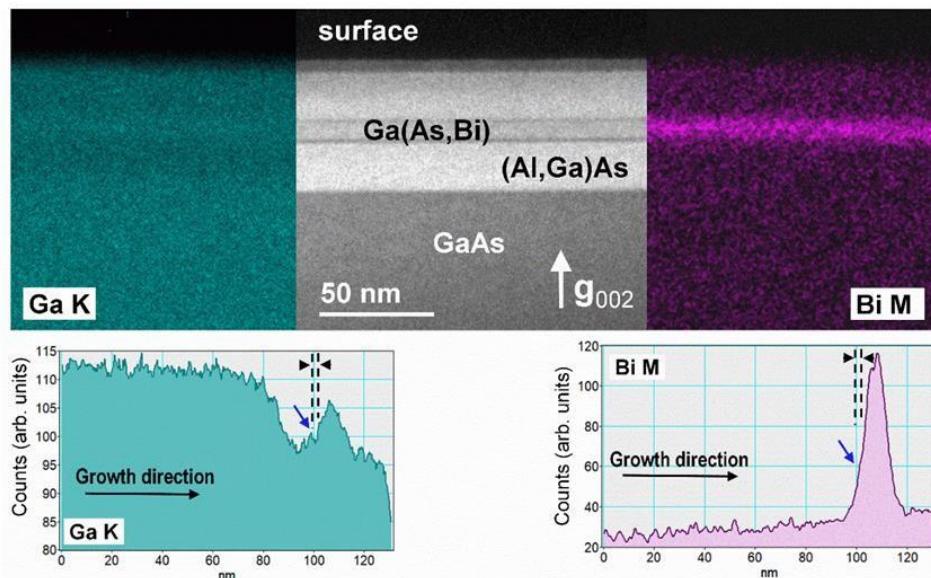


Fig 2. Energy-dispersive x-ray spectrometry (EDS) elemental maps reveal Bi-rich and Ga-depleted features at the location of the dark-line at the Ga(As,Bi)-on-(Al,Ga)As interface in g_{002} DFTEM micrographs. The "dark-lines" are explained by the presence of Bi_{Ga} hetero-antisites at this location. [4].

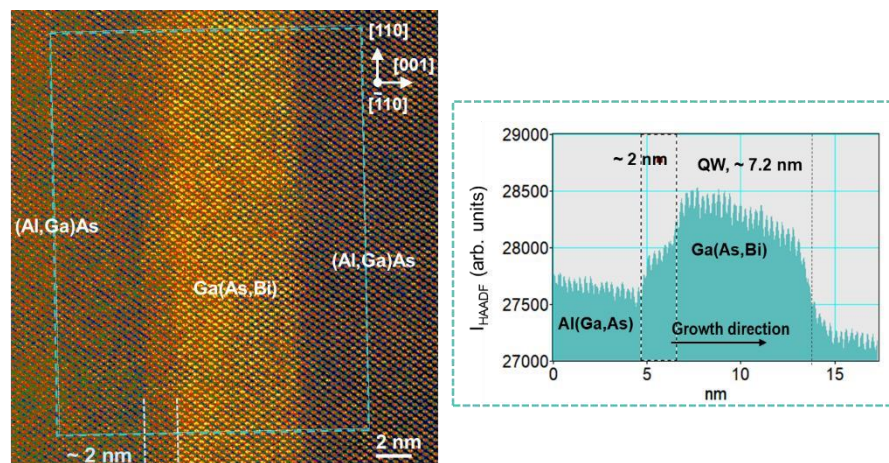


Fig 3. Features in aberration-corrected STEM image at the Ga(As,Bi)-on-(Al,Ga)As interface which match the position and width of the dark-line in g_{002} DFTEM micrographs associated to Bi_{Ga} hetero-antisites at this location.



S11.1: GaAs growth on graphene covered substrates towards substrate recycling

Naomie Messudom¹, Carlos Macias^{1,2}, Antonella Cavanna¹, Ali Madouri¹, Laurent Travers¹, Nathalie Bardou¹, Stéphane Collin^{1,2}, Jean-Christophe Harmand¹, Amaury Delamarre^{1,2*}

¹Centre for Nanoscience and Nanotechnology (C2N), CNRS, Univ. Paris-Saclay, 10 Boulevard Thomas Gobert, 91120 Palaiseau, France, ²Institut Photovoltaïque d'Ile-de-France (IPVF), Palaiseau F-91120, France.

*E-mail: amaury.delamarre@cnrs.fr

The purpose of this work is to obtain transferable III-V thin films, by epitaxy above a graphene covered substrate. Studies showed that monocrystalline layers could be obtained, which are sufficiently weakly attached to the substrate thanks to the graphene plane to allow for their exfoliation. Ideally, the substrate could be recycled for several growth. In the field of photovoltaics, this would provide cost reductions by more than 30%, for devices presenting the highest efficiencies among available materials.

It was suggested that growth could occur *via* remote interaction through the graphene¹. We have not observed this behavior in previous work, which resulted in a polycrystalline layer formation. A potential competing growth mechanism could proceed by nucleation at graphene holes, followed by lateral growth towards coalescence. We propose to explore this route, since we have evidenced that graphene can play the role of a mask compatible with selective area growth. In our case, graphene is grown on a germanium substrate and dry-transferred to GaAs², before patterning by electron beam lithography.

We investigate the growth behavior on graphene patterned as parallel stripes along different directions of the GaAs substrate. Before coalescence (fig. 1), we find that the $\langle 100 \rangle$ directions provide structures with smooth morphologies, and significant lateral growth over the graphene. $\langle -110 \rangle$ resulted in nanowalls with negligible lateral growth, and $\langle 110 \rangle$ presented significant roughness, which could be due to twin formation on the formed $\{111\}$ walls. Those results are consistent with the literature with silica masks³. Higher index directions present nanostructures with multi-atomic steps. After coalescence however, high index directions provided layers with the smoothest morphologies (fig. 2), while $\langle -110 \rangle$ did not show significant coalescence, and $\langle 100 \rangle$ preserved a more significant roughness. Above a 500 nm buffer GaAs, we have grown a $\text{Al}_{0.8}\text{Ga}_{0.2}\text{As}/\text{Al}_{0.2}\text{Ga}_{0.8}\text{As}/\text{Al}_{0.8}\text{Ga}_{0.2}\text{As}$ (100/200/100 nm) heterostructure for luminescence tests (fig. 3). Consistently, no signal could be observed on directions $\langle 110 \rangle$ and $\langle -110 \rangle$ while it increases for higher indexes. More precise studies as a function of graphene coverage and stripes orientation are ongoing, as well as cathodoluminescence and TEM.

Exfoliation tests have been carried out. First, a 30 nm Ti layer to enhance adhesion is deposited, followed by a 250 nm Ni layer and a thermal release tape. This tape is manually peeled off. Fig. 4 show an SEM picture of the remaining material on the substrate. The polycrystalline GaAs formed on graphene covered GaAs is successfully exfoliated. Coalesced GaAs structure on patterned graphene can be exfoliated for sufficiently large graphene coverage ratio. A dependance on the stripe orientation is observed, which is suspected to be related to the manual peel off direction. This dependance will be further investigated in the coming months.

1 Kim, Y. et al. Nature 544, 340–343 (2017), 2 Macías, C. et al. Appl. Surf. Sci. 676, 160913 (2024), 3 Ironside, D. J. et al. Cryst. Growth Des. 19, 3085–3091 (2019)

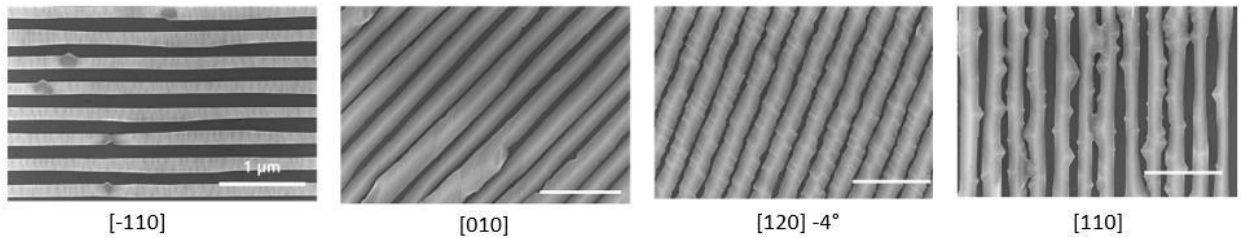


Figure 1 Deposition of 360 ML GaAs, at $T_g \sim 615^\circ\text{C}$ and V/III ratio of 2, on a graphene covered GaAs substrate, patterned as stripes along various substrate orientations. Stripes opening are 50 nm wide, with a 300 nm repetition period.

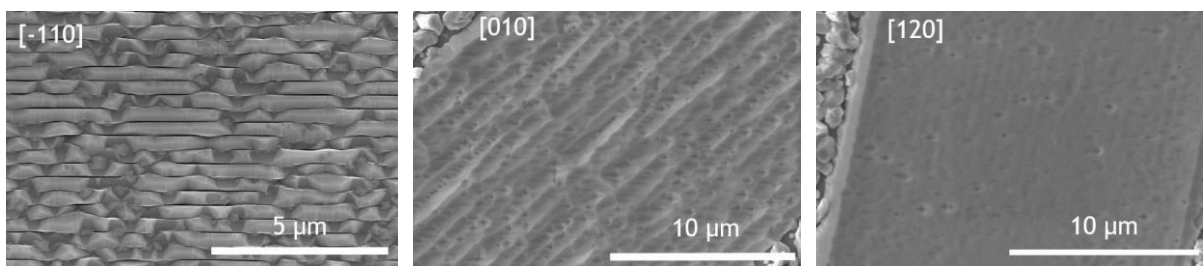


Figure 2 500 nm GaAs deposition, beyond coalescence on patterned graphene on GaAs. Stripes opening are 150 nm wide, with a 300 nm repetition period.

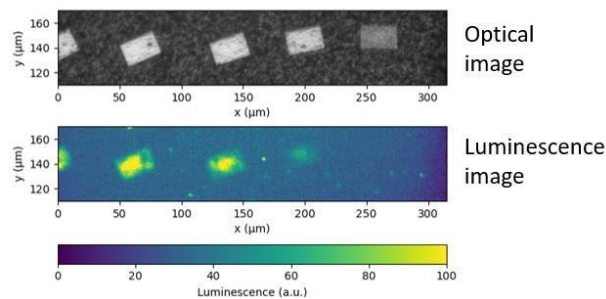


Figure 3 Optical image and corresponding luminescence under an LED illumination at 405 nm, for a $\text{Al}_{0.8}\text{Ga}_{0.2}\text{As}/\text{Al}_{0.2}\text{Ga}_{0.8}\text{As}/\text{Al}_{0.8}\text{Ga}_{0.2}\text{As}$ (100/200/100 nm) heterostructure, on a 500 nm GaAs buffer grown on a patterned graphene covered GaAs substrate.

Graphene coverage

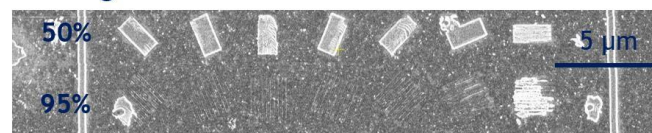


Figure 4 Remaining structures on the substrate after an exfoliation test. Exfoliation is obtained by depositing 30 nm Ti and 250 nm Ni, and attaching a thermal release tape, before manual peel off. Exfoliation depends on the graphene coverage. The angle between the graphene stripe orientation and peel off direction is suspected to play a role and has not been carefully investigated so far.



S11.2: Earth abundant oxynitrides alloys for tandem solar cells

Khiem Tu Tran,¹ Christiane Deparis,¹ Maxime Hugues,¹ Ileana Florea,¹ Marie-Pierre Chauvat³, Jesús Zúñiga Pérez^{1,2} and Hélène Rotella¹

¹Université Côte d'Azur, CNRS, CRHEA, rue B.Grégory, 06560, Valbonne, France

²MajuLab, International Research Laboratory IRL 3654, CNRS, Université Côte d'Azur, Sorbonne Université, National University of Singapore, Nanyang Technological University, Singapore, Singapore

³Normandie University, CIMAP, ENSICAEN, UNICAEN, CAEN, 14000, France

e-mail: ktt@crhea.cnrs.fr

Owing to the increasing energy demand due to the rising population, there is a crucial need for sustainable energy resources. Government regulations focus on the reduced dependency on fossil fuels and gases, but also on the control of environmental pollution. This promotes the demand for renewable energy sources such as solar energy, thus driving the photovoltaic (PV) energy development. Different PV devices are being developed, including high-efficiency tandem cell devices but also lower cost thin films alternatives. However, these devices are often made of materials whose elements are considered scarce, like indium, or toxic, like lead.

The studies of earth-abundant nitrides started a decade ago, guided by the desire to replace critical materials in III-nitrides technology. Semiconducting earth-abundant nitrides are therefore an emerging group of materials, opening the way to a wide range of key technological devices, including solar cell absorbers. Among them, the nitrides Zn_3N_2 and Mg_3N_2 are both earth abundant and non-toxic semiconductors. Recently, we successfully grew by molecular beam epitaxy these two binary materials and we determined room temperature direct bandgap energies around 1.0 eV and 2.9 eV for Zn_3N_2 and Mg_3N_2 , respectively, thanks to transmission measurements. Besides, we analyzed their electrical properties, both carrier concentration and electronic mobilities, in view of developing absorber materials for tandem solar cells[1, 2, 3].

In this context, and based on these two materials, we aim to develop a top cell based on indium free, earth abundant and non-toxic quaternary nitride alloy, namely the $(Zn_{1-x}Mg_x)_3(N_{1-y}O_y)_2$ alloy, compatible with bottom crystalline Si technology. The targeted tandem cell architectures rely on a gap stacking of 1.7 eV/1.1 eV, which provides the maximum theoretical power conversion efficiency with Silicon as a bottom cell [4] (*Figure 1*).

In this work, we will discuss the epitaxial growth of ZnMgON thin films, which was performed by plasma assisted molecular beam epitaxy (PA-MBE) in order to stabilize monocrystalline epitaxial layers on insulating MgO(100) substrate. The crystalline quality was characterized by X-ray diffraction and transmission electron microscopy on cross sections. STEM of epitaxial ZnMgNO on MgO substrates confirms a homogenous crystallinity along the layer. (fig 3). The Zn/Mg ratio was evaluated by energy dispersive X-ray analysis. The proof of the incorporation of oxygen was revealed by measuring the

element profiles extracted from XPS measurements through successive in-situ etchings with an argon ion gun as well as EDXSTEM mapping. The atomic profiles show that oxygen has been incorporated across the entire ZnMgN thickness (fig 2). The optical band gaps were measured by transmission while the carrier densities and the mobilities of the newly synthesized quaternary alloys were extracted from Hall effect measurements. By adjusting the growth conditions, in particular substrate temperature, N₂ flow, presence of O₂ during growth and the temperature of the Mg cell, we achieved monocrystalline layers of (Zn,Mg)(O,N) with the targeted 1.7 eV band gap, a carrier density around 4-5x10¹⁹ [cm⁻³] and a mobility of 45-50 [cm²/V/s].

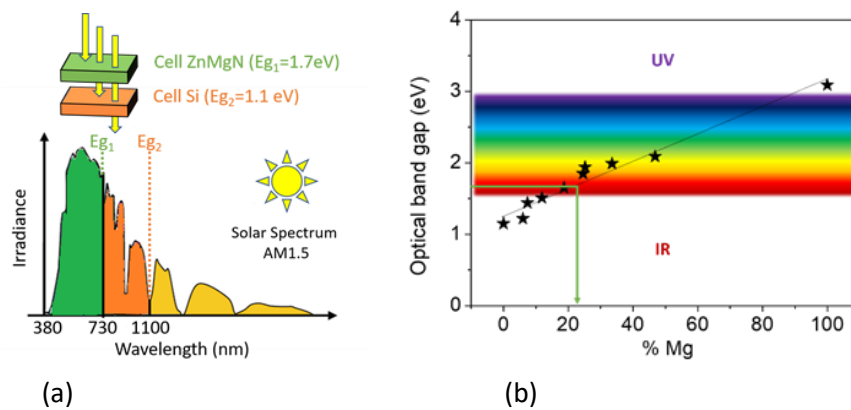


Figure 1. a) Absorption of the ZnMgN solar cell combined with a silicon bottom cell in the solar irradiance spectrum. b) Band gap of ZnMgN as a function of Mg concentration.

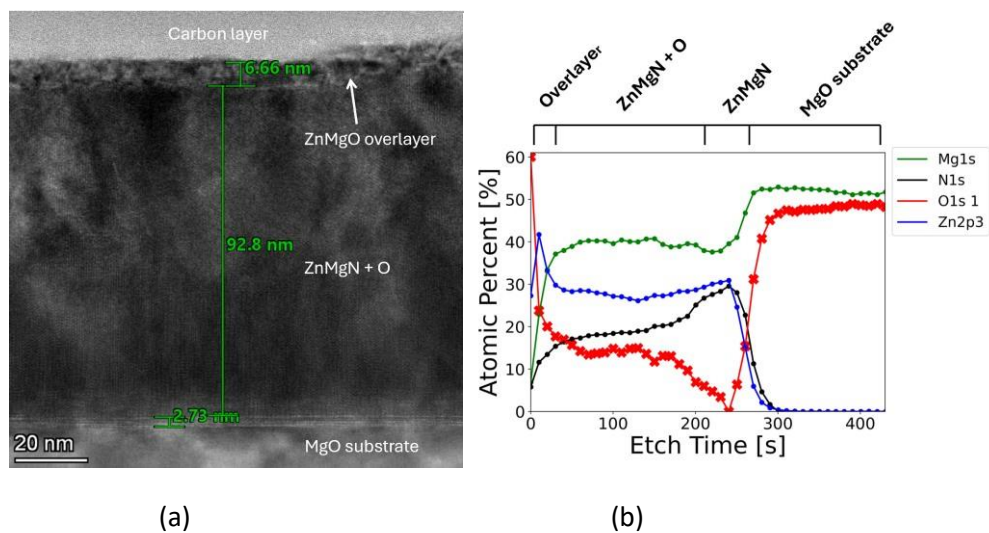


Figure 2. a) TEM image of ZnMgNO on MgO substrate. b) XPS atomic profile of ZnMgON with a control ZnMgN control layer and the MgO substrate.

- [1] P. John, et al., Phys. Rev. Materials 4, (2020) 054601
- [2] P. John, et al., J. Appl. Phys. 130, (2021) 065104
- [3] P. John, et al., J. Appl. Phys. 129, (2021) 095303
- [4] A. Marti and G.L. Arujo, Solar Energy materials and Solar Cells, 43 (1996) 203

Acknowledgments:

We acknowledge support from the Agence Nationale de la Recherche (No. ANR-22-CE50-0006-01) through the project NITA.

S11.3: The correlation between the microstructure and the optoelectronic properties of Zn_3P_2 grown by Selective Area Epitaxy

Raphaël Lemerle^a, Helena R. Freitas^b, Leo Webb^a, Thomas Hagger^a, Didem Dede^a, Valerio Piazza^a, Maria Chiara Spadaro^b, Jordi Arbiol^b and Anna Fontcuberta i Morral^a

^aLaboratory of Semiconductor Materials, Institute of Materials, School of Engineering, Ecole Polytechnique Fédérale de Lausanne, 1015, Lausanne, Switzerland ^bCatalan Institute of Nanoscience and Nanotechnology (ICN2), CSIC and BIST, Campus UAB, Bellaterra, Barcelona, Catalonia, 08193, Spain.

Zinc phosphide (Zn_3P_2) is a promising material for low-cost photovoltaics made of earthabundant elements. Its direct band gap of 1.5 eV makes it ideal for efficient photovoltaics. However, the record efficiency of 6% for a Zn_3P_2 solar cell achieved in the 1970s has never been outperformed ever since [1]. The main obstacle is the synthesis of Zn_3P_2 with high crystal quality and controllable properties. We have previously reported the growth of monocrystalline Zn_3P_2 on InP by Molecular Beam Epitaxy (MBE) [2]. Furthermore, we showed that the hole concentration can be controlled by tuning the Zn:P stoichiometry [3]. Nevertheless, the high lattice mismatch with the substrate induces strain in the layer with consequent formation of defects that limit the mobility. In this work, we explore selective area epitaxy (SAE) to improve the carrier transport by reducing the defect density [4]. The idea is to grow the thin film starting from a nanoscale pattern enabling Zn_3P_2 pyramidal growth and subsequent merging.

Here, we report on the combination of Hall Measurements and Photoluminescence Measurements on thin films grown by Selective Area Epitaxy. The highest hole mobility ever measured for Zn_3P_2 ($520 \text{ cm}^2/\text{Vs}$) was obtained from high-quality thin films. Furthermore, Transmission Electron Microscopy (TEM) is used to characterize the microstructure of the samples. We determined which defects have the greatest impact on the optoelectronic properties of the films. The investigation extends to the effect of the hole size and the pitch size on the structure and, on the optoelectronic properties (see Figure 1 and 2).

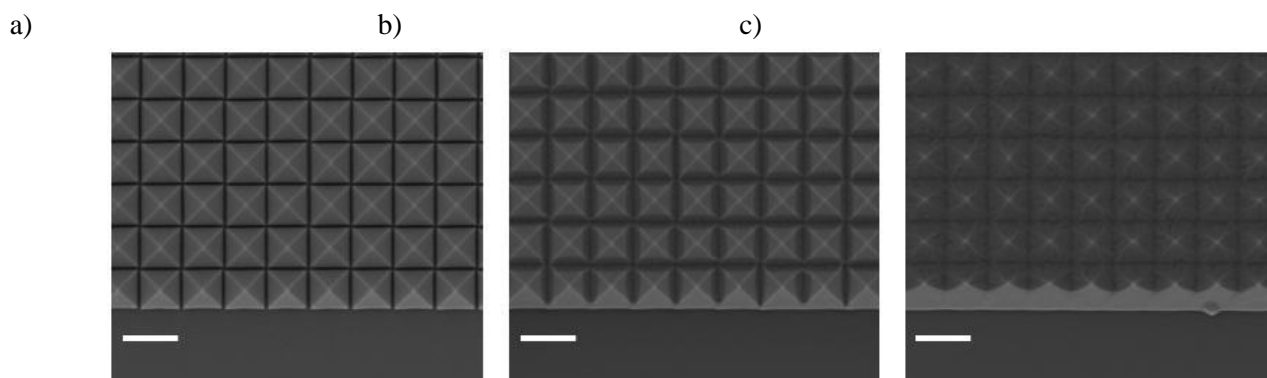


Figure 1: SEM images of Zn_3P_2 grown by SAE on InP (scale bar=500nm). (a) 40/400. (b) 75/400. (c) 120/400 (hole radius in nm/hole pitch in nm).

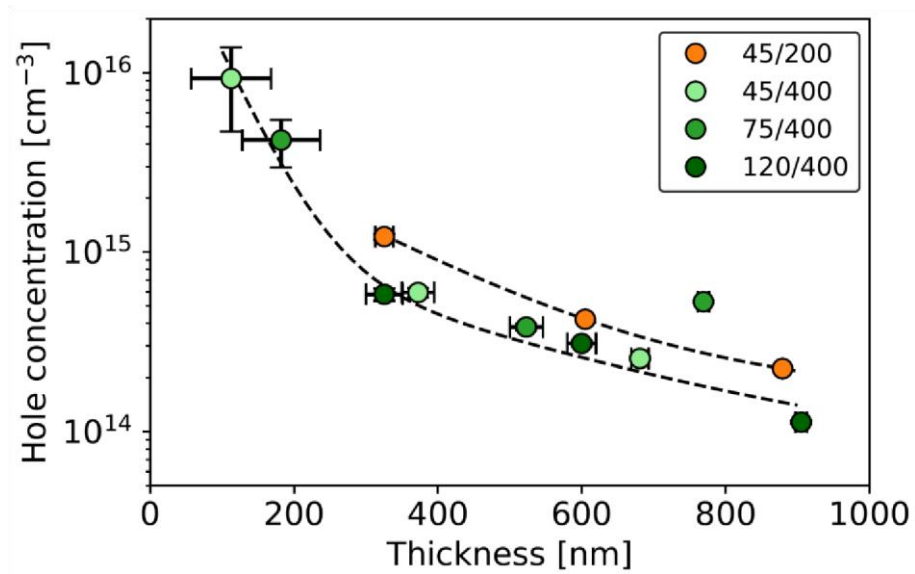


Figure 2: Evolution of the carrier concentration with the thickness for thin films grown from different patterns (hole radius in nm/hole pitch in nm).

[1] Bhushan, M. (1980). *Appl. Phys. Lett.* 38, 39–41 [2] Zamani, M (2021). *JPhys Energy*, 3(3).

[3] Paul, R. (2023). *Solar Energy Materials and Solar Cells*, 252

[4] Escobar Steinvall, S (2021). *Nanoscale Advances*, 3(2), 326–332



S11.4: Remote epitaxy of III-V films on a universal template

T. Henksmeier^{1,2,*}, P. Mahler¹, A. Wolff¹, D. Deutsch¹, M. Voigt³, L. Ruhm³, A. M. Sanchez⁴,
D. J. As¹, G. Grundmeier³, D. Reuter^{1,2}

¹Paderborn University, Department of Physics, Warburger Str. 100, 33089 Paderborn

²Institute for Photonic Quantum Systems (PhoQS), Paderborn University, 33098 Paderborn ³Paderborn University, Department of Chemistry, Warburger Str. 100, 33089 Paderborn ⁴Warwick University, Department of Physics, Coventry CV4 7AL, UK

*tobias.henksmeier@upb.de

In remote epitaxy, a thin 2D material layer placed on a semiconductor substrate induces an interaction gap between substrate and growing layer allowing to peel-off the epitaxial layer from the substrates and to recycle the substrate [1], therefore reducing production cost of freestanding heterostructures and enabling versatile stacked heterostructures fabrication [1,2]. The thin 2D material layer is either manually transferred to a substrate or grown directly on a substrate at high temperature, thus limiting the process scalability or the choice of substrates. Here, we present a low-temperature (300 °C), cheap and wafer-scale fabrication process of ultrathin 2D-like sp²-hybridised amorphous carbon layer templates on various substrates and their subsequent overgrowth [3]. High crystal-quality group III-arsenides layer growth on amorphous carbon covered InP and GaAs substrates is demonstrated as well as growth of metastable cubic group III-nitride layers on amorphous carbon covered 3C-SiC.

Atomic force microscopy measurements (Fig. 1a)) reveal an atomically smooth surface of the monolayer-like thin amorphous carbon layer and Raman and X-ray photoelectron spectroscopy measurements reveal a predominant sp²-hybridisation of the carbon bonds (Fig. 1b-c)); key factors for successful remote epitaxy [2]. We show that precisely tailoring the carbon layer thickness allows superior tunability of the substrate-layer interaction allowing to tune the nucleation behavior on the amorphous carbon coated substrates (Fig. 2a-b)) while transferring the substrate crystal orientation to the epilayer (Fig. 2c)). Photoluminescence measurements of droplet etched In_{0.57}Ga_{0.43}As quantum dots (Fig. 3b)) (important for infrared applications) on our amorphous carbon templates and high-resolution X-ray diffraction measurements (Fig. 3a)) verify a high crystal quality of the epitaxial layers; dislocation densities <math><1 \times 10^7 \text{ cm}^{-2}</math> are determined for optimized growth conditions. Our results show a universal approach to fabricate templates for remote epitaxy, e. g., for remote epitaxy on temperature sensitive substrates like GaAs or InP and growth of metastable phases. Lift-off of layers from their substrates is demonstrated by employing a Ni stressor approach (Fig. 3c)) [3].

[1] Kim, Y. et al. Nature 544, 340–343 (2017)

[2] Park, B-I. et al. ACS Nano. 24, 10 (2024)

[3] Henksmeier, T. et al. arXiv:2410.15487 (2024)

Fig. 1: Characterization of the fabricated monolayer-like amorphous carbon layer. a) $5 \times 5 \mu\text{m}^2$ AFM image with surface roughness ≤ 0.3 nm, b) XPS spectrum and c) Raman spectrum both revealing sp^2 -hybridised amorphous carbon.

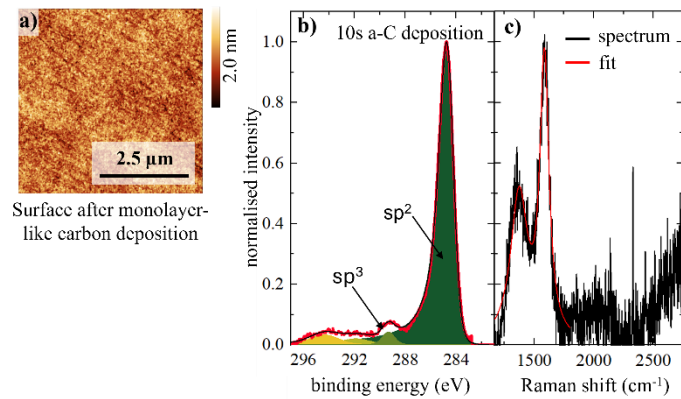
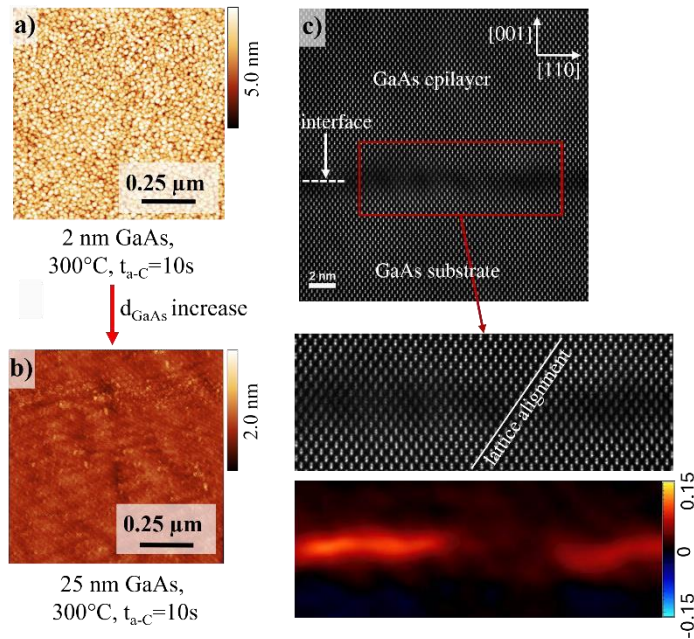


Fig. 2: Characterization of nucleation layers on amorphous carbon template. a), b) $1 \times 1 \mu\text{m}^2$ images after 2 nm and 25 nm GaAs deposition, respectively, c) ADF-STEM image and GPA of the substrate-carbon-epilayer interface indicating a crystal lattice stretching and lattice alignment through the interface.



the
AFM
analysis

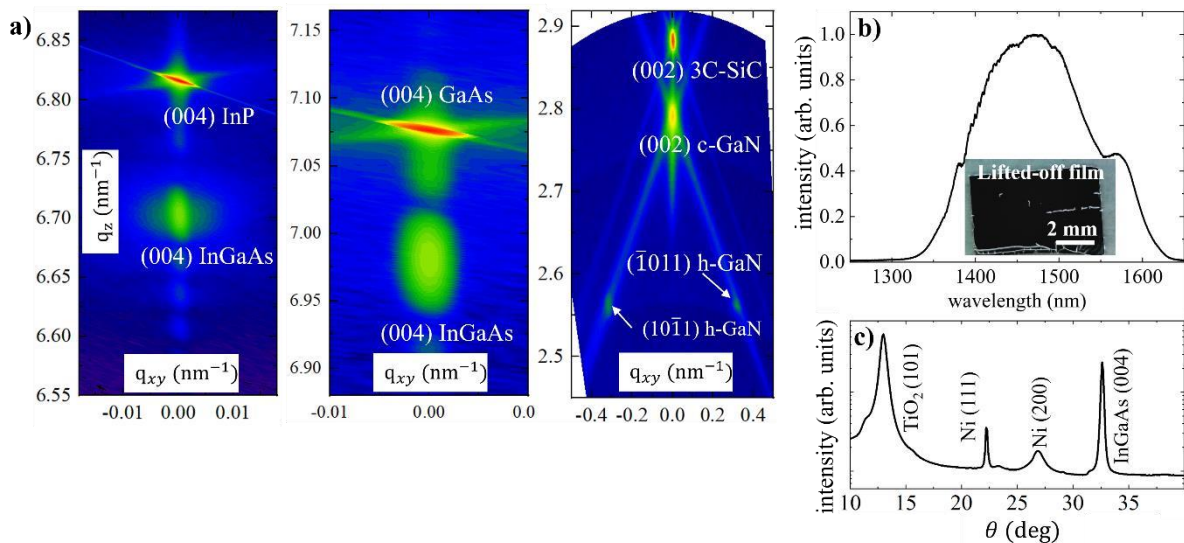


Fig. 3: HR-XRD and photoluminescence measurements of epitaxial films grown on amorphous carbon templates. a) HR-XRD measurements of $\text{In}_{0.65}\text{Ga}_{0.45}\text{As}$ on InP, $\text{In}_{0.09}\text{Ga}_{0.91}\text{As}$ on GaAs and c-GaN on 3C-SiC substrates. b) Photoluminescence measurements of droplet etched $\text{In}_{0.57}\text{Ga}_{0.43}\text{As}$ quantum dots; the inset shows a 200 nm thick film lifted-off by applying the Ni-stressor approach. c) $\theta/2\theta$ -scan of the lifted-off film.

SMART TOOLS,
SMARTER MBE

RIBER

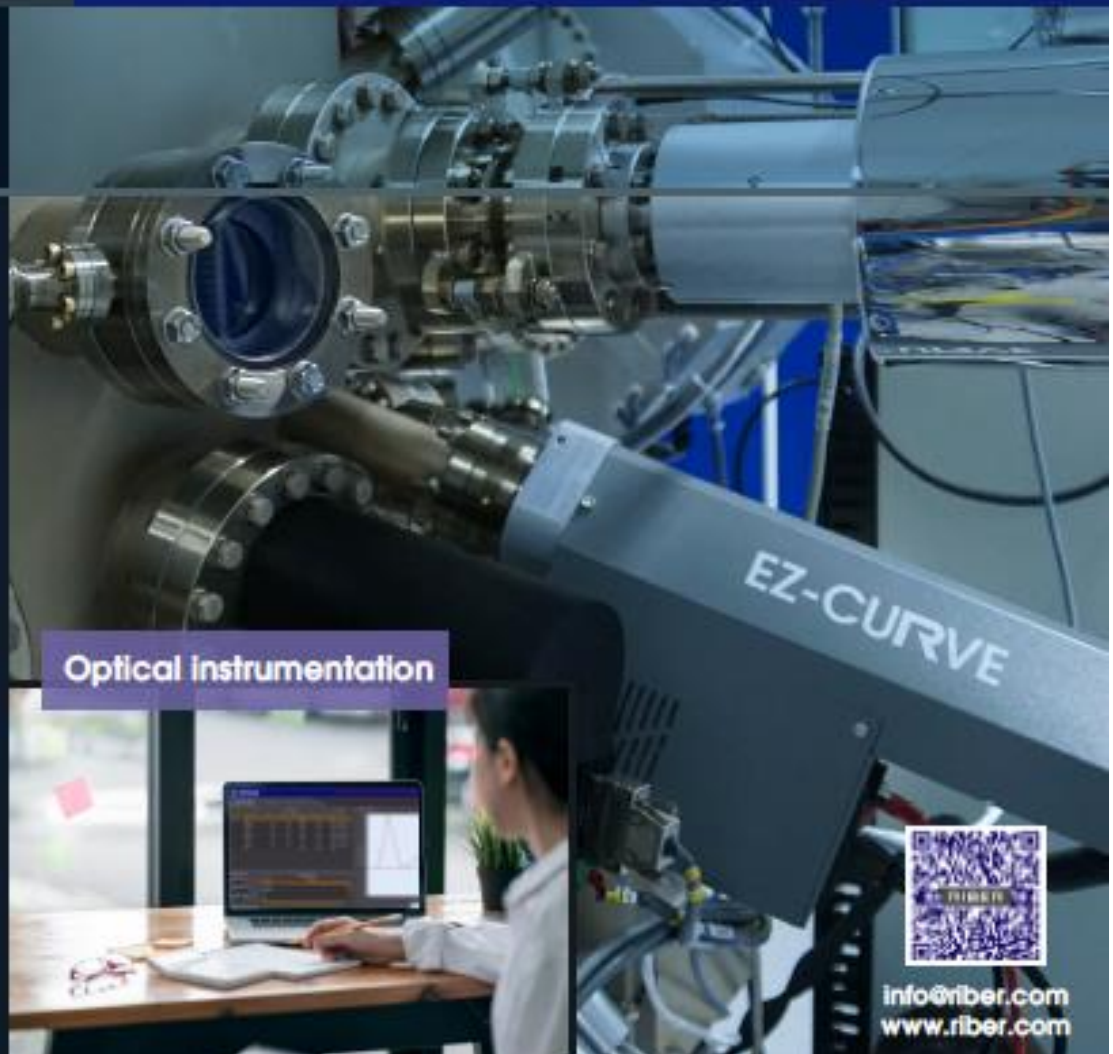
INNOVATIVE SOLUTIONS FOR SEMICONDUCTOR INDUSTRY

MASTER
your Epitaxy with
EZ-instruments

IN SITU
Growth monitoring

AUTOMATED
Process

REAL TIME
Analysis &
adjustment



Optical Instrumentation



info@riber.com
www.riber.com



MAKING A MATERIAL DIFFERENCE

Enabling Next Generation Semiconductor, Compound Semiconductor & Cloud Computing Devices

Differentiated Technology Solutions Driving Global Megatrends

Megatrends



Leading Edge Computing / AI

Mobility and the Immersive User Experience



5G, Sensors, AR/VR, Advanced Displays

High Performance Computing and Artificial Intelligence



EV, Hybrid, Autonomous Driving

Transformation of the Automotive Industry



Data Centers, High Speed Communication, Data Storage

The Cloud

Markets Served

Semiconductor

Compound Semiconductor

Cloud Computing

Core Technologies



Laser Annealing



AP Lithography



IBE/IBD



MOCVD



SIC CVD



Wet Processing



ALD



IBE/IBD



Wet Processing



Wafer Dicing



MBE



MBE Equipment for Scientific Innovation

Industry-leading MBE Systems and Sources for R&D and Production



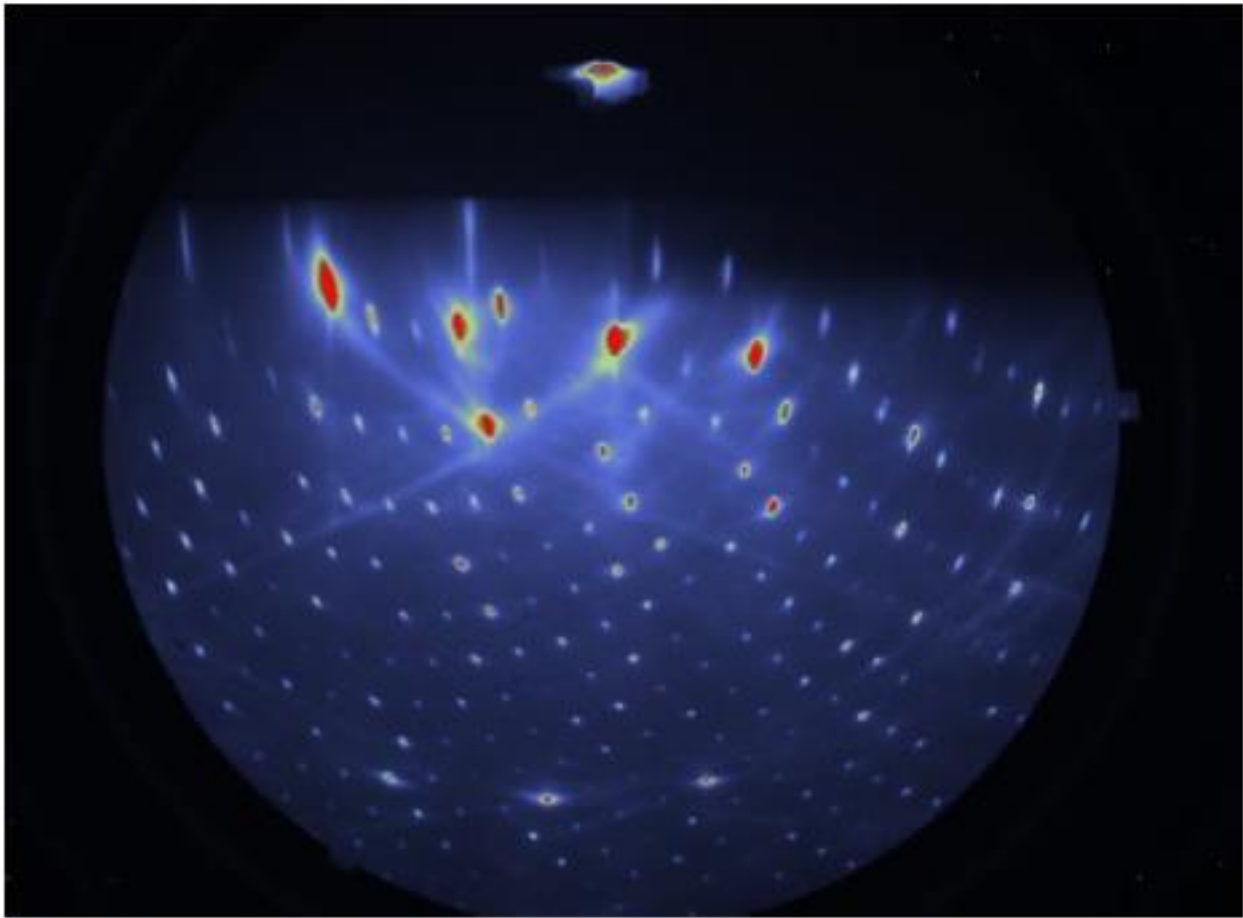
To learn more, visit www.veeco.com



A Material Science Company with Deep Expertise in Compound Semiconductor Solutions



RHEED Systems and Accessories



Everything you need for a RHEED pattern like this:



RHEED Electron Guns
15kV – 20kV -30kV



RHEED Camera and
Data analysis systems



RHEED Screens



High Pressure



Your Partner for MBE Film Growth Around the World



12" Production MBE

MBE
molecular
beam
epitaxy

hybrid
MBE
systems

MBE
components



M-Series
MBE System



R-Series
MBE System

Come and talk with us about our latest generation of MBE systems,
each individually tailored for your growth demands.

contact: martyn.green@dca.fi

www.dca.fi

MBE Systems and Components



Substrate Manipulator
BH



Production Effusion Cell
PEZ



Hydrogen Atom Beam
Source HABS



Valved Arsenic Cracker
Source VACS

Fields of application

SiGe, III/V MBE
 High Mobility GaAs / AlGaAs MBE
 Metals / Magnetics
 Graphene
 Oxides
 II/VI MBE
 Topological Insulators
 Thin Film Solar Cells
 Organics



Dr. Eberl MBE-Komponenten GmbH
 Josef-Beyerle-Str. 18/1
 71283 Weil der Stadt, Germany

Phone +49 7033 8937-0
 Email info@mbe-components.com
 Web www.mbe-components.com

Distribution partners

USA / Canada United Mineral & Chemical Corp. www.umocorp.com
 China BE-Instrument Trading Co. Ltd. www.be-instruments.com
 Japan Toyama Co., Ltd. www.toyama-en.com
 India Mack International www.mack.in
 Singapore Torque Science Pte Ltd. www.torquesci.com



COMPLETE MBE



STANDARD or CUSTOM MBE

REALLY AFFORDABLE AND
LOW OPERATING COST

GUARANTEED PRIORITY
REPAIRS AND SERVICE



FLEXIBLE AND FROM ONE
SOURCE FOR COMPATIBILITY

FULL PROCESS SUPPORT
FROM MBE SCIENTIST AND LAB

DEPOSITION COMPONENTS



RF Plasma
DN40-DN200



Effusion Cell
Valved Cracker



Electron Beam
Deposition



SMART NanoFab MBE System



Hybrid/Organic
Epitaxy

IN-SITU PROCESS MONITORING



AccuFlux™



AccuTemp™

EPI WAFER Service
In-House MBE LAB



MBE Modules with In-Situ Characterization



Stand-alone MBE System for 1-12" Sample Size



axt



The Compound Semiconductor Materials Specialist

Substrates

Gallium Arsenide
2", 3", 4", 5", 6", 8"
Indium Phosphide
2", 3", 4", 6"
Germanium
4", 6"

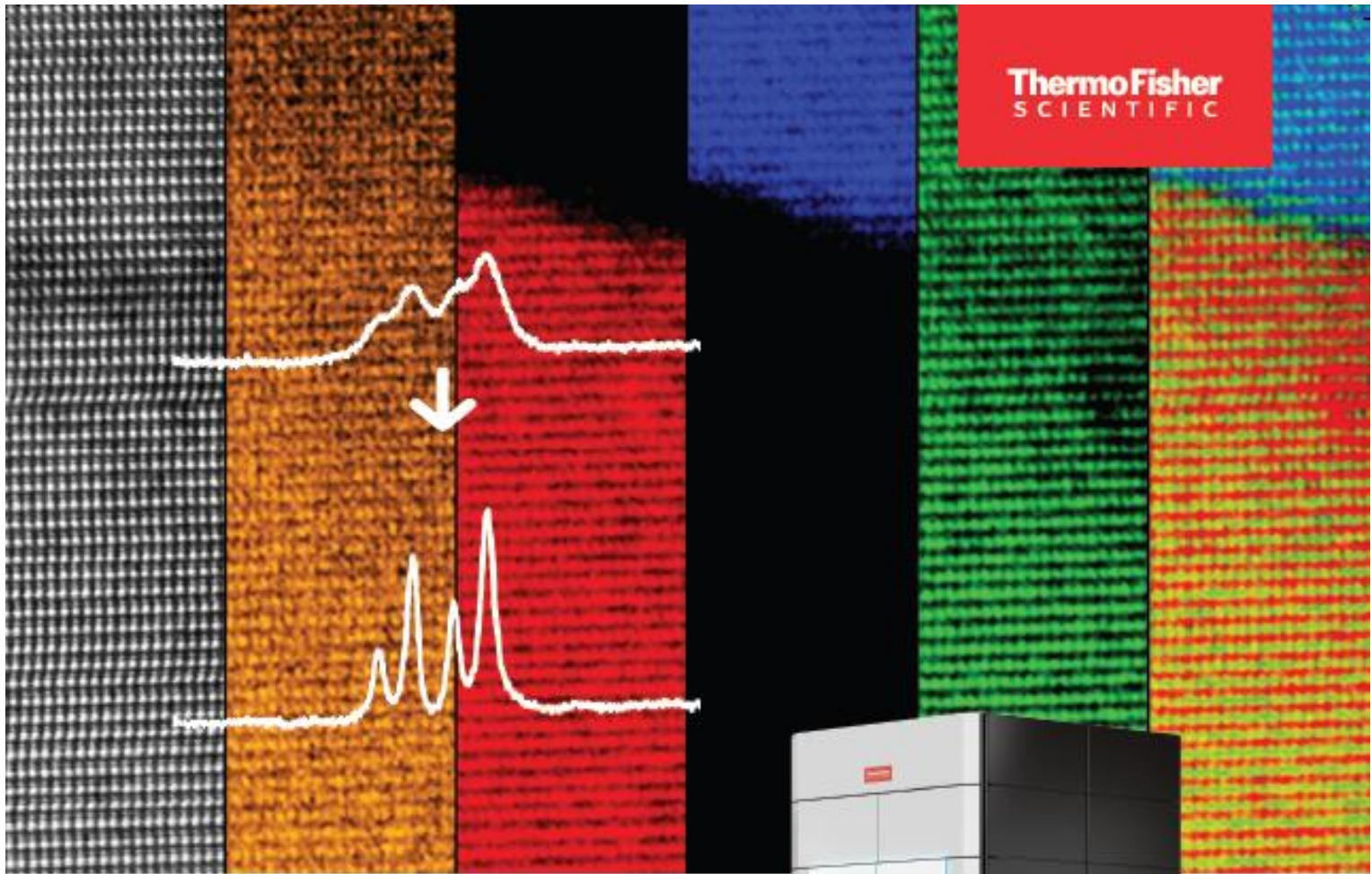
High Temperature Materials and Coatings

PBN Crucibles
PBN Boats
PBN Rings, Rods, Etc
PBN Coatings
PG Coatings

www.axt.com

sales@axt.com

+33-(0)6-89-85-65-74



Iliad S/TEM:

Seamlessly integrated EELS and EDS

- Unique integration of superior hardware
- One software for complete and intuitive control
- State-of-the-art (S)TEM with future proof capabilities
- Advanced (S)TEM control and automation



Learn more at thermofisher.com/iliad



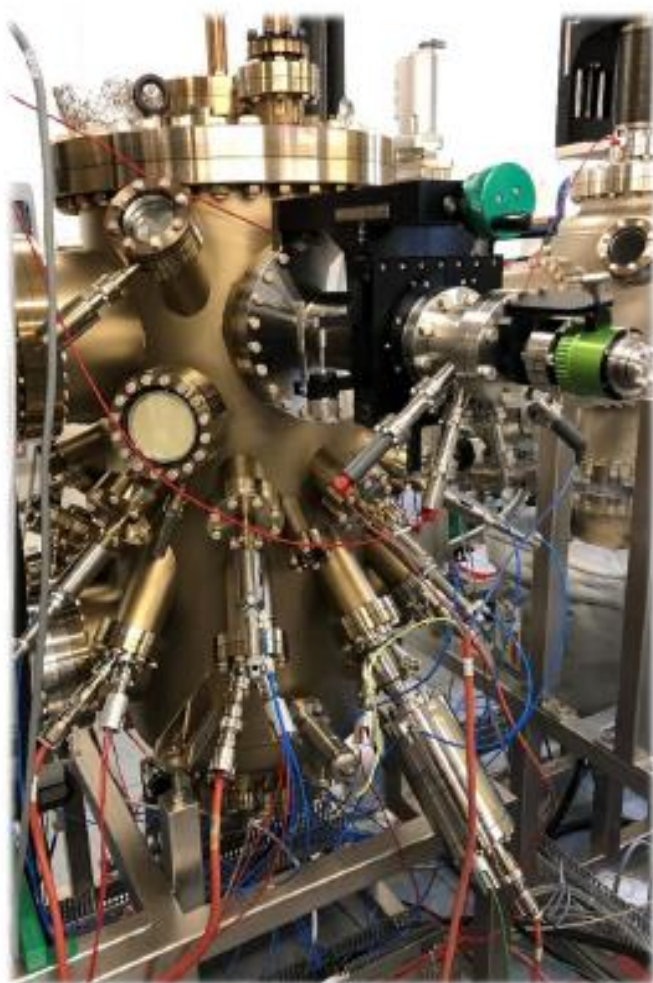
UHV SYSTEMS

Tailored for laboratories & industries

Vinci Technologies began by manufacturing specialized laboratory and field instruments. Committed to R&D, we have continuously evolved to address emerging challenges like carbon footprint and environmental concerns. Today, we provide cutting-edge laboratory instruments and sensors for high-tech industries, including chemicals, health, civil engineering, and materials.

In 2008, Vinci Technologies acquired **MECA2000**, a pioneer in the UHV industry since 1980. With this integration, our Vacuum division team expanded its expertise, enabling the development of advanced UHV MBE systems, preparation chambers, UHV linear transport, sputtering, PLD, thermal & E-beam evaporators, to provide a full lab-scale solution.

With 45 years of expertise, we design and manufacture high-performance UHV equipment, delivering full turnkey solutions.



ENHANCE YOUR PROJECTS

with Vinci's MBE expertise!

Cutting-edge technology:

- ◆ *Advanced Source Options*
- ◆ *Comprehensive Pumping Groups*
- ◆ *Ultra-High Vacuum Capability (10^{-11} mbar)*
- ◆ *Real-Time Growth Feedback*
- ◆ *Versatile Sample Accommodation*
- ◆ *Dynamic Temperature Control*
- ◆ *Efficient Cooling*
- ◆ *Full Process Control*
- ◆ *Supervisory Control And Data Acquisition*
- ◆ *Secured by PLC*

The Vinci Advantage:

- ◆ *Expert technical support (2D TMDs, GaN...)*
- ◆ *Full integrated UHV platforms (MBE with PVD, annealing, PLD... cluster or linear transport)*

Visit our Website:



Phone: +33(0)1-41-37-92-20
Email: vincinet@vinci-technologies.com
Website: www.vinci-technologies.com
Address: 27 B, rue du Port, 92022 Nanterre (FRANCE)
www.linkedin.com/company/vinci-technologies-sa/

RELIABILITY EFFICIENCY PRECISION PERFORMANCE



Pioneering ultra-clean
heterostructures by
thermal laser epitaxy

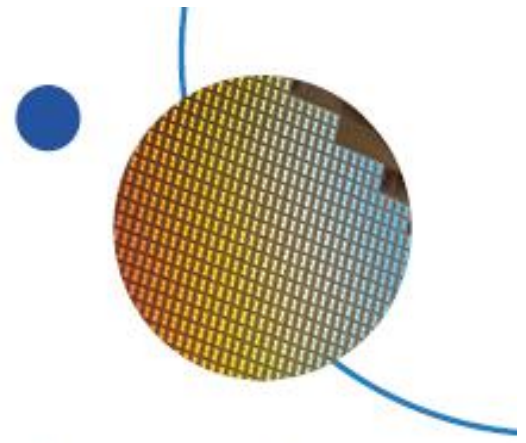
Clean, simple,
fast & versatile

www.epiray.de





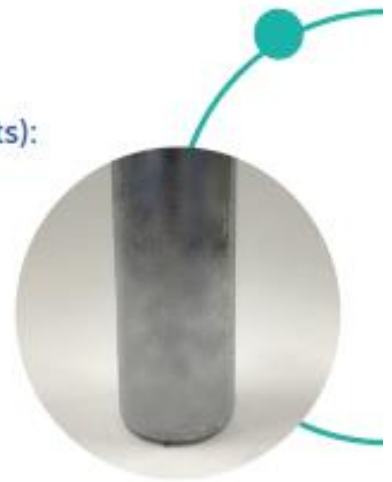
Innovation
through
formulation



Your only supplier for the **highest purity**
and state of the art products for MBE,
MOCVD, substrates and chip bonding

**Purest
in the
world!**

- Arsenic 7N,7N5 MBE (chunks & ingots): **Furukawa**
- Antimony 7N, 7N5+ MBE
- Gallium 7N5+ (RRR > 75000) MBE
- Aluminium 6N, 6N5+ MBE
- Indium 7N, 7N5 MBE
- Red phosphorous 6N, 7N MBE
- Beryllium 4N+ MBE
- GaTe 6N, Mg 6N, Mn 5N8, Se 6N, Zn 6N, Te 6N, ZnTe 6N, CdSe 6N, Bi 6N, S 6N...
- Silicon wafers, ultrapure silicon dopant MBE
- GaAs, InP GaSb, GaP, InAs, InSb wafers
- PBN crucibles
- Wafers Reclaim & Thinning
- Precursors for MOCVD, ALD... technologies
- Bonding Wires and Ribbons
- Bonding Caps-Wedges, Pick up tools, Die Collets: **SPT Roth**



www.azeliselectronics.com

azelis.electronics@azelis.fr

Azelis France - 8-14 av. de l'Arche - 92400 Courbevoie - France

Automatic LN₂ Circulation for MBE

Engineered to be safe, reliable and easily interface
with all production and research MBE systems



THE WORLD'S LEADING SUPPLIER OF LIQUID NITROGEN PIPING SYSTEMS

- Automatic liquid nitrogen circulation
- Constant liquid nitrogen temperature and pressure
- Modular components to simplify installation
- Vacuum jacketed cryopanel connections

**VACUUM
BARRIER** **VBC**
CORPORATION

4 Barten Lane, Woburn, MA 01801, USA
T 781 933 3570 | F 781 932 9428
sales@vacuumbarrier.com
vacuumbarrier.com



VacuumBarrierSystems

Avenue Landas 17, B-1490 Saintes (Tubize), Belgium
T +32 2 354 71 77 | F +32 2 354 72 21
sales@vbseurope.com
vbseurope.com

WAFER ECV PROFILER CVP21

ECV Measurement of Doping Profiles

Patents: DE-10256821, US-7026255 (further pending)



CVP21 including option FP: Footprint
60*80cm for minimum required clean room
space

ECV Profiler CVP21: The **COMPLETE** Solution.

COMPLETE Material Range:

Group IV: Si, Ge, SiC
Standard III-V: GaAs, InP, ...
Ternary: AlGaAs, GaInP, ...
Quaternary: AlGaInP, ...
Nitrides: GaN, AlGaN, AlInN, ...
II-VI: ZnO, CdTe, CdHgTe, ...

COMPLETE Sample Range:

Stacked layers no problem
No restrictions concerning substrate
Sample size: 4*2 mm² ... 8" Wafer

COMPLETE Resolution Range:

< 10¹² cm⁻³ ... > 10²¹ cm⁻³ (*)
1 nm ... 100 μm (*)
(*) may depend on material type/ sample quality.
Please ask for sample measurements.

COMPLETE System:

HiRel - Calibration-free - Easy-to-Use
Wafer-Stepping - Camera-Control
Recipes - Auto-Load/Unload/Reload
Manual/SemiAuto/FullAuto

WEPcontrol.com



STAIB

STAIB INSTRUMENTS

MBE Real Time Growth Monitoring

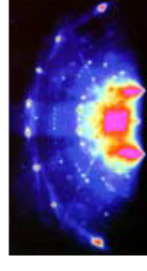
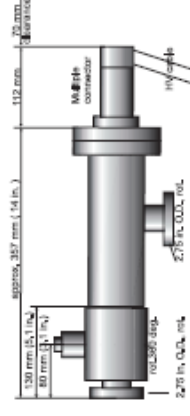
In-situ and On Site Surface Characterization



STAIB

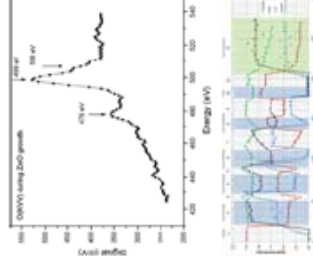
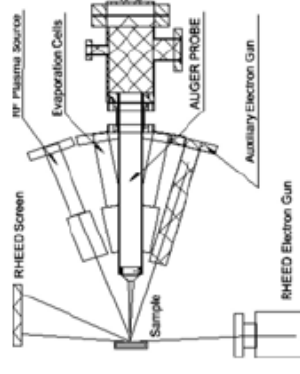
RHEED

STAIB RHEED systems, the gold standard for *in-situ* diagnostics during growth. Growth rate, lattice spacing, crystal structure
STAIB RHEED for MBE, Oxide / Nitrogen MBE Laser MBE, PLD, Sputtering



In-situ AugerProbe™ **NEW!**

STAIB AugerProbe for real time *in-situ* AUGER electron spectroscopy during growth. Surface stoichiometry



STAIB MultiTech™

The **STAIB MultiTech™** System Plus is an affordable, modular surface analysis chamber, for use as a **stand-alone system** or for **incorporation in multi-chamber installations**. It can be configured, as a **basic research and analysis tool** for AES and ELS, with **upgrade options for additional techniques**, like XPS, SAM, SEM, UPS, ISS, and Depth Profiling



Systems for MBE

Mass spectrometers for vacuum, gas, plasma and surface science

XBS

- ▶ In-situ beam monitoring
- ▶ Wide, 70° beam acceptance
- ▶ Water-cooled for thermal stability

Modular SIMS

- ▶ Add high performance surface analysis to your MBE system
- ▶ Complete bolt-on SIMS instrument built onto a single flange
- ▶ Incoming wafer quality and post process static thin film characterization

TDSLab Series

- ▶ Advanced thermal desorption studies for materials characterization
- ▶ Measurement of desorbed species from thin films
- ▶ Simultaneous detection of known and unknown species for contamination and quality control

RIGAKU ADVANCED THIN FILM SOLUTIONS

Best-in-class instrumentation for thin films and semiconductors

All methods in one tool: XRD, XRR, Rocking Curve and Reciprocal Space Mapping, 2D-GISAXS, GI-XRD, Residual Stress, and Texture



SmartLab XE

- Global data consistency with auto-alignment concept
- Automatic optical component recognition ensures error-free handling
- 7x faster data acquisition due to 9 kW X-ray source
- Ultrafast, single photon sensitive 2D HyPix-3000 detector with unmatched robustness



Five-circle goniometer for thin film application

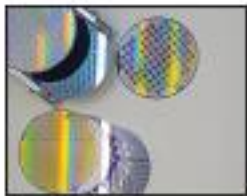
- Most brilliant and powerful line and microfocus X-ray sources available
- High-resolution optics for double- and triple-axis geometries
- HyRES automatic, switchable analyzer
- Ultrafast & Wide Range RSM using HyPix-3000 2D detector



EVO50 MOLECULAR BEAM EPITAXY SYSTEM

Your vision, your plan... ...our smart solution

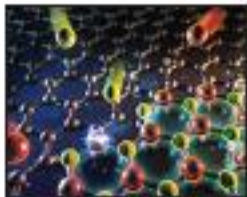
Nexus: The first MBE software with Recipe Builder



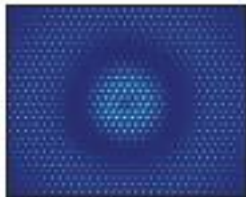
Classic III-V



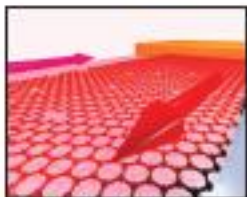
Nitrides



Oxides



TMDC



Topological Insulators



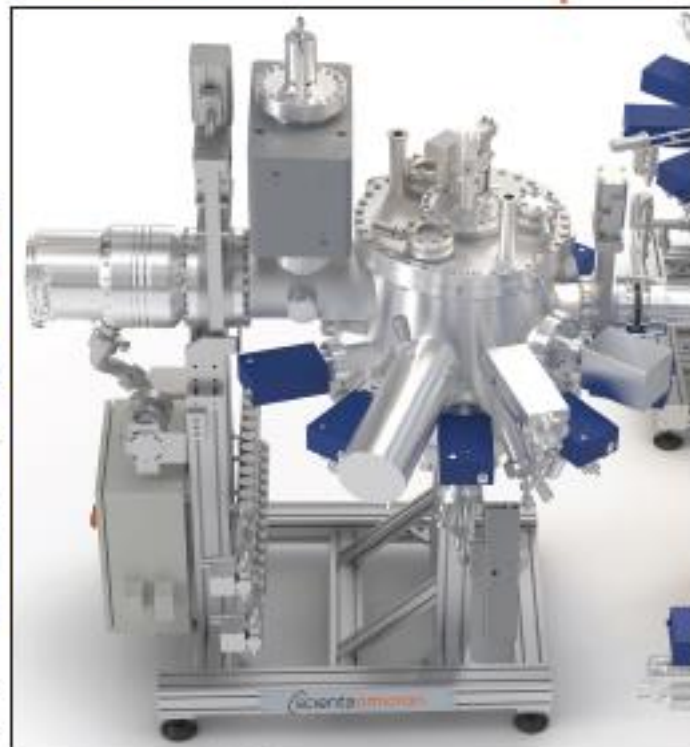
Metals



Heusler alloys



Graphene



Optoelectronics



Power electronics



Spintronics



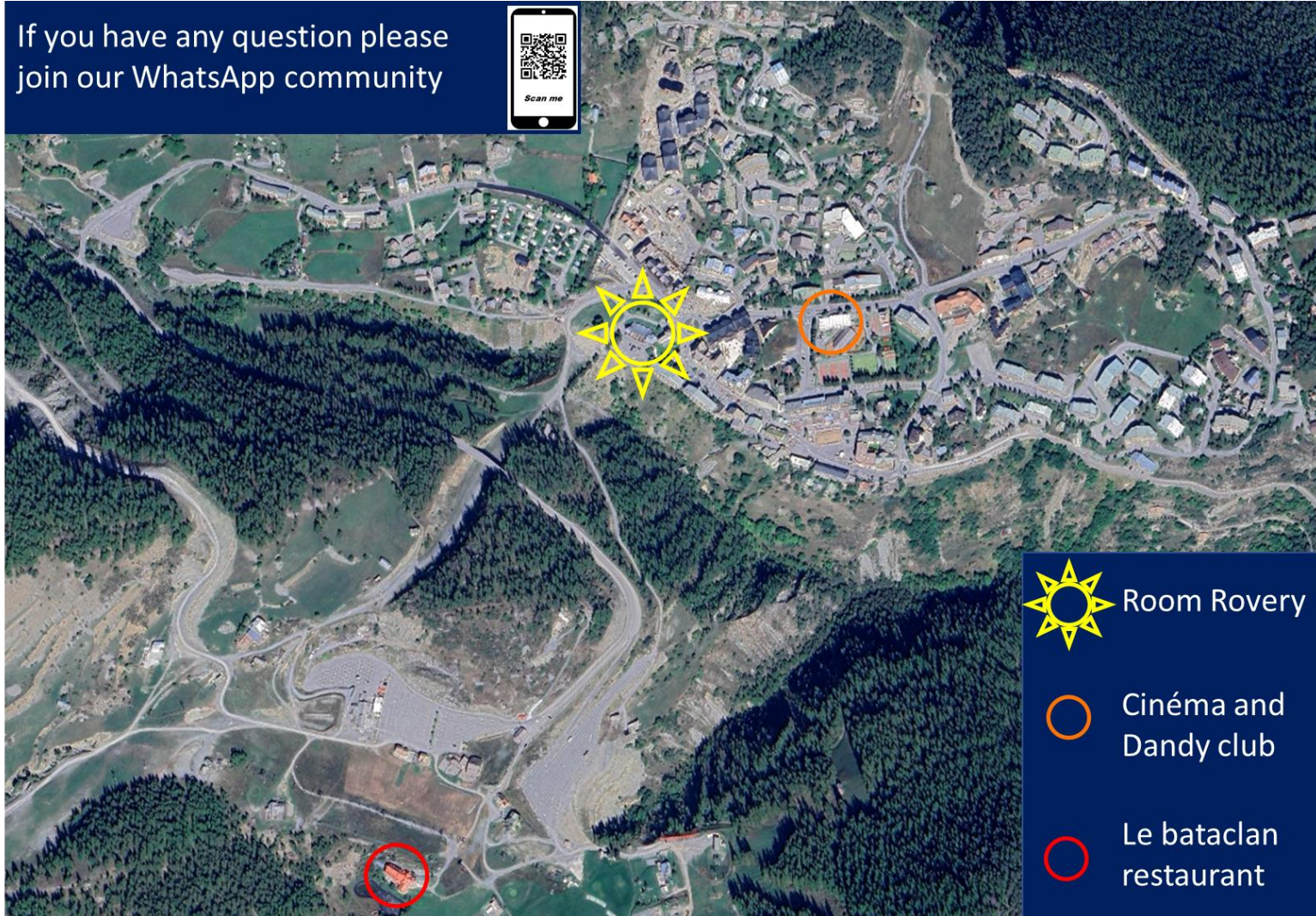
Superconductors




- Unique recipe builder technology with graphical sample composition information
- Scheduled sample transfer and detailed tracking with batch processing
- Automatically gather and utilise cell flux data
- Integrated in situ metrology for self-calibration of samples during growth
- Safeguard your system with programmable interlocks and system watchdog
- Full history, logging and cloud integration

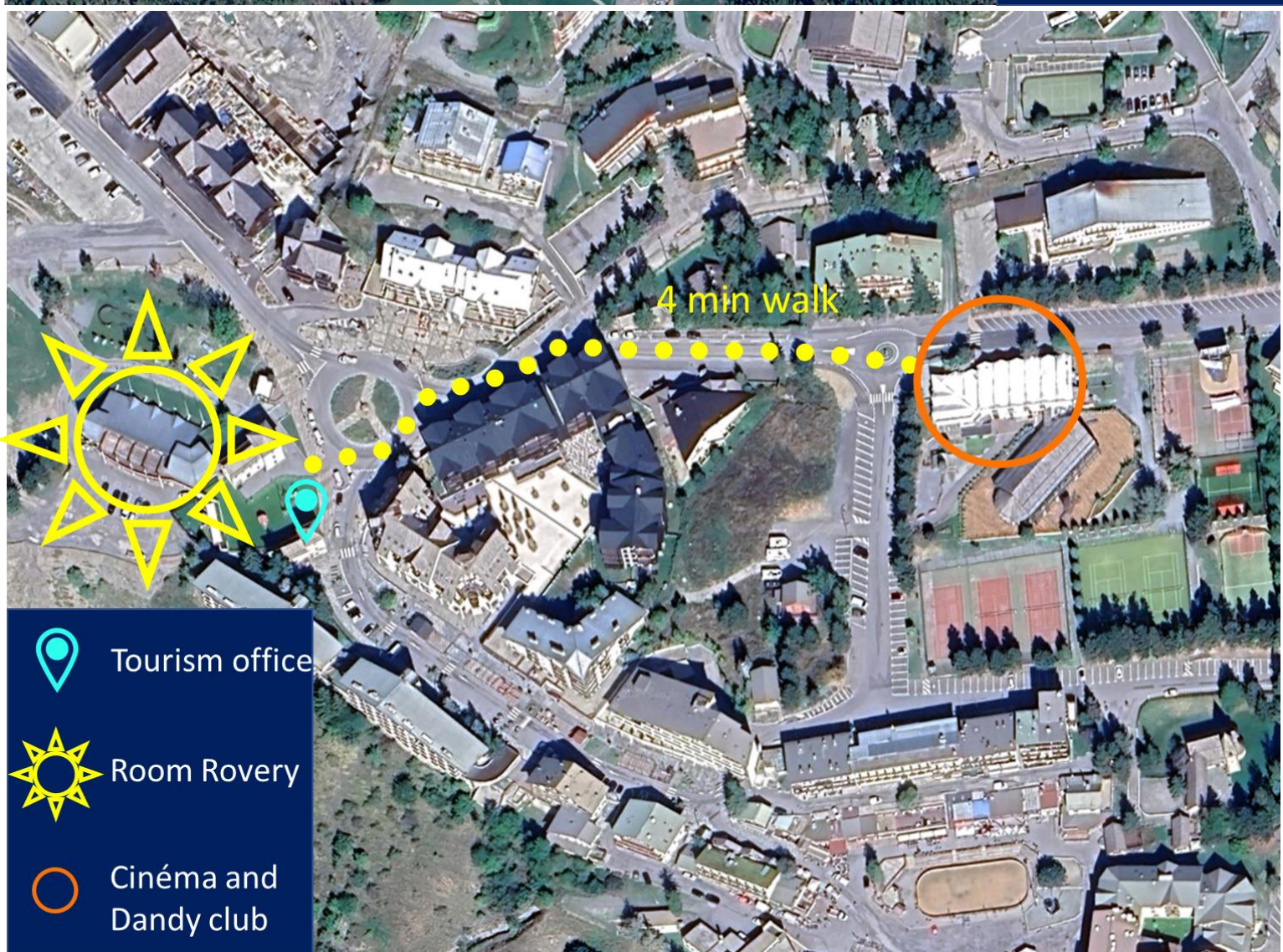
Read more at:



If you have any question please join our WhatsApp community



-  Room Rovery
-  Cinéma and Dandy club
-  Le bataclan restaurant



-  Tourism office
-  Room Rovery
-  Cinéma and Dandy club